2021

The Role of Vps54 in Drosophila melanogaster Neuronal Development and Age Progressive Neurodegeneration

Emily Wilkinson
University of Denver

The Role of Vps54 in *Drosophila melanogaster* Neuronal Development and Age Progressive Neurodegeneration

---

A Dissertation

Presented to

the Faculty of the College of Natural Sciences and Mathematics

University of Denver

In Partial Fulfillment

of the Requirements for the Degree

Doctor of Philosophy

---

by

Emily Wilkinson

March 2021

Advisor: Dr. Scott A. Barbee

Author: Emily Wilkinson
Title: The Role of Vps54 in *Drosophila melanogaster* Neuronal Development and Age Progressive Neurodegeneration
Advisor: Dr. Scott A. Barbee
Degree Date: March 2021

ABSTRACT

Vps54 is a subunit of the Golgi-associated retrograde protein (GARP) complex, which is involved in tethering endosome-derived vesicles to the *trans*-Golgi network (TGN). The "wobbler" mouse is the phenotypic result of a destabilizing point mutation in Vps54. This mutation causes neurodegeneration and is subsequently used as a model for human motor neuron disease. Presently, it is unclear how disruption of GARP complex function leads to motor neuron degeneration. To better understand the role of Vps54 in motor neuron development, function, and age-related neurodegeneration, we disrupted expression of the Vps54 ortholog in *Drosophila* and examined the impact on larval neuromuscular junction morphology, locomotor function, and longevity. We show that functional null mutants and motor neuron specific knockdown of Vps54 lead to NMJ overgrowth and partial disruption of Syntaxin-16 localization. We also see reduced lifespan and severe locomotor defects in adult flies. We show that Vps54 may be interacting with small GTPases Rab7 and Rab11 at different life stages to further regulate motor neuron development and function. Taken together, these data suggest that Vps54 plays a major role in the development and functional regulation of motor neurons, while additionally interacting with differing endosomal trafficking components associated with disease phenotypes.

ACKNOWLEDGEMENTS

I would like to thank Dr. Scott Barbee for his mentorship and guidance over the past few years as well as his support and understanding throughout my time at the University of Denver. I would like to thank all of my committee members: Dr. Nancy Lorenzon, Dr. Robert Dores, and Dr. Daniel Linseman, for their support and advice over the course of my degree. I would also like to thank all of the other faculty that supported my growth and education: Dr. Joseph Angleson, Dr. Cedric Asensio, Dr. Schuyler Van Englenburg, Dr. Nancy Sazaki, Dr. Kristen Andrud, and Angela Hebel. I would like to thank Kelly (Sinak) DellaGrotte, Kristen Dew, Keelan Zius, Larissa Ikenouye and Emily Starke for all of their help and support as my lab mates and friends over the past few years. I would also like to thank all of my peers who were always available for advice, conversation, and reagent swaps, especially Brianne Hoglin, Dr. Perry Davis, Dr. Navneeta Kaul and Elizabeth Ignowski. Finally, I would like to thank my friends and family for all of their love and support over the duration of my degree, especially my parents Susan and Erik Wilkinson and my partner McCrae Kempf. I couldn't have done it without every one of you.

TABLE OF CONTENTS

LIST OF FIGURES

CHAPTER 1: AN INTRODUCTION TO NEURODEGENERATION

Neurodegeneration and disease

Neurodegeneration is a devastating and fatal neurological disease characterized by gliosis and the irreversible loss of neurons [1]. The increased prevalence of age-dependent neurodegenerative diseases in recent years poses a major threat to human health [2-4]. The manifestation of these disorders can be seen impacting both the central and peripheral nervous systems. Symptoms such as memory loss or other cognitive impairments are associated with loss of nervous function in the brain, while locomotor dysfunction affecting mobility, speech, and respiratory function are associated with peripheral nervous function [5-8]. Disruption of normal cellular function, ranging from the regulation of RNA metabolism to the general homeostatic maintenance of neuronal proteins, have been characterized in neurodegenerative disorders such as Parkinson's Disease (PD), Alzheimer's Disease (AD), Amyotrophic lateral sclerosis (ALS), Frontotemporal dementia (FTD), and Charcot-Marie-Tooth (CMT) disease [1, 9]. There are very few effective treatments for neurodegenerative disorders. As such, a deeper understanding of the mechanistic causes of such disorders is needed to further target potential therapies [10]. Several intracellular pathways have been implicated in neurodegenerative disease pathogenesis associated with mutations found in specific genes. These genes can be

categorized by their control of or assistance in; RNA metabolism, axonal and cytoskeletal dynamics, and protein trafficking [7].

RNA regulation and neurodegeneration

RNA binding proteins (RBPs) are required for stabilization of RNA, transcription, splicing, and RNA degradation in both the nucleus and cytoplasm. Because of this, metabolism of RNA can be regulated by RBPs [1]. Mutations in proteins such as TAR DNA-binding protein-43 (TDP-43) and nuclear protein fused in sarcoma (FUS) have been identified in neurodegenerative disorders such as ALS and FTD [11-17]. TDP-43 functions ubiquitously in RNA processing and is involved in RNA stability [18-20], transport [21], and splicing [22-25]. Similar to TDP-43, FUS regulates RNA transcription by recruiting RBPs to non-coding RNA via its interactions with serine-arginine RNA splicing associated proteins [26, 27].

When mutated both proteins show a characteristic mis-localization from the nucleus to the cytoplasm, where in some cases they form large protein aggregates [11, 16, 17]. Other RBPs, such as hnRNPA1 and A2B1 have also been shown to localize to cytoplasmic RNA stress granules [28-31]. The utilization of mRNA during stress is in part controlled by RPBs and the formation of RNA stress granules. RNA stress granules are generally transient membrane-less organelles formed through liquid-liquid phase separation. However, there is evidence that indicates that age related chronic stress causes the persistent appearance of stress granules, which act as foci associated with aggregation of disease related proteins [32].

It has previously been shown that there is a positive correlation between the number and size of cytoplasmic aggregates and cytoplasmic RNA granules to the risk of neuronal cell death [33]. However, the specific disease-causing mechanisms involved in RBP regulated RNA metabolism, such as those associated with TDP-43 and FUS dysfunction, are yet to be fully understood.

In a TDP-43 deficient mouse model, global RNA expression of over 600 genes were altered showing a particular bias toward neuronal genes [34]. Similarly, immunoprecipitation of TDP-43 and FUS from mouse brain tissue and rat primary neuronal cultures show binding to 3' untranslated regions (UTRs) of thousands of different mRNA [25, 34, 35]. Together this suggests that disease pathogenesis may be the result of altered gene expression and global RNA dysregulation [1].

Aberrant microsatellite sequence expansions produce RNA with tandem repeat sequences beyond that of normal nucleotide threshold lengths [36]. Sequestration of RBPs away from their target RNA by microsatellite repeat expansions can also alter RNA metabolism [37-39]. There are several examples of disease-causing genes that contain these pathogenic repeat expansions including *DMPK*, *FMR1*, and *C9orf72*. A CTG expansion in the 3' UTR of *DMPK* causes muscleblind-like proteins (MBNLs), an RBP that regulates alternative splicing, to sequester into RNA foci rendering them incapable of functioning [40-44]. Similarly, RBPs such as hnRNPs and MBNL1 are found to alter microRNA (miRNA) biogenesis and splicing in individuals with a repeat expansion in the UTR of the *FMR1* gene that causes Fragile X-associated tremor/ataxia syndrome (FXTAS) [45-48]. Finally, a hexanucleotide (G_4C_2) expansion in *C9orf72* causes the formation of

mutant nuclear RNA aggregates. These sequences sequester RBPs such as hnRNPs and alter RNA splicing, thus affecting metabolism [39, 49-53]. Further still, there are other types of RNA such as miRNA and non-coding RNA (ncRNA) that have been implicated as effectors on neurodegenerative disease-causing genes [54, 55]. Taken together, it is clear that regulation of RNA metabolism contributes to the devastating pathology associated with neurodegenerative disorders.

Axonal and cytoskeletal involvement in neurodegeneration

Protein aggregation by defective cytoskeletal components

The formation of abnormal filamentous protein deposits in neurons have been found in cases of familial and sporadic neurodegenerative diseases [56]. Specifically, disorders known as neuronal intermediate filamentopathies or tauopathies are caused when intra-cellular inclusions are present in intermediate filament proteins and in the microtubule-associated protein (MAP) tau [57]. The two are often present in pathological neurofibrillary tangles, neuropil threads, and dystrophic neurites. In PD and dementia, neuronal filament and alpha-internexin triplet proteins are present, although it is unclear what their role is in lesion formation or neurodegeneration [58, 59]. It was realized that mutations in neuronal intermediate filament genes and the *tau* gene, were sufficient to invoke neurodegeneration associated with diseases such as CMT, ALS, FTD and parkinsonism linked to chromosome 17 [60-67].

Tau proteins, specifically, have been implicated in the onset of neurodegeneration because filamentous tau aggregates have been found in progressive neurodegenerative

disease neurons in the absence of other neuropathological abnormalities [56]. Pathogenic *tau* mutations in heterogeneous FTDP-17 disorders further established a role for tau in neurodegenerative diseases [66, 68-70]. Tau proteins are low molecular weight MAPs predominantly expressed in abundance in neuronal axons both in the central and peripheral nervous systems [71-73]. From the human *tau* gene, six distinct isoforms of tau protein can be generated by alternative splicing of the 16 exons within the mRNA [74, 75]. Tau binds to microtubules promoting polymerization and aiding in stabilization [71, 76]. There are 4 highly conserved microtubule binding motifs where phosphorylation-dependent tau binding can occur [77-82]. It has been shown that hyperphosphorylation of tau is the principal component of filamentous neuronal aggregates found in AD and FTD [83-85].

Normally, very low levels of phosphorylation are associated with neuronal filaments located in the proximal axonal segments, perikaryon, and dendrites of neurons; conversely, distal axonal segments are heavily phosphorylated [86, 87]. Although the significance of neuronal filament phosphorylation is unclear, in ALS, affected neurons show accumulation of phosphorylated neuronal filaments localized to swollen axons, the perikaryon and cytoplasmic spheroids [88-90]. It has been speculated that abnormal aggregate hyperphosphorylation, protecting against proteolysis, may contribute to neuronal dysfunction via impediment of axonal transport [91].

The protein alpha-internexin plays a role in neuronal cell differentiation preceding the expression of neuronal filament protein triplets. It is normally found to be minimally expressed in adult brains compared to neuronal filament proteins [92]. This said, it has been implicated as a major component of the pathological inclusions of neuronal

intermediate filament inclusion disease (NIFID) and FTD. Although not found to have altered mobility in most neurodegenerative diseases, alpha-internexin along with tau, are absent in the neuronal cytoplasmic inclusions of NIFID affected neurons suggesting a role in neuronal dysfunction phenotypes [93-97].

Cytoskeletal defects and dysfunction of axonal transport

Axonal transport is required for neuron viability and is dependent on microtubule architecture and integrity [98]. The bidirectional transport of cellular cargo in neurons is facilitated by molecular motors. Kinesins are responsible for anterograde cargo transport to axon terminals, while dyneins are involved in retrograde transport to the soma [99]. Neuronal microtubules have a lower grade of dynamic instability than other cells, presumably due to their role in axonal transport [100]. It has been speculated that the faulty axonal transport observed in neurodegeneration could be a result of microtubule structural alterations or molecular motor dysfunction [101, 102]. Microtubule abnormalities in nigral dopaminergic neurons in PD affected cells and axonal breakage due to traumatic brain injury, seen in chronic traumatic encephalopathy (CTE) affected cells, clearly show the neurodegenerative nature of axonal dynamic dysfunction [103-106].

Several protein coding genes have been implicated in neurodegenerative diseases, such as PD and ALS, that appear to cause pathogenic microtubule alterations. Normally, alpha-synuclein plays a role in synaptic function, however, it has been observed that overexpression in cells leads to reduced microtubule network complexity, Golgi fragmentation, microtubule-dependent trafficking dysfunction and neuritic degeneration

[107, 108]. An A53T mutation of alpha-synuclein has been found in cases of familial PD [109]. In the A53T transgenic mouse model, reduction of microtubule stability is observed along with hyperphosphorylation of tau, suggesting that tau disengagement acts as a precursor to microtubule dysfunction [110-112]. A hereditary mutation in the leucine-rich repeat kinase 2 (LRRK2), associated with familial PD, causes phosphorylation of bound tau thereby releasing it from microtubules, which further links microtubule stability to neurodegeneration [113-116]. Mutations in the protein Parkin have also been shown to reduce microtubule stability resulting in reduced neurite complexity and length [117-119]. This disease phenotype can be rescued by introduction of the drug paclitaxel, which stabilizes microtubules [119]. This direct interaction of Parkin and microtubules is not well understood; however, it is speculated that that deacetylation of microtubules by HDAC6 may play a role due to Parkin and HDAC6 interactions [120].

Mutations in the *superoxide-dismutase-1* (*SOD1*) gene are found in about 10% of inherited ALS cases and display axonal transport deficits that sometimes precede neurodegeneration [121, 122]. Increased microtubule dynamics have been observed in the neurons of several transgenic mutant SOD1 mouse models, further supporting the role of axonal transport in neurodegeneration [123, 124]. A mutation in the $p150^{glued}$ subunit of dynactin causes dysfunction of axonal retrograde transport, which has been linked to motor neuron disease and possibly ALS [125, 126]. Axonal transport dysfunction has also been observed in *Drosophila* and mouse models with mutations in *TDP-43*, *FUS*, and *C9orf72* genes, all of which are involved in RNA metabolism as well [11, 127-130].

Neurodegeneration associated with dysfunction of secretory protein trafficking and membrane trafficking

Trafficking disruption associated with beta-amyloid plaque formation

Dysregulation of endocytic trafficking is apparent in many neurodegenerative diseases including AD, PD, ALS and even Down syndrome [131-134]. In AD beta-amyloid plaques (AB) form as trafficking of upstream components such as beta-amyloid precursor protein (APP) and its proteolytic secretases like beta-secretase 1 (BACE1) are mis-localized due to subcellular trafficking dysfunction [135, 136]. BACE1 is a transmembrane protease which catalyzes the first step of AB formation. ADP-ribosylation factor-binding protein GGA3 has been shown to act as a BACE1 transporter to lysosomes, regulating BACE1 expression, however, increased levels of BACE1 have been implicated in AD pathology suggesting the transport by GGA3 is required for normal cellular function [137-141].

Similarly, transmembrane glycoprotein lipoprotein receptor-related protein 1 (LRP1) has been shown to affect APP trafficking leading to similar results [142-144]. Due to overexpression of genes such as *APP* and *synaptojanin 1* (*SYNJ1*), an increase in AD pathology is found in Down syndrome cases, further supporting the neurodegenerative role of such proteins [145, 146]. Genes that express both *alpha-synuclein* and *LRRK2* have been found to have a role in neuronal protein sorting. *LRRK2* mutations cause defects in protein degradation via lysosomes and cause Golgi fractionation, while dopamine release in PD affected animals is linked with alpha-synuclein function [147-151].

Trafficking components, such as the sorting nexin (SNX) family of proteins, have been found to regulate APP cleavage. Loss of function of sorting nexins has been linked with increased accumulation of AB plaques in mammalian cells and disrupted recycling of LRPs [152-154]. To the same effect, SNX33 has been found to bind dynamin and reduce APP endocytosis, while acting as an activator of APP cleavage [155]. SNX6 is a key component of the retromer complex involved in retrograde transport and SNX12 down-regulation is linked with decrease in BACE1 via accelerated endocytosis [156, 157].

Regulation of protein trafficking by Rab GTPases

It has also been shown that the small GTPase ADP ribosylation factor 6 (ARF6) is involved in the regulation of BACE1 internalization and sorting to Rab5-positive early endosomes [158]. Other Rab GTPase components have also been found to regulate protein trafficking associated with neurodegeneration. An example is Rab1B, which has been shown to have a role in trafficking of APP from the endoplasmic reticulum (ER) to the Golgi [159, 160]. Rab7 mediates subcellular localization of lysosomes and interacts with late endosomes. In PD Rab7 interaction with *LRRK2 Drosophila* ortholog cause alterations in lysosomal positioning associated with neurodegeneration [149]. In CMT type 2B missense mutations in Rab7 causes altered function associated with neurodegeneration. There is evidence suggesting that mutant variants of Rab7 result in reduced endolysosomal capacity, a change to which neurons are very sensitive [161]. Rab6 is involved in intra-Golgi trafficking, While Rab11 is involved in the facilitation of axonal and dendritic BACE1 trafficking [162-165].

Disruption of endosomal recycling and neurodegeneration

Endosome recycling to the *trans*-Golgi network (TGN) is regulated in part by the retromer complex [166]. The retromer complex localizes on endosomes and plays a key role in endosomal protein sorting [167]. This is composed of a trimer core sub-complex of vacuolar protein sorting (VPS) proteins VPS26, VPS29, and VPS35 and a membrane-associated dimer of SNXs including SNX1, SNX2, SNX5, and SNX6 [168]. The core subunit VPS35 is presumed to be responsible for the majority of cargo-binding with evidence of direct interaction with cargo proteins such as CI-Manose-6-phosphate receptors (M6PR), wntless, and sortilin [166, 169-173]. In cell culture, knockdown of VPS35 causes an upregulation of AB peptides, while overexpression leads to a stark downregulation of the generation of AB. It has been observed that expression levels of VPS26 and VPS35 are reduced in brain tissue of AD individuals [174]. Presumably, modulation of BACE1 by the retromer complex is responsible for the neurodegenerative phenotypes seen in Vps26 and Vps35 knockout mice [175, 176]. Involvement by the retromer complex is further supported by the stabilization of APP transportation by a chemical chaperone. That chaperone acts by stabilizing the retromer complex [177]. Finally, a missense mutation, D620N, of the VPS35 protein has been identified in multiple cases of familial PD [178-180].

Similar membrane protein involvement has been implicated in neurodegeneration caused by endocytic trafficking dysfunction. The Sortilin-related receptor with A-type repeats (SorLA) has reduced expression in AD brain tissue, with some hereditary variants being linked to late-onset AD [181, 182]. Recycling of APP is modulated by SorLA and

the knockdown of SorLA causes an increase in APP sorting into the compartments associated with AB generation [182]. It is speculated that interaction between Vps26 and SorLA play a role in disruption of Golgi function associated with neurodegenerative phenotypes [183]. The mutation S498A in BACE1 targets it to SorLA-positive compartments that attenuate reduction of AB peptides [184]. Additionally, there is some evidence that Munc18 interacting proteins (Mints) are involved in synaptic function and neuronal protein transport, although their involvement in neurodegeneration is unclear [185, 186].

Cell surface protein expression and endosomal trafficking defects

There are several genes that have been linked to neurodegenerative disorders such as hereditary spastic paraplegia (HSP) and ALS. Specifically, genes that are involved in the regulation of membrane trafficking include; *Alsin* (*ALS*2), *C9orf72*, *Optineurin* (*OPTN*), *Spastin* (*SPG4*), *Strumpellin* (*SPG8*), *Spatacsin* (*SPG11*), *Spastizin* (*SPG15*), *AP5*, and *Vps37A* [187-197]. Although the precise mechanism affected by the hexanucleotide expansion in C9orf72 is unclear in terms of the cause of motor neuron degeneration, in effected cells elevated levels of cell surface proteins such as NR1, the receptor for NMDA, and GlurR1, the receptor of AMPA, have been observed leading to disease phenotypes. M6PRs, involved in lysosomal enzyme trafficking, are also affected by C9orf72 mutations, this can be seen by the mis-localization of M6PRs to the cytosol and defects in lysosomal degradation [198]. There is also evidence that C9orf72 interacts with Rab-GTPases involved in several intracellular trafficking steps [130, 199, 200].

Trafficking disruption caused by alterations in TDP-43 have also been described in ALS. Knockdown of TDP-43 expression has been linked with reduced cell surface levels of ErbB4 and epidermal growth factor receptor (EGFR). It has been suggested that defects in receptor recycling following receptor activation are the cause of neurodegeneration, as EGFR activation promotes neuronal outgrowth, maturation, and survival [201-203]. Depletion of TDP-43 in *Drosophila* also affects BMP receptors, activation of which is involved in endosome sorting to either the recycling or degradation pathways [204]. Downstream phosphorylation of MAD, involved in facilitating synaptic growth, is also altered by changes in TDP-43 expression leading to receptor mis-sorting [205].

More than 12 different mutations in the gene encoding Alsin-2 have been reported in cases of juvenile ALS and primary lateral sclerosis (PLS). Alsin-2 functions as a guanine-nucleotide exchange factor (GEF) for Rab5 [206]. Prevention of endosomal fusion has been observed in cells co-expressing truncated Alsin-2 and Rab5, while accumulation of Rab-5 positive early endosomes has been noted in an Alsin-2 transgenic mouse model [207]. Taken together, these findings suggest a disruption of downstream trafficking effectors by dysfunction of Rab5 due to alteration of Alsin-2 function.

Age progressive neurodegeneration by alteration of GARP complex function

Transfer of cellular components to and from endosomal vesicles and the *trans*-Golgi network require a physical link between tethering factors and soluble N-ethylmaleimide-sensitive fusion protein attachment protein receptors (SNAREs) prior to compartmental fusion executed by small GTPases [208]. The evolutionarily conserved

Golgi-associated retrograde protein complex is a tethering factor localized to the TGN and is involved in the retrograde transport of early and late endosomes to the TGN. The heterotetrameric core is made up by Vps proteins Vps51, Vps52, Vps53, and Vps54. The N-terminus of Vps54 binds SNARE proteins, including Syntaxin-16 (Stx16) Syntaxin-6 (Stx6) and Vamp4, while the C-terminus interacts with endosomes [209, 210]. Most of the core subunits of GARP are shared by the endosome-associated recycling protein (EARP) complex. The composition of the EARP complex core has the protein Syndetin, an uncharacterized protein, found in lieu of Vps54. This difference in core subunits determines the differential localization of the EARP complex to Rab4-positive recycling endosomes. The EARP complex has been shown to regulate endosomal cargo sorting to dense-core vesicles and act as a tethering complex in endocytic recycling [211, 212].

In yeast, non-lethal GARP component deletion mutants display temperature-sensitive growth impairments, mis-sorting of carboxypeptidase (CPY), and aberrant vacuolar morphology including lysosomal enlargement [208, 213, 214]. Knockdown of GARP subunits in mammalian systems inhibits transport of recycling proteins including cation-independent mannose 6-phosphate receptor (CI-M6PR) and TGN46. Retrograde transport of the Shiga toxin B subunit is also inhibited in similarly affected mammalian cells [215]. It has been speculated that the GARP complex may be involved in anterograde membrane trafficking as well due to the defective transport of some glycosylphosphatidylinositol (GIP)-anchored TGN derived transmembrane proteins in systems with GARP subunit disruption [216].

Complete loss of function of the Vps54 protein in mice is characterized by embryonic lethality around gestational day 10.5, thought to be caused by the clear underdevelopment of cardiac muscle and motor neurons [217]. The underdevelopment of neuronal tissue can be specifically seen by the extensive membrane blebbing of the neural tube which, is believed to be a consequence of impaired vesicle transport [218]. There is an additional neurodegenerative mouse model where heterozygous mutation of *Vps53* causes symptoms used to model human pontocerebellar hypoplasia type 2E [219]. However, GARP complex dysfunction cannot be solely implicated in this neurodegenerative model due to the shared core subunit, Vps53, with the EARP complex. This said, this stands to further demonstrates the role of endosomal trafficking in neurodegenerative disorders.

The wobbler mouse: a model for motor neuron disease

In the wobbler mouse model, a destabilizing point mutation (L967Q) in the last exon of the gene encoding Vps54 located on chromosome 11, causes age-progressive motor neuron degeneration. The spontaneous missense mutation found in the wobbler mouse causes a reduction of GARP complex function leading to an impairment of retrograde endosome transport resulting in protein mis-sorting and accumulation in enlarged endosomes [217, 220]. The destabilizing point mutation greatly reduces the half-life of Vps54 causing reduced levels of expression in the mouse. Due to the reduced levels of Vps54 and even further the unstable nature of the mutant protein, the GARP complex when assembled is not stable and therefore has reduced function [208].

The wobbler mouse phenotype shares many pathological features with human ALS cases. The ‘wobbler’ name came from the unsteady or ‘wobbly’ gait exhibited in homozygous individuals due to severe muscle weakness in the forelimbs, head and neck. Overall, it is characterized by spinal neurodegeneration, muscular atrophy, astrogliosis, microgliosis [221], mitochondrial dysfunction [222], hyperexcitability [223], neurofilament aggregation [224], axonal transport defects [225], and ubiquitin-positive protein aggregations [226]. Because of these numerous similarities the wobbler mouse is commonly used to model human motor neuron disease, specifically sporadic ALS (sALS) [220]. This said, there have yet to be any cases of ALS that are linked to mutations in Vps54 [227, 228]. However, it is believed that continued study of the wobbler mouse model will illuminate key factors in overall motor neuron degeneration caused by impairment of endocytic trafficking.

Male sterility is a unique phenotype seen in the wobbler mouse. At this point, sterility has not been directly associated with human motor neuron diseases. The wobbler mutation has a pleiotropic effect on spermatogenesis, which causes an overall decrease in the production of sperm cells and those that are produced have abnormal round-headed morphology and reduced motility [229]. The round-headed morphology of sperm cells is caused by a failure of nuclear condensation resulting from defective acrosome granule formation, a Golgi dependent process [208, 229-231].

During spermatogenesis Vps54 has been shown to follow the same trafficking route as de-ubiquitinating enzyme, USP8, and the endosomal sorting complex, ESCRT-0 [231]. USP8 is associated with acrosomal structures and is involved in endosomal sorting. Most

notably, it is highly expressed in both male germ cells and neurons, suggesting function in both spermatogenesis and neuronal development, much like that associated with Vps54 function [232-234].

The *Drosophila* Vps54 ortholog scattered

Both neurodevelopmental and neurodegenerative processes have been studied in the well characterized glutamatergic neuromuscular junction (NMJ) of *Drosophila melanogaster* larvae [204]. *Drosophila* have a single ortholog of *Vps54* which is known as *scattered* or *scat*. It was first discovered during a large-scale screen to determine if allelic disruption by P-element insertion caused male sterility in *Drosophila* [235]. To this point, scat has been relatively understudied except in the case of male sterility [235, 236]. The *Drosophila* mutant $scat^{1}$ was developed by inserting a transposon P-element insertion into the *scat* allele resulting in complete loss of function. The $scat^{1}$ mutant exhibits partial lethality and, like the wobbler mouse, has severe spermatogenesis defects causing complete male sterility [230, 235, 236]. Specifically, homozygous $scat^{1}$ male fly seminal vesicles are devoid of mature sperm. The early steps of spermatogenesis such as meiotic division are not disrupted, however, defects in acrosome formation and nuclear elongation, as a result of compromised Golgi integrity, are found in $scat^{1}$ males [230].

Neuronal processes and scat

Our initial interest in scat stemmed from a screen Prajal Patel did to identify possible interactions with the protein HPat. HPat is a decapping activator that interacts with

miRNA and has been suggested to play a role in larval NMJ development [237]. In flies, dysfunctional mutations of HPat cause severe synaptic hyperplasia [238]. In the screen, scat was positively identified, due to its homology with Vps54 and known neurodegenerative phenotype characterized in the wobbler mouse. Because of this we pursued scat and its role in neuronal processes.

Our goal is to characterize the role of scat in both neurodevelopmental and neurodegenerative processes. Specifically, we would like to establish *scat* mutants as models for neurological study; in essence developing novel "wobbler fly" models. The *Drosophila* larva NMJ has previously been used to model other neurodegenerative diseases [239]. These models show synaptic abnormalities such as changes in bouton number and synaptic branch number in cases where AD causing proteins APP and BACE were expressed [240]. Similarly, larvae that were arrested in the third instar (ATI) stage also exhibited neurodegeneration and the appearance of ghost boutons [241]. By characterizing NMJ morphologies in developing *scat* mutants and describing adult neurological phenotypes we can establish *scat* mutants as viable neurodegenerative models.

The development of wobbler flies would allow for the use of unique and powerful *Drosophila* specific genetic tools commonly used to study neurological conditions and morphology. The characterization of scat loss-of-function and reduction-of-function in the development and maturation of *Drosophila* would allow for the continued study of neurodegenerative and neurodevelopmental mechanisms such as interaction with Rab GTPases.

The following chapters detail the role of scat in the neurodevelopment of larval motor neurons and the age progressive neurodegeneration of adult motor neurons. Unique mechanistic interactions with scat and small GTPases Rab7 and Rab11 are also described, each associated with distinct timepoints in the *Drosophila* lifecycle.

CHAPTER 2: REGULATION OF *DROSOPHILA* NEURODEVELOPMENT BY SCAT

Introduction

The fruit fly has long been used to study neuromuscular function and development because of the genetic tools available for manipulation and isolated expression of variable alleles. Its relatively simple nervous system mirrors the neural circuitry found in more complex mammalian systems, such as our own, which contains motor neurons with elaborate NMJ morphology, multinucleate muscle cells, and sensory neurons. The fundamental mechanisms of neuromuscular processes such as action potential propagation, generation and contractile coupling with myocytes at the NMJ are well conserved between mammals and *Drosophila*. In the past several decades it has been shown that nearly 75% of all genes involved in human disease have *Drosophil*a orthologs [242]. These traits in addition to numerous behavioral motor functions, allows for an in depth study of neurodegenerative phenotypes associated with gene specific disease mutations [243].

Endocytic trafficking is critical for maintenance of neuronal cellular homeostasis [244]. Disruption of endocytic trafficking components have been shown to cause neurodevelopmental defects and neurodegeneration [245]. Loss of function of the GARP complex components results in defects in retrograde vesicular transport and some disruption of anterograde transport of transmembrane proteins [209, 210, 213, 216, 246].

Loss of GARP complex function has also been associated with lysosomal dysfunction [209, 246].

Specifically, in mice, loss-of-function of core subunit Vps54, and thus loss of function of the overall GARP complex, causes underdevelopment of cardiac muscle tissue and motor neurons leading to embryonic lethality [217, 218]. In order to better understand the role of Vps54 in motor neuron development we examined how loss of scat, the *Drosophila* Vps54 ortholog, affects larval motor neurons. Unlike in mice, depletion of scat in *Drosophila* does not cause embryonic lethality in all individuals [230]. This allows for examination of larval NMJs to determine specifically how GARP complex disruption leads to motor neuron dysfunction and the mechanistic interaction with additional endocytic trafficking components.

The data presented in figures 1-10 comes directly from our previously published work [247]. Data in this paper was provided by Prajal Patel, Malea McGimsey, Emily Starke, and I, specific contributions are indicated in the corresponding figure descriptions. If a contribution is not specified, the work was my own.

Results and Discussion

Neuromuscular junction axon terminal growth requires scat

To determine if scat has any function in motor neurons, we examined the morphology of neuromuscular junctions in developing third instar larvae. In fly homozygotes expressing the classic $scat^{1}$ allele, protein expression is completely disrupted in the testes suggesting that they are scat null [230]. The $scat^{1}$ allele has a P-element

insertion close to the 5' end of the second exon of the *scat* gene, rending any product of translation non-functioning (Fig. 1A) [235]. We confirmed that expression of scat is disrupted in the CNS of $scat^{1}$ mutant larva by quantitative real-time PCR (qPCR) (Fig. 1B).

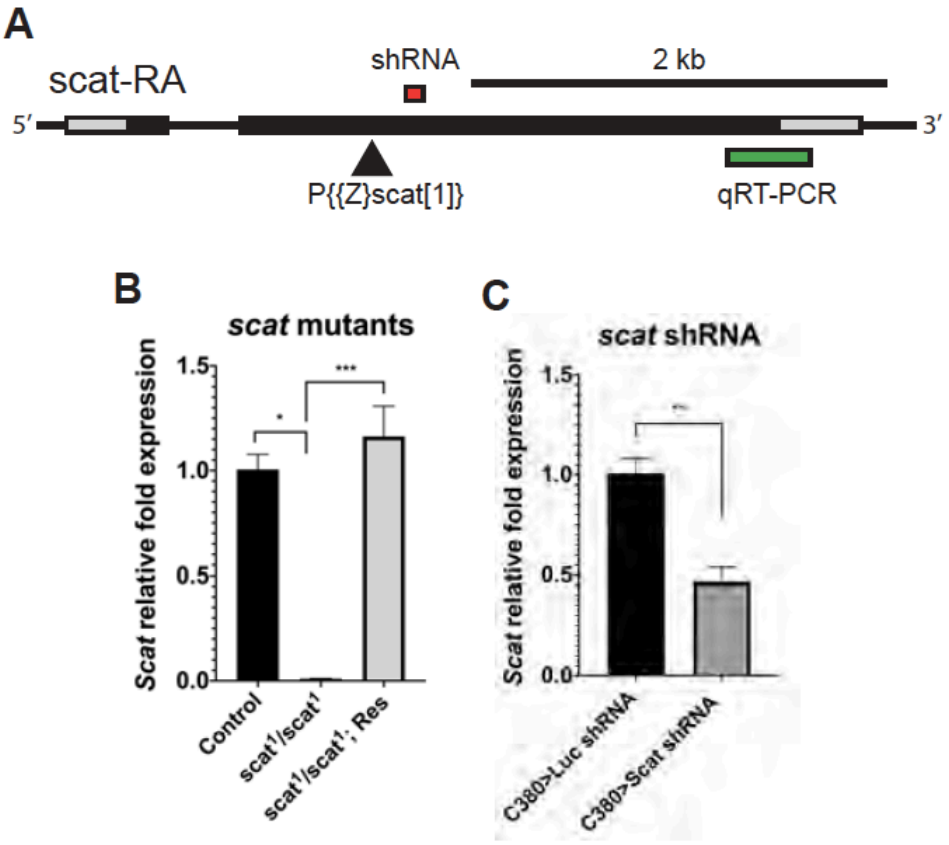

Figure 1. The *scat*^{1} allele (A) Provided by Scott Barbee. This is a diagram showing the structure of the *scat* gene in *Drosophila*. Exons are indicated by boxes and the single intron indicated by a line. Gray boxes at the 3' and 5' ends indicate the untranslated regions (UTRs) and black boxes indicate coding sequence. The triangle shows the location of the P-element insertion in the second exon of the *scat* locus. Using an antibody targeting the N-terminal 200 amino acids of the scat protein, it has previously been shown that this is a null allele (Fari et al., 2016). The region targeted by the *UAS-TRiP(HMS01910)* shRNA line is indicated by the red box. The green box at the 3' end indicates the location of the amplicon analyzed for qRT-PCR. (B) Provided by Emily Starke. Results of qRT-PCR analysis of *scat* mRNA levels in the larval CNS of controls, *scat*^{1} homozygotes, and the *scat*^{1}/*scat*^{1}; *scat-HA:scat/scat-HA:scat* rescue (Res) lines. *scat* mRNA is reduced in *scat*^{1} homozygotes and restored to near control levels in the rescue line. (C) Provided by Emily Starke. Results of qRT-PCR analysis of *scat* mRNA levels in control *(C380>Luc shRNA*) and *scat* (*C380>scat shRNA*) larval ventral ganglia. Levels of *scat* mRNA are reduced by at least 50%. Note that this is likely an underrepresentation because *C380-Gal4* drives expression in only a subset of neurons in the ventral ganglion. In both B and C, levels of *scat* transcripts were determined as described in the Methods and then normalized to the control. N = 7 ventral ganglia for each genotype. qPCR datum shown in B was analyzed by one-way ANOVA followed by a Holm-Sidak multiple comparison test. qPCR datum shown in C was analyzed by a two-way Student's t-test. Data are represented as the mean ± SEM for three technical replicates. * $p < 0.05$, ** $p < 0.01$, *** $p < 0.001$.

We found that *scat*^{1} mutants have a synaptic overgrowth morphology in the NMJ with an overelaboration of synaptic boutons, 114% relative to that of controls (Fig 2A-B). Quantification of synaptic arbor branch points correlated strongly with the number of synaptic boutons (Fig. 2C). A similar morphology was observed when the *scat*^{1} allele was put in *trans* to the overlapping *Df(2L)Exel8022* deficiency (Fig 2A-B). We then created a *scat-HA:scat* rescue line with the introduction of a transgene into the *scat*^{1} background. The rescue transgene contains a minimal *scat* promoter and ~350 bp of upstream genomic DNA that controls the expression of hemagglutinin (HA)-tagged *scat* cDNA restoring scat expression in larval CNS (Fig 1B). The *scat*^{1} synaptic overgrowth phenotype was rescued in *scat-HA:scat* larvae (Fig 2A-C). This data shows that scat has a role in the control of NMJ axon terminal growth during larval development.

The differences in NMJ phenotypes also manifest in bouton morphology. The NMJ at muscle 6/7 has two distinct types of synaptic boutons, type 1b (big) and type 1s (small). The different types of boutons are derived from distinct motor neurons and differ in physiology and morphology [248]. Postsynaptic densities in 1b boutons usually have stronger signal than that of 1s boutons when immunostained by Discs large (Dlg). Dlg is the fly ortholog of postsynaptic density protein, PSD-95 [249]. We show that Dlg staining in *scat*^{1} homozygotes is spotty and discontinuous in both 1b and 1s boutons. Additionally, we see a reduction in size of both types of boutons and all boutons have roughly the same intensity of staining, contrary to what is seen in controls (Fig. 2D). Quantification of synaptic area revealed a significant 2-fold decrease in *scat*^{1} homozygotes and an increase in total synaptic length. Bouton morphology and synaptic length phenotypes seen in the

scat^{1} mutants were rescued in *scat-HA:scat* larvae (Fig. 2E-F). Interestingly, a reduction of bouton size was not seen in *scat*^{1}*/Df* larvae (Fig. 2E). However, the deletion that causes the deficiency may include neighboring genes, about 60 kb of flanking sequence is included in the deletion. We speculate that there may be an uncharacterized effect by the heterozygosity of one or more of the neighboring loci, and thus we do not see the same reduction in bouton size.

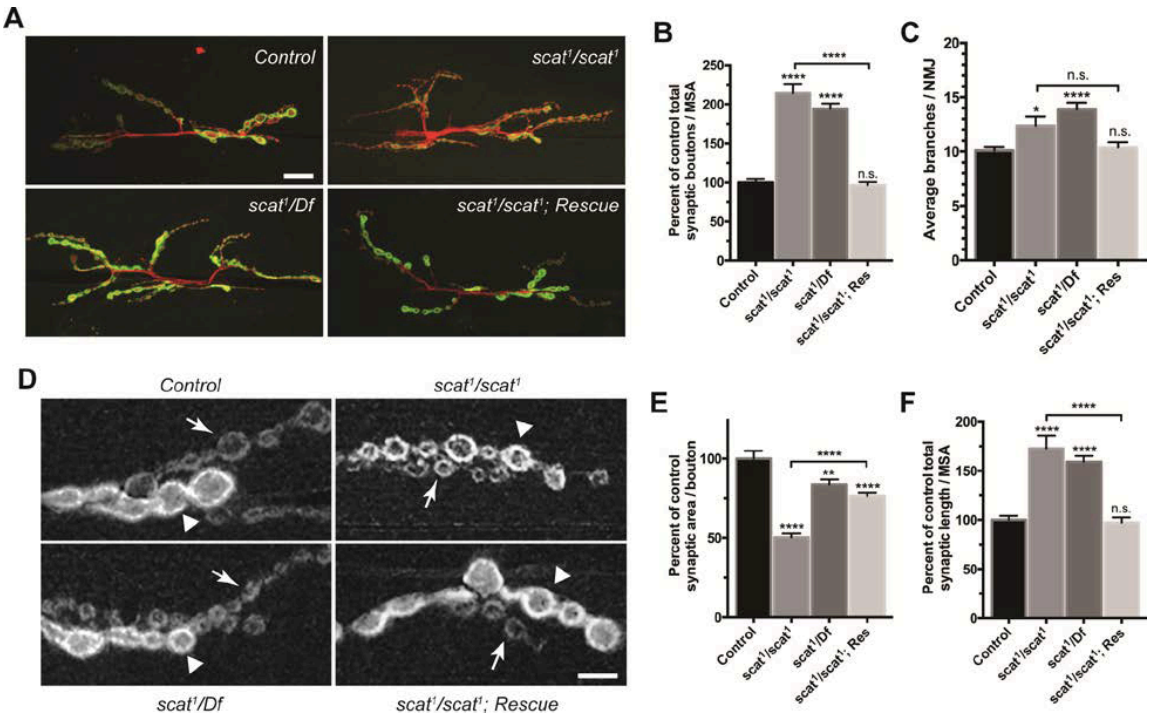

Figure 2. scat is a negative regulator of synaptic development at the larval NMJ. Provided by Prajal Patel. (A) scat loss-of-function causes defects in NMJ structure. Wandering third instar larvae from controls, *scat*^{1} homozygotes, *scat*^{1}*/Df(2L)Exel8022*, and the *scat*^{1}*/scat*^{1}*; scat-HA:scat/scat-HA:scat* rescue (Res) lines were stained with antibodies targeting the postsynaptic density marker, Dlg (green) and the neuronal membrane marker, Hrp (red). Images show maximum Z-projections. The NMJs innervating body wall muscles 6/7 in abdominal segment 3 (m6/7 in A3) were analyzed. *scat* mutants have an increased number of boutons and synaptic arbors in comparison to controls. Scale bar, 20 μm. (B) Total bouton number/MSA (normalized to control) and (C) synapse branch points are significantly increased in *scat* mutants. Both were quantified by counting manually and both phenotypes are rescued by the introduction of the *scat-HA:scat* transgenic construct. N = 23, 21, 24, and 25. (D) scat loss-of-function causes defects in the size of both type 1b (arrowhead) and 1s boutons (arrows). Wandering third instar larvae from controls, *scat*^{1} homozygotes, *scat*^{1}*/Df(2L)Exel8022*, and the *scat*^{1}*/scat*^{1}; *scat-HA:scat/scat- HA:scat* rescue lines were stained with an antibody targeting Dlg. Images shown are single focal planes through the equator of the type 1b boutons. *scat*^{1} homozygotes have noticeably smaller boutons than controls. The NMJs innervating muscle 6/7 in body segment A3 were analyzed. Scale bar, 5 μm. (E) Total synaptic length/MSA (normalized to control) is significantly increased and (F) synaptic area per bouton is decreased in *scat*^{1} homozygotes. Both features were quantified using the Morphometrics algorithm. N = 23, 19, 24, and 25. Data are represented as the mean ± SEM. All statistical analysis was done by Kruskal-Wallis followed by a Dunn's multiple comparison test. Unless otherwise indicated, all comparisons have been made to the control. * $p < 0.05$, ** $p < 0.01$, **** $p < 0.0001$.

Function of scat in motor neuron and muscles is required for NMJ development

Due to the NMJ morphology we observed in *scat*^{1} mutants we wanted to determine where in the synapse scat function plays a role. Because of the motor neuron degeneration seen in the wobbler mouse we predicted that scat would play a presynaptic role. To test this, we targeted the knockdown (KD) of *scat* expression in motor neurons using a transgenic short hairpin RNA (shRNA) driven by a motor neuron specific driver, *C380-Gal4* (Fig. 1A). This *scat* KD reduces mRNA levels of *scat* in the larval CNS by around 50% (Fig. 1C). Similar to the *scat*^{1} mutant, we saw a highly significant increase in the number of boutons in the presynaptic KD larvae as well as an increase in the number of synaptic arbor branches. To recapitulate these findings, we observed NMJ morphology in larvae expressing the same *scat* shRNA driven by a second, weaker, motor neuron driver *D42-Gal4*. We observed similar NMJ morphology with an increase in the number of synaptic boutons in our second motor neuron-specific test (Fig. 3A-B). To determine if scat function is restricted to the motor neuron, we examined the larval NMJ in muscle-specific *scat* KD. We expressed the *scat* shRNA transgene driven by the muscle-specific driver *24B-Gal4*. Postsynaptic KD in the muscle resulted in a small, but significant, increase in bouton number relative to controls (Fig. 3A-B). Presynaptic KD of *scat* shows a significant reduction in the size of boutons when driven by both *C380-Gal4* and *D42-Gal4* with a 58% and 41% reduction respectively (Fig. 3E). There is also a modest, but significant, 27% increase of NMJ length observed in *C380-Gal4* driven KD. In motor neuron *scat* KD we also see a partial disruption of normal Dlg expression and localization of postsynaptic densities, similar to what is seen in *scat*^{1} mutants (Fig. 3F). We also observed that

disruption of scat in the muscle shows a significant decrease in average bouton size (21%) and increase in NMJ length (28%) (Fig. 3E). Together, these data suggest that scat function controls NMJ development in presynaptic and postsynaptic compartments controlling bouton morphology.

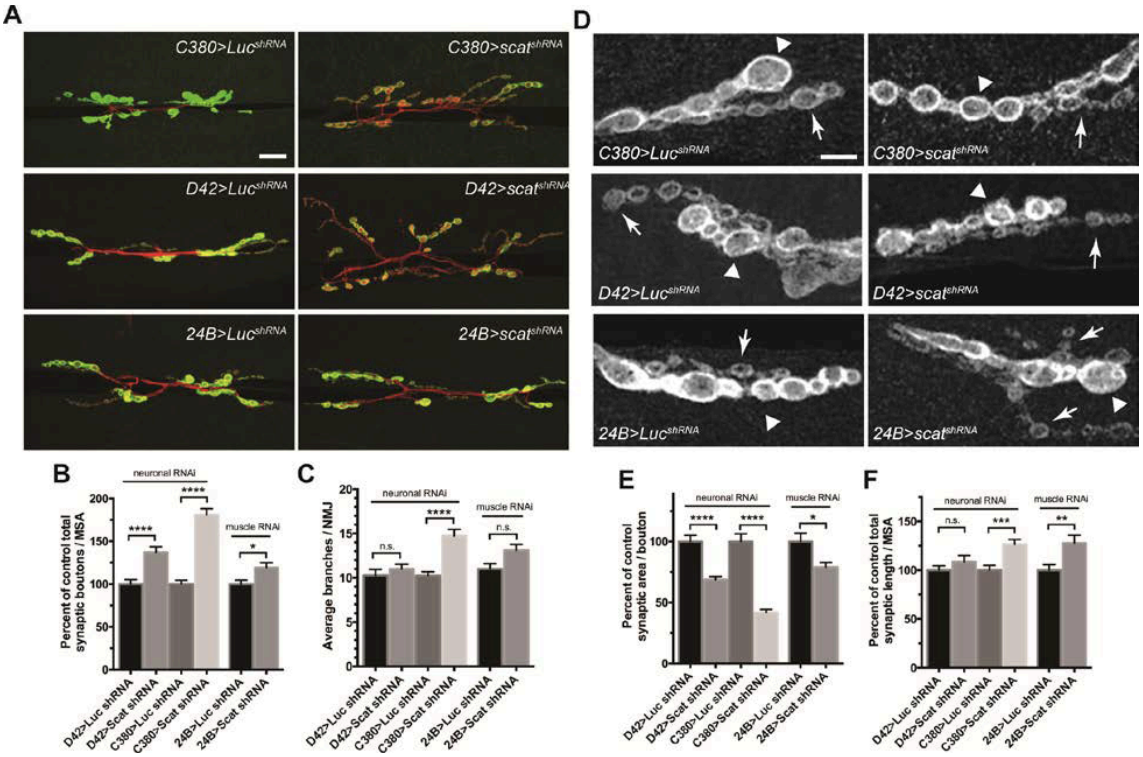

Figure 3. scat has a presynaptic function in the control of NMJ development. Provided by Prajal Patel. (A) Knockdown of *scat* expression in the presynaptic motor neuron by RNAi causes defects in NMJ structure. An inducible transgenic shRNA targeting *luciferase* (*UAS-LUC.VALIUM10*) or *scat* (*UAS-TRiPHMS01910*) was expressed in motor neuron using the *C380-Gal4* or the weaker *D42-Gal4* driver or in muscle using *24B-Gal4*. NMJs at muscle 6/7 in body segment A3 in late third instar larvae were stained with antibodies targeting Dlg (green) and Hrp (red). Images show maximum Z-projections. Presynaptic knockdown of *scat* causes an increased number of boutons and synaptic arbors. Scale bar, 20 μm. (B) As in *scat* mutants, the total bouton number/MSA (normalized to the respective control) and (C) synapse branch points are significantly increased by presynaptic *scat* knockdown. N = 18, 18, 17, 18, 20 and 25. (D) Presynaptic *scat* knockdown causes defects in the size of type 1b (arrowhead) and 1s boutons (arrows). Wandering third instar larvae from genotypes indicated in A were stained with an antibody targeting Dlg. Images show single focal planes through the equator of type 1b boutons. Presynaptic *scat* knockdown causes a reduction in the size of type 1 boutons. Scale bar, 5 μm. (E) As in *scat* mutants, total synaptic area per bouton/MSA (normalized to control) is significantly decreased and (F) length is increased by presynaptic *scat* knockdown. Effects are statistically significant but not as dramatic following *scat* RNAi in the postsynaptic muscle. Both features were quantified using the Morphometrics algorithm. N = 18, 17, 17, 18, 20, and 19. All statistical comparisons shown have been compared to driver-specific controls (driver/+ heterozygotes) using a two-tailed Mann-Whitney U test. Data represented as the mean ± SEM. * $p < 0.05$, ** $p < 0.01$, *** $p < 0.001$, **** $p < 0.0001$.

Because of the significant effects on NMJ morphology we observed in *scat*^{1} mutants and *scat* KD larvae, we asked if *scat* overexpression has any impacts on NMJ development. To test this, we constructed transgenic fly lines with global overexpression and pan-neuronal overexpression of *HA:scat*. The global overexpression line was made by crossing a Gal4-inducible version of HA-tagged *scat* cDNA (*UAS-HA:scat*) line with a *tubulin-Gal4* line (*tub-Gal4>UAS-HA:scat*). Global overexpression of *scat* did not show any significant impact on NMJ development (Fig. 4A-G). The fly line with pan-neuronal overexpression of scat was made using the same *UAS-HA:scat* driven by a strong pan-neuronal driver *elav-Gal4*. We observed a minor, but significant (p=0.0159), increase in NMJ branching and a 21% increase in synaptic bouton area. In larvae overexpressing *scat* in the muscle (*Mef2-Gal4>UAS-HA:scat*) we also observed a significant increase in synaptic bouton number by 25% and number of synaptic branches (Fig. 4B-F). There were no observed changes in bouton morphology (Fig. 4A). These data taken together indicate that development of the larval NMJ is affected by both loss- and gain-of-function of scat.

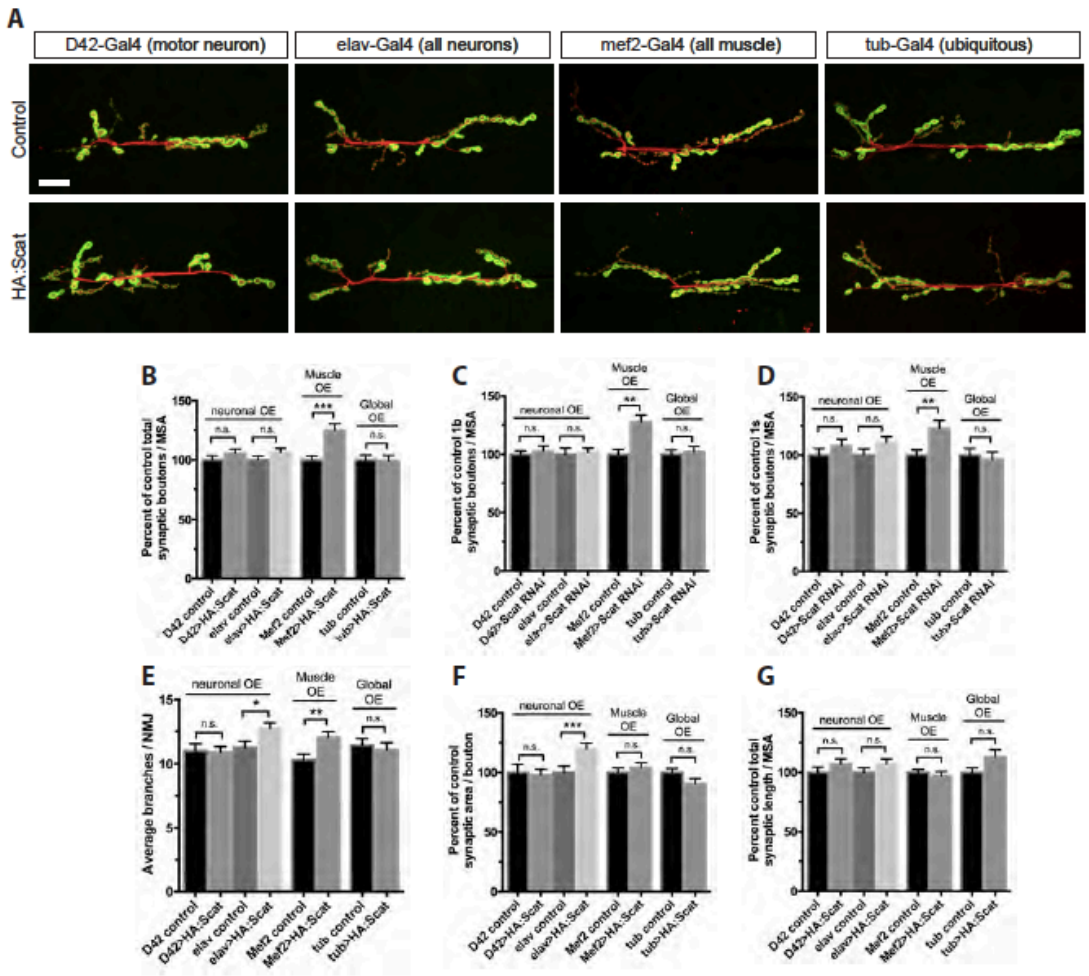

Figure 4. Overexpression of scat has an effect on NMJ development. Provided by Prajal Patel. (A) The inducible *UAS-HA:scat* transgene was expressed using a motor neuron-specific driver (*D42-Gal4*), a strong panneuronal driver (*elav-Gal4*), a strong muscle-specific driver (*Mef2-Gal4*), or ubiquitously (*tubulin- Gal4*). NMJs at m6/7 in body segment A3 have been stained with antibodies targeting Dlg (green) and Hrp (red). Images show maximum Z-projections. Scale bar, 20 μm. Quantification of the (B) total number of boutons, (C) type 1b boutons, and (D) type 1s boutons shows that bouton number is increased when *HA:scat* is overexpressed in larval muscle but not when expressed ubiquitously or in neurons. (E) The number of branches is significantly increased when *HA:scat* is strongly expressed in either neurons or muscle. For B-E, N = 22, 23, 19, 24, 30, 30, 23, and 23 in the order shown in graphs. (F) Total synaptic area is increased when strongly expressed in muscle. (G) There is no impact on total synaptic length. Synaptic area and length where quantified using the Morphometrics algorithm. For F and G, N = 22, 23, 19, 24, 28, 30, 24, and 27 in the order shown in graphs. All statistical analysis was done by Kruskal-Wallis followed by a Dunn's multiple comparison test. Unless otherwise indicated, all statistical comparisons shown have been compared to driver-specific controls (driver/+ heterozygotes). * $p < 0.05$, ** $p < 0.01$, *** $p < 0.001$.

Localization of scat in the larval neuromuscular system

In yeast and mouse spermatids Vps54 has been shown to primarily localize to the TGN [213, 250]. In *Drosophila* expressing fluorescently tagged scat, a similar pattern of localization to the TGN has been seen in the testes [230]. Based on these previous findings, we predicted that in larval motor neurons and muscle cells scat would localize primarily to the TGN. In our hands, the only antibody available that targets scat, did not work in immunostaining neurons. Therefore, to examine the subcellular localization of scat, we drove global expression of the Gal4-inducable *UAS-HA:scat* protein with *tubulin-Gal4* , allowing us to observe immunofluorescence by targeting HA. First, we counterstained tissue with anti-HA antibody and an antibody that recognized the golgin Lava lamp (Lva), a marker for the *cis*-Golgi in *Drosophila* [251]. We found that Lva was juxtaposed to a majority of overexpressed HA:scat protein in the ensheathing glial cells surrounding peripheral nerves (Fig. 5B), the soma of larval motor neurons (Fig. 5A), and the larval muscle body wall (Fig. 5C). HA:scat and Lva were found to be absent for the axons of motor neuron and presynaptic boutons (Fig. 5B-C). The localization of HA:scat in close proximity to the *cis*-Golgi suggests that scat localizes to the TGN of neurons and muscle cells, consistent with previous findings.

Because of the obvious presynaptic role scat plays in the development of larval NMJs, we wanted to further characterize the subcellular localization of scat with known components of the endocytic trafficking pathway. We started by counterstaining HA:scat with an antibody targeting *Drosophila* Syntaxin-16 (dStx16). Syntaxin-16 is a core

component of the t-SNARE complex involved in retrograde transport of endosome-derived vesicles to the TGN [210, 252].

In mammalian cells the N-terminus of Vps54 interacts with t-SNAREs, but there is evidence suggesting that both Vps53 and Vps54 are required to form a functional SNARE binding site. The coiled-coil SNARE motif and possibly the Habc domain are the domains found on t-SNAREs that interact with the GARP complex. It has been observed that t-SNAREs, specifically syntaxin-6, syntaxin-16, and Vamp4 colocalized with Vps54 at the TGN suggesting that GARP and t-SNARE interaction occurs at the TGN [209]. As expected, we found HA:scat to strongly colocalize with foci containing dStx16 in motor neuron cell bodies (Fig. 5D-G; Pearson's correlation coefficient = 0.55±0.02), further supporting our claim that scat localizes to the TGN. Vps54 has also been shown to localize to early endosomes in yeast via a conserved C-terminal domain that is required for retrograde transport of early endosomes to the TGN [210].

Next, we used small GTPases Rab5, Rab7, and Rab11 as markers for early endosomes, late endosomes and recycling endosomes, respectively, in order to determine localization of HA:scat in differing compartments of the endosomal trafficking pathway. In contrast to dStx16 we found colocalization of HA:scat with Rab5, Rab7 and Rab11 to be remarkably low (Fig. 5H-S; Pearson's correlation coefficient =0.15±0.01, 0.22±0.04, 0.178±0.02 respectively). However, we did sometimes observe HA:scat to localize to a structure immediately adjacent to Rab5-positive early endosomes (Fig. 5K). Although we cannot rule out that these findings may be due to the high-density of Rab5-positive early endosomes in larval motor neurons, we did not observe similar results with Rab7 or Rab11

positive foci, which have similar numbers (Fig. 5O and S). These results together suggest that majority of scat localize to the TGN, but a possible interaction with Rab5 positive early endosomes may also occur (Fig. 5K).

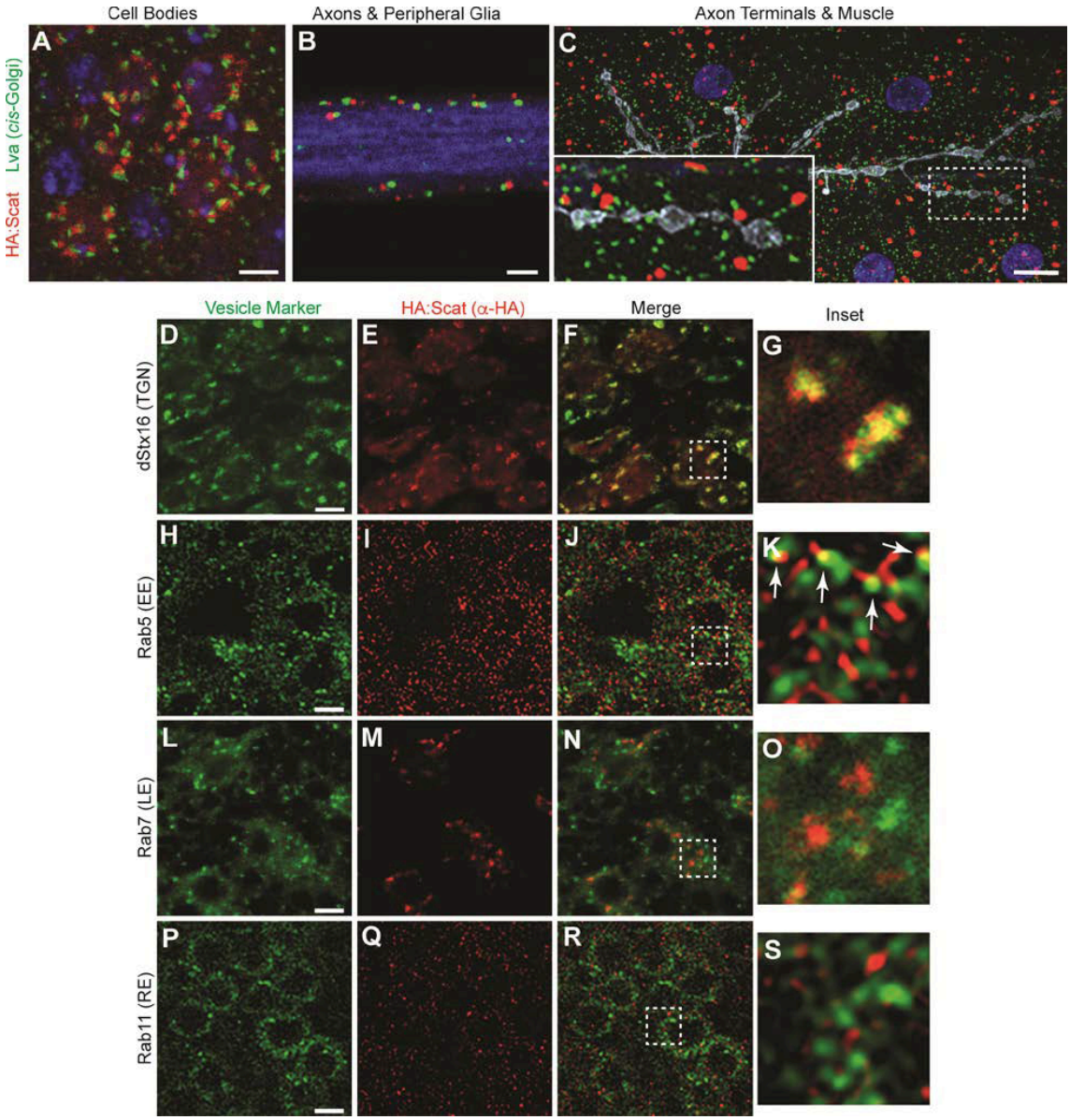

Figure 5. scat localizes to the TGN in MN cell bodies. (A-C provided by Prajal Patel) scat localizes to a structure adjacent to the *cis*-Golgi in (A) motor neuron cell bodies, (B) peripheral glia, and (C) body wall muscle. (A-B) Ventral ganglia and (C) body wall muscle preps from wandering third instar larvae expressing inducible *HA:scat* under control of the *tubulin-Gal4* driver were stained with antibodies targeting the HA tag (red) and the *cis*-Golgi marker, Lva (green). Single focal planes are shown in A and B while C is a maximum Z-projection. HA:scat localizes to the motor neuron cell body but not peripheral axons or axon terminals. Most HA-positive structures are adjacent to the Lva-positive *cis*-Golgi. Blue is DAPI (DNA) in A and C and Hrp (axon) in B. Grey in C is Hrp (axon). Scale bars are 2.5 μm in A and 10 μm in B and C. (D-S) *tub-Gal4>HA:scat* animals were counterstained with antibodies targeting the HA tag (red) and the indicated marker (green). Images shown are single focal planes through MN cell bodies in the larval ventral ganglion. Vesicle trafficking markers shown are the TGN marker, Syntaxin 16 (D-G provided by Malea McGimsey), the early endosome marker, Rab5 (H-K), the late endosome marker, Rab7 (L-O provided by Malea

McGimsey), and the recycling endosome marker, Rab11 (P-S). Larvae showing the colocalization of HA:scat with Rab5 and Rab11 were fixed with Bouin's reagent which provided much better signal to noise. Larvae showing HA:scat with dStx16 and Rab7 were fixed with paraformaldehyde. The boxed areas indicated in the merged images (F, J, N, and R) are shown in G, K, O, and S (respectively). The arrows shown in K are indicating localization of HA:scat in spots immediately adjacent to Rab5. Scale bars in D, H, L, and P are 2.5 μm.

Effects of scat mutants on endocytic trafficking pathway components in motor neurons

It is important during synaptic development that membranes and receptor proteins be regulated. It is believed that the bi-directional transfer of such endosomal cargos plays an important role in regulation of neuronal homeostasis [253]. In response to the synaptic overgrowth phenotype seen in *scat* mutant NMJs, we postulated that components of the endocytic trafficking pathway might be impacted by loss-of-function of scat thus causing malfunction in endosome transport. It has been shown that GARP complex function is required to tether vesicles derived from early and late endosomes to the TGN in yeast and mammalian cells [254, 255]. This is done, in part, by controlling the assembly of the t-SNARE complex [209]. Because of this, we wanted to determine if t-SNARE component, dStx16, localization was disrupted in scat loss-of-function or reduction-of-function mutant motor neurons. As predicted, immunofluorescent staining of dStx16 was observed to be more diffuse in $scat^{1}$ mutant larval motor neurons. This phenotype was rescued by the introduction of the *scat-HA:scat* transgene into the $scat^{1}$ background. The results observed in larvae with motor neuron specific shRNA KD of *scat* were similar to those seen in $scat^{1}$ mutants (Fig. 6A). These data indicate that scat has a contributing role in the localization of dStx16 to membrane at the TGN. Thus, suggesting that an integral component of the retrograde trafficking pathway is partially disrupted by the loss of function of scat. However, some punctate dStx16 is still observed in the motor neurons of *scat* mutants and motor neuron specific *scat* KD (Fig. 6A). It could be speculated that only partial disruption of dStx16 could represent a real functional difference between scat and mammalian Vps54,

as complete loss of function in mammals leads to embryonic lethality but is only semi-lethal in flies [217, 235].

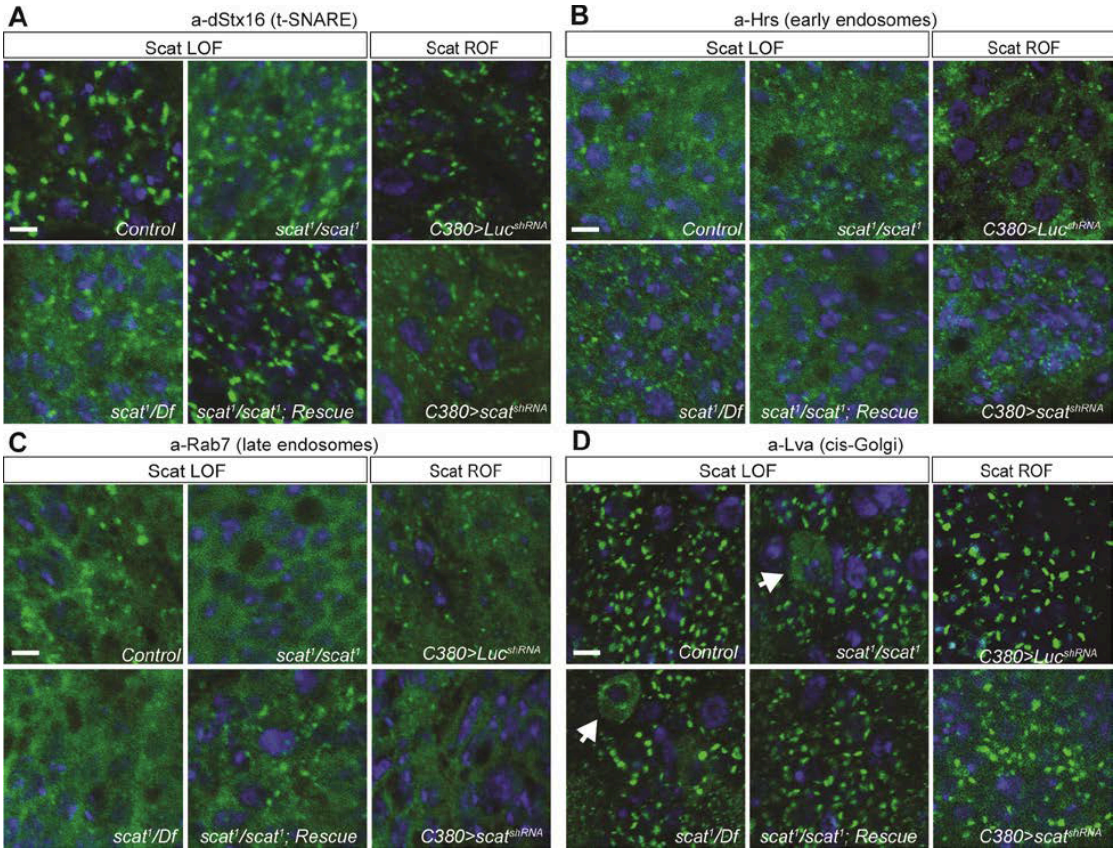

Figure 6. *scat* mutant MNs have defects in Syntaxin-16 localization and *cis*-Golgi integrity. (A) Provided by Malea McGimsey, localization of Syntaxin-16 to the TGN is disrupted in *scat*^{1} mutants. Images shown are single focal planes. Ventral ganglia from wandering third instar larvae from controls, *scat*^{1} homozygotes, *scat*^{1}*/Df(2L)Exel8022*, and the *scat*^{1}*/scat*^{1}*; scat-HA:scat/scat-HA:scat* rescue lines were stained with an antibody targeting (A) dStx16 (green) and DAPI to visualize nuclei (blue). dStx16 staining is significantly more diffuse (but still clearly punctate) in *scat*^{1} mutants compared to controls. The *scat*^{1} mutant phenotype is rescued by the introduction of the *scat-HA:scat* transgene. Similar results were observed *in C380>scat shRNA* MNs. (B) Provided by Malea McGimsey, EEs are not affected in *scat*^{1} mutants. The indicated genotypes were stained with an antibody targeting the EE- and multivesicular body-associated protein, Hrs (green) and DAPI (blue). (C) Provided by Malea McGimsey, LEs are not affected in *scat* mutants. The indicated genotypes have been stained with an antibody targeting Rab7 (green) and DAPI (blue). (D) Provided by Malea McGimsey and Prajal Patel, localization of the *cis*-Golgi marker, Lva is partially disrupted in the cell body of some *scat* mutant and motor neurons (arrows). The indicated genotypes have been stained with an antibody targeting Lva (green) and DAPI (blue). This phenotype is never observed in control or rescue larvae. More global effects are observed in *C380>scat shRNA* MNs. Scale bar, 2.5 μm.

In the wobbler mouse motor neuron, there appears to be an accumulation of large Rab7-positive late endosomes [256]. In yeast, disruption of *Vps54* causes the accumulation of vesicles containing early endosome markers [210]. As such, we were interested in determining if scat loss of function in *Drosophila* showed any impact on endosomal pools within motor neurons. To test this, we examined the localization of endosomes targeted with antibodies against Hrs and Rab7, marking early and late endosomes respectively [257]. Interestingly, we observed no effect on endosome size or number of either marked endosome type in $scat^{1}$ mutant larval motor neurons (Fig. 6B-C). Hrs is traditionally used as a marker of multi-vesicular bodies, not necessarily specific to early endosomes. As a result, we repeated this experiment again using a different set of antibodies targeting Rab5 positive early endosomes and Rab7 positive late endosomes [258]. This second set of staining showed similar negative results (Fig. 7). This datum suggests that disruption of scat does not have a significant impact on endosomal populations during this stage of development.

In cultured mammalian cells, Vps54 loss-of-function causes defects in vesicle trafficking pathways with no apparent impact on Golgi structure or function [218]. Conversely, Golgi fragmentation and dysfunction, associated with early stages of neurodegeneration, are observed in motor neurons of the wobbler mouse [256]. To determine if Golgi structure is affected by the disruption of scat function in *Drosophila* larvae, we stained motor neurons with antibodies targeting *cis*-Golgi market Lva. We found that in both $scat^{1}$ mutants and $scat^{1}/Df(2L)Exel8022$ larvae there were diffuse cytoplasmic fractions of Lva along with the typical Golgi localized fractions. This cytoplasmic fraction

was never observed in controls or transgenic rescue motor neurons (Fig. 6D). We speculate that partial disruption of *cis*-Golgi integrity may lead to an increase of Golgi associated markers being found in the cytoplasm. A similar phenotype was observed in larvae with motor neuron targeted depletion of scat, however, Lva staining was globally more diffuse and punctate structures remained more intact (Fig. 6D). Taken together, these data suggest that *scat* expression is involved in maintaining Golgi integrity in larval motor neurons and that global Golgi defects may be responsible for the partial disruption of dStx16. In both yeast and humans, Stx16 interacts with GARP and EARP subunit Vps51, showing Golgi dysfunction in both cases, and other trafficking defects in humans [259, 260]. Similarly, depletion of *fat free*, the zebrafish ortholog of *Vps51*, shows disruption of Golgi structural morphology and endosomal trafficking in intestinal cells [261]. This suggests that GARP and or EARP function is important in the control of Golgi structure. Previous work in the post-mitotic *Drosophila* spermatids of $scat^{1}$ mutants has shown mislocalization of a conserved golgin, Golgin245 [230].

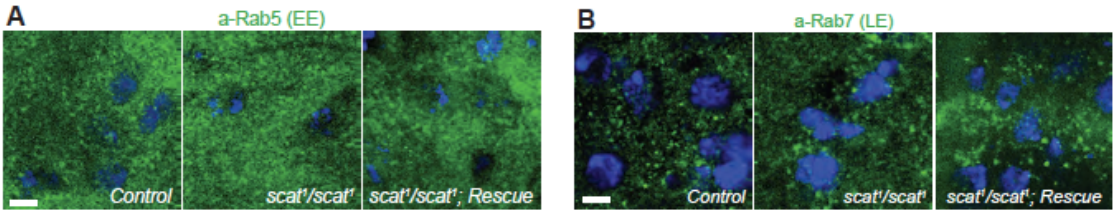

Figure 7. *scat* mutants do not have defects in Rab5- or Rab7-positive endosomes. Using polyclonal antibodies targeting Rab5 and Rab7 (Hirata et al., 2015), there is no visible defect in the size, number, or distribution of EE or LE in *scat*^{1} mutant MNs. Images shown are single focal planes. Ventral ganglia from wandering third instar larvae from controls, *scat*^{1} homozygotes, and the *scat*^{1}/*scat*^{1}; *scat-HA:scat/scat-HA:scat* rescue lines were stained with antibodies targeting (A) Rab5 or (B provided by Malea McGimsey) Rab7 (both green). Nuclei are marked by DAPI (blue). Scale bar, 2.5 μm.

Axon terminal growth is regulated by genetic interactions of scat and Rab proteins

Not only do Rab proteins associate with specific endosomal compartments, their activity is also required in the mediation of every step of membrane trafficking [262]. Rab's ability to bind to specific Rab effector proteins is determined by its state. GTPases switch between inactive GDP- and active GTP-bound forms [263]. We were interested in gaining insight into how mechanistically, disruption of scat leads to axon terminal overgrowth. To test this, we used transgenic *Drosophila* lines that contain Gal4-inducible Rabs along with our Gal4-inducible *scat* KD flies. The Gal4-inducible Rab lines caused overexpression of either wild type Rab proteins or GTP-binding defective Rab conferring dominant negative (DN) activity allowing for the cell autonomous disruption of Rab function [264]. We concurrently drove motor neuron specific expression of wild type or DN Rab5, Rab7, or Rab11 with our shRNA *scat* KD using the driver *C380-Gal4*. In our hands, we saw no effect on the number of type 1 synaptic boutons by expression of wild type or DN Rab5, Rab7, or Rab11 compared to controls (Fig. 8A-B). We speculated that if *scat* were genetically interacting with any Rab proteins, we would see an enhanced or suppressed synaptic overgrowth phenotype when wild type or DN Rabs were expressed in *scat* KD larvae respectively. Interestingly, we found that co-expression of either wild type or DN forms of Rab5, Rab7, and Rab11 all significantly suppressed the *scat* shRNA NMJ overgrowth phenotype. In most cases the NMJs from these larvae were indistinguishable morphologically from the negative controls (Fig. 8A). However, there were two exceptions that are worth note.

The first exception being that the co-expression of *scat* shRNA and wild type *Rab5* cause clustering of synaptic boutons at the ends of axon terminals compared to the normal linear alignment of boutons. This bouton clustering phenotype has been observed in several other instances of synaptic regulation. Mutations in the gene *spastin* cause bouton clustering defects that can be suppressed by loss of *kinase 3* [265]. CaMKII is a regulator of DLG synaptic localization. Hyperphosphorylation by constitutively active CaMKII mutant causes bouton clustering in the NMJ [266]. Mutations in the positive regulator of glutamate receptors, Kismet, are also found to cause bouton clustering [267].

Second, in animals expressing *DN Rab7* and *scat* shRNA we see a slight but appreciable disruption of postsynaptic Dlg staining (Fig. 8C). The disruption of Dlg staining in *DN Rab 7/scat* KD individuals resulted in a significant decrease in total bouton number compared to *C380>scat shRNA* (54%) and *C380>DN Rab7* (46%) controls (Fig. 8B). Overall, we observed disruption of both scat and Rab7 function in motor neurons to significantly reduce the complexity of larval NMJs. Together these data suggest that the normal regulation of NMJ development by *scat* requires the activity of Rab5, Rab7, and Rab11. The developmental defects seen in *DN Rab7/scat* KD larval NMJs are not unprecedented as similar synaptic defects have been observed to preclude neurodegeneration in ALS, AD, PD, and FTD fly models [268-270]. This said, neurological morphology during metamorphosis is not well understood and we cannot rule out that processes during this period may further impact motor neuron degeneration in our model.

Rab5, Rab7, and Rab11 all have well characterized trafficking functions involved in the control of axon growth and guidance [9, 244, 271, 272]. Rab5 and Rab7 are involved in the local retrograde transport of membrane proteins through the recycling pathway, while Rab11 is required for transport of membrane and transmembrane proteins to axon terminals [273, 274]. In *Drosophila*, loss of function of Rabs is linked with several distinct neuronal morphologies. In olfactory projection neurons and sensory neurons with a loss of function mutation in *rab5,* defects in axonal elongation were observed [275, 276]. When a *rab7* mutation linked to CMT was expressed in flies, defects in both axon growth and guidance were seen in sensory neurons [9]. Moreover, *rab11* mutant larvae have a characteristic increase of synaptic bouton number and show bouton clustering in defective NMJs similar to what we observe in *DN Rab 7/scat* KD mutants [274]. Taken together, it is clear that *scat* likely interacts with Rabs in the regulation of neuronal development.

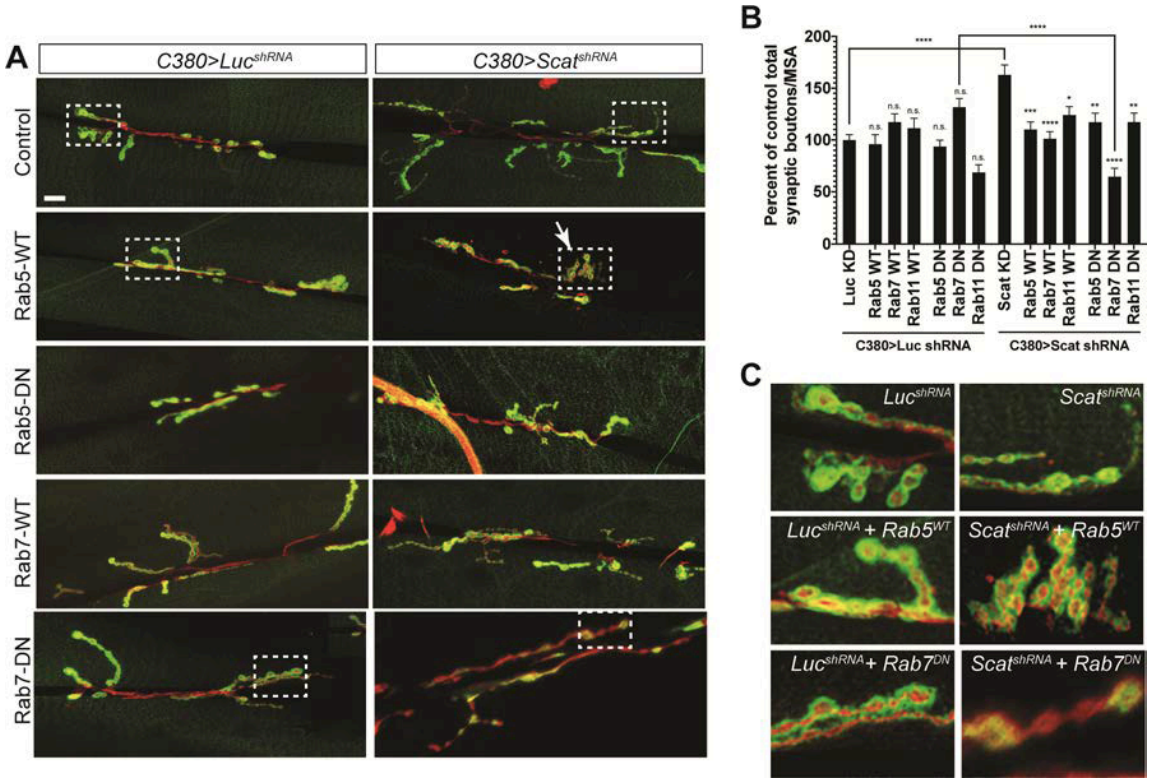

Figure 8. scat interacts genetically with Rab5, Rab7, and Rab11 to control NMJ development. (A) NMJ phenotypes caused by the motor neuron-specific knockdown of *scat* expression by RNAi are suppressed by overexpression of wild type and dominant-negative transgenes for Rab5, Rab7, and Rab11 (Rab11 images are not shown). An inducible transgenic shRNA targeting *luciferase* (*UAS-LUC.VALIUM10*) or *scat* (*UAS-TRiPHMS01910*) was expressed in motor neuron using the *C380-Gal4* driver in combination with an inducible YFP-tagged wild type or dominant negative Rab5, Rab7, or Rab11 (*UAS-YFP:Rab*). NMJs at muscle 6/7 in body segment A3 in wandering third instar larvae were stained with antibodies targeting Dlg (green) and Hrp (red). Images show maximum Z-projections. The boxed areas are blown up in C to show altered synaptic bouton or PSD morphologies. Scale bar, 20 μm. (B) As shown in Fig. 2, the total bouton number/MSA (normalized to the respective control) are significantly increased by presynaptic *scat* knockdown. This phenotype is suppressed by co-expression of wild type and dominant negative Rabs. *C380>scat shRNA, Rab7 (DN)* double mutant NMJs are significantly smaller. N = 18, 12, 16, 13, 22, 17, 21, 17, 18, 20, 20, 22, 21, and 23. (C) Boxed areas in A. Many *C380>scat shRNA, Rab5 (wild type)* NMJs have a clustered bouton phenotype similar to many endocytic mutants. Dlg staining and bouton morphology is significantly disrupted in *C380>scat shRNA, Rab7 (DN)* double mutants. Data are represented as the mean ± SEM. Unless otherwise indicated, all comparisons have been made to the control. Statistical analysis was done using a one-way ANOVA followed by a Holm-Sidak multiple comparison test. * $p < 0.05$, ** $p < 0.01$, *** $p < 0.001$. **** $p < 0.0001$

NMJ synaptic integrity is regulated by scat and Rab7 genetic interactions

There appears to be a partial disruption of postsynaptic Dlg staining in *scat*^{1} mutants and larvae with presynaptic KD of *scat* by RNAi (Fig 2D, 3D). We see a further exacerbated disruption of Dlg when both *scat* and *rab7* have been disrupted in motor neurons (Fig. 8C). In *Drosophila*, Dlg forms a multimeric scaffold that is required for the clustering of postsynaptic glutamate receptors (GluRs) at the NMJ. It has been shown that mutations in *dlg* have no effect on GluRs containing the subunit GluRIIA, however, the levels of subunit GluRIIB are significantly decreased by the same mutations [277]. Because of this, we asked if GluR localization to postsynaptic sites was altered following the disruption of both scat and Rab7 function. High resolution single focal plane images of NMJs confirmed that in *C380-Gal4>scat shRNA, DN Rab7* larvae Dlg staining was reduced and spotty in type 1b synapses when compared to controls (Fig. 9A). Similar to mutations in *dlg,* we found that in *C380-Gal4>scat shRNA* animals there was a slight reduction of GluRIIB, which was further disrupted in *C380-Gal4>scat shRNA, DN Rab7* larval NMJs (Fig. 9B). In contrast, there appeared to be no effect on GluRIIA localization in the same backgrounds (Fig. 9C) suggesting that the core GluR had not been lost from postsynaptic sites. We cannot rule out that GluRIIB staining at the NMJ is reduced because of a reduction in expression. However, these data suggest that scat is required in the presynaptic cell to regulate the localization of Dlg and GluRIIB via an unknown trans-synaptic mechanism involving Rab7 activity.

There is a growing body of evidence suggesting trans-synaptic regulation in fly NMJs. An example of presynaptic mechanisms affecting post synaptic density composition

can be seen in larvae with altered presynaptic phosphorylated Smad (pMad) regulating GluRIIA accumulation via a noncanonical BMP signaling pathway [278]. In this case, GluRIIA levels are also regulated by conserved Rab5 effector dMon1 via uncharacterized transsynaptic mechanisms [279-281]. It was proposed that release of dMon1 from boutons, much like other signaling molecules, may be responsible for its transsynaptic regulatory properties [282-284]. Although it is unclear what the transsynaptic mechanism is in our model, our work suggests an interesting signaling relationship across the synapse.

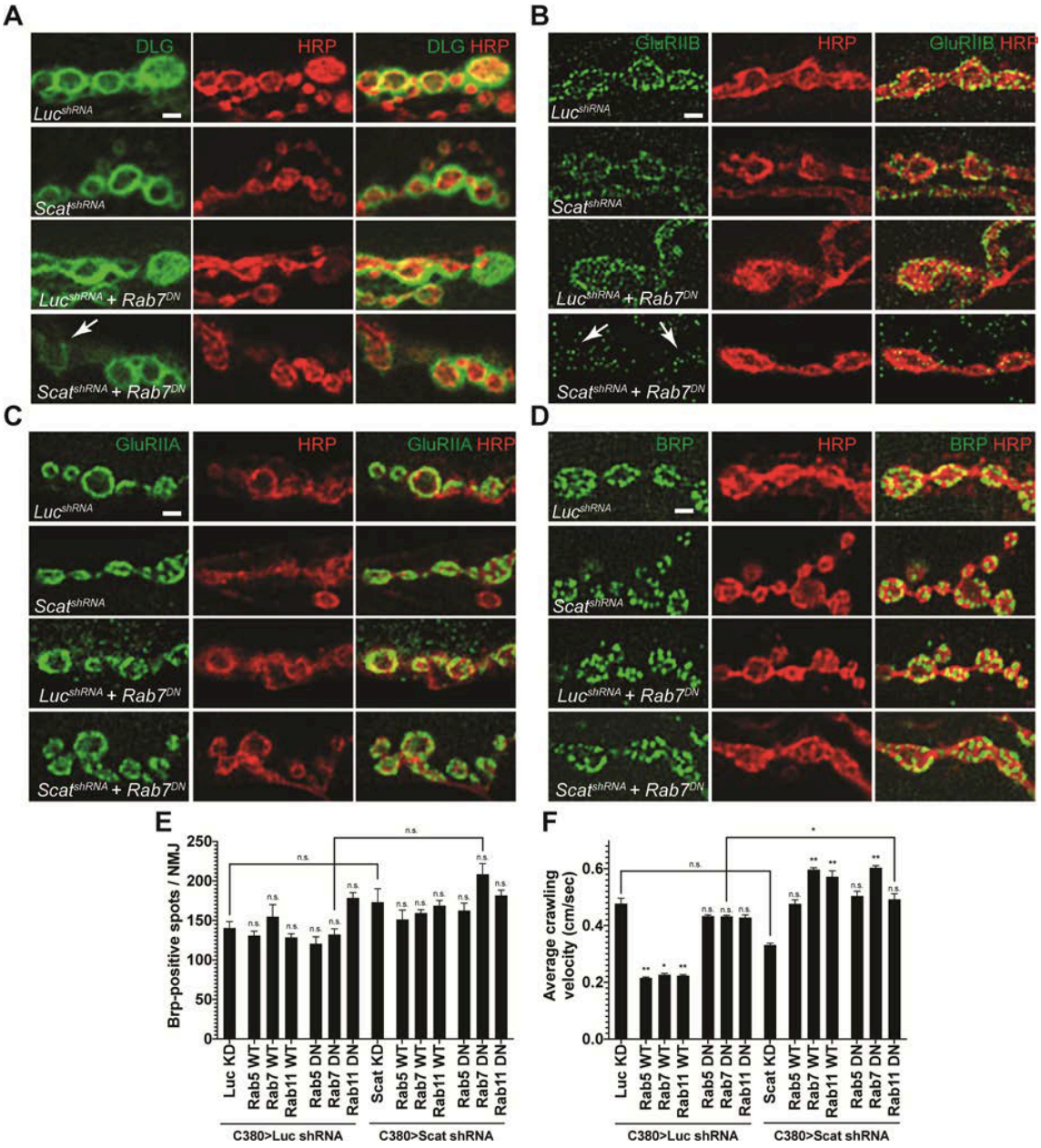

Figure 9. scat interacts genetically with Rab7 to control the composition of the PSD. Localization of the PSD proteins (A) Dlg, (B) GluRIIB, (C) GluRIIA, and the AZ marker (D) Brp to synaptic boutons at muscle 6/7 in body segment A3 in late third instar larvae are shown in green. All NMJs have been counterstained with an antibody targeting Hrp (red). Merged images are included to confirm pre- or post-synaptic localization. All images are single focal planes. Synaptic bouton structure has been better preserved here using Bouin's fixative. The arrow in (A) points to a type 1b bouton with abnormally low levels of Dlg and neighboring boutons have spotty Dlg staining. Arrows in (B) point to synaptic boutons where GluRIIB localization has been significantly disrupted (compare *scat* shRNA, Rab7DN to any of the control genotypes). Scale bar, 2.5 μm. (E) Quantification of the number of Brp-positive spots per NMJ. No significant difference was observed in any genotype (N = 5 each). Statistical analysis was done using a one-way ANOVA followed

by a Holm-Sidak multiple comparison test. (F) Average crawling velocity of third instar larvae for each genotype (N = 10 each). MN-specific overexpression of wild type Rab5, Rab7, and Rab11 alone significantly suppressed larval crawling velocity while overexpression of dominant negative Rabs had no effect. Overexpression of both wild type and dominant negative forms of all Rabs suppressed the *C380>scat shRNA* phenotype. Statistical analysis was done by Kruskal-Wallis followed by aDunn's multiple comparison test. * $p < 0.05$, ** $p < 0.01$.

In order to further explore the role of scat on NMJ synaptic architecture, we next asked if localization of the active zone regulating protein, Bruchpilot (Brp), was affected by scat dysfunction. Brp is required to regulate active zone structure and function at the synapse. It is similar to the human ELKS/CAST family of proteins [285]. In *Drosophila* larvae, Brp localizes to presynaptic active zones of the NMJ. Lack of Brp causes defects in Ca^{2+} channel clustering, vesicle release, and active zone assembly [286]. In all *C380-Gal4>scat shRNA* genotypes tested, we observed no significant difference in the total number of Brp puncta per NMJ compared to controls (Fig. 9D-E). Similar results were seen in $scat^{1}$ mutant larvae when compared to transgenic rescues *scat-HA:scat*. We did observe a significant decrease in the number of active zones per synaptic bouton, which was partially rescued in *scat-HA:scat* larval NMJs (Fig. 10). However, this result may be due to the increased number of overall boutons seen in the mutant NMJs. Taken together, these results suggest that there is no disruption in overall presynaptic active zone localization by disruption of scat.

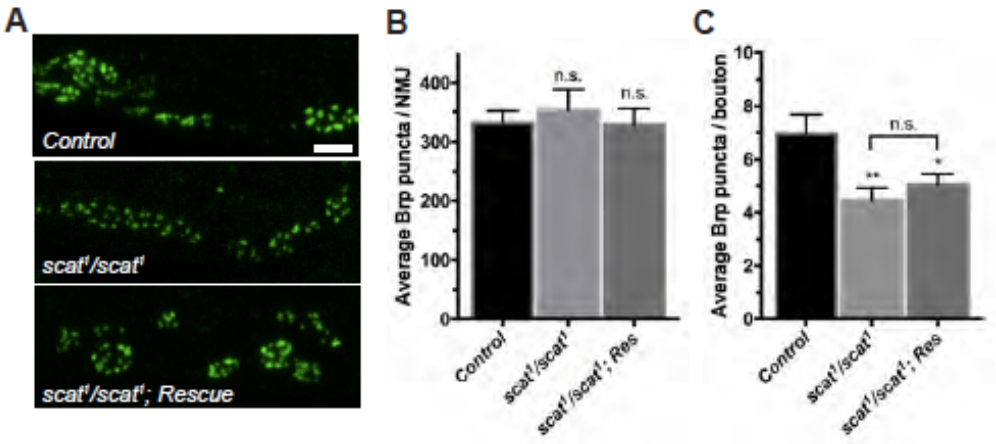

Figure 10. *scat* mutants do not have active zone defects. Provided by Emily Starke. A) NMJs innervating muscle 6/7 in body segment A3 from the indicated genotypes stained with an antibody targeting Brp (green). *scat* mutants have an increased number of small boutons with fewer Brp-positive puncta. Scale bar, 5 μm. B) The total number of Brp-positive punctae per NMJ does not change C) The number of Brp-positive punctae per synaptic bouton increases in *scat* mutants. N = 10 for each genotype. Statistical analysis was done using a one-way ANOVA followed by a Holm-Sidak multiple comparison test. Data in graphs are represented by the mean ± SEM.

Next, we wanted to see if the changes in synapse morphology and composition we observed in larval NMJs, due to the disruption of scat, affected larval crawling behavior. Locomotor defects are commonly seen in animals with neuronal dysfunction and have been directly linked with synaptic dysfunction [287, 288]. We see no statistical differences in the speed of crawling when comparing *C380-Gal4>scat shRNA* larvae to controls (Fig. 9F). Interestingly, the motor neuron specific expression of DN Rab5, Rab7, and Rab11 did not show any effect on larval crawling speeds. However, wild type expression of the same Rab proteins all significantly decreased larval crawling velocity by 55%, 53% and 53% respectively. Conversely, in animals with motor neuron specific *scat* KD expressing wild type Rab7, Rab11, and DN Rab7, all showed significant increases in larval crawling velocity when compared to *C380-Gal4>scat shRNA* control animals (Fig. 9F). Because of the non-correlative nature of these data, we do not believe there to be a relationship between synaptic morphology or post-synaptic density composition and larval locomotor function. However, this datum clearly supports our findings suggesting that scat is interacting with Rab GTPases to regulate neuronal function.

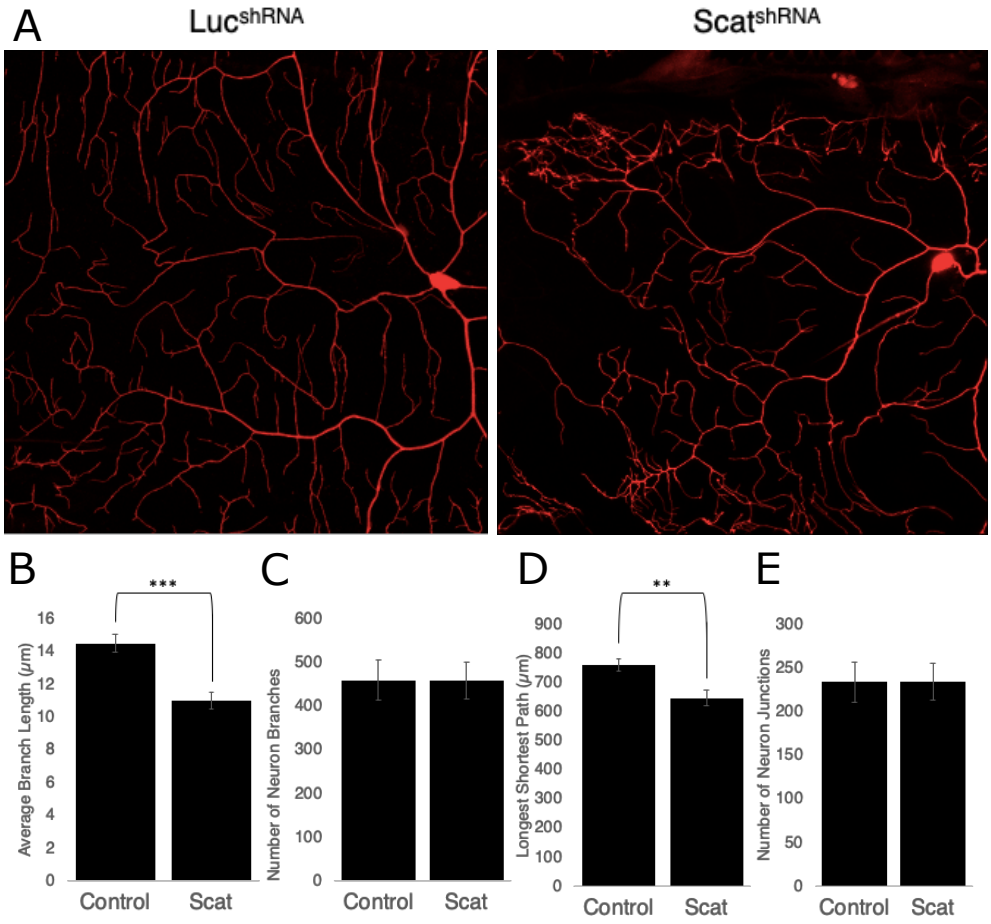

Figure 11. scat is a regulator of larval Class IV ddaC sensory neuron dendritic development. Images of wandering third instar larvae Class IV ddaC sensory neurons from dorsal segments A4-A6 collected from larvae co-expressing *Luc*^{shRNA} or *scat*^{shRNA} and membrane-tethered td:tomato driven by sensory neuron specific driver *ppkGal4* (A) scat sensory neuron specific reduction-of-function cause changes in dendritic morphology of sensory neurons. Z-projections of ddaC neurons show distinct phenotypic differences between *scat*^{shRNA} and control neurons with a characteristic disorderly clumping of distal neurite branches in KD *scat* neurons. (B) Average dendritic branch length of ddaC neurons in animals described above. Control animals have significantly longer average branch lengths. (C) The average number of dendritic branches in ddaC sensory neurons, no difference is seen between KD of *scat* and control animals. (D) Average longest-shortest path of KD of *scat* and control larvae, sensory neuron specific *scat* KD shows shorter longest-shortest paths compared to controls. (E) Average number of dendritic neuron junctions of ddaC neurons in *scat* KD and control animals. No differences were seen. n = 11 control and 15 *scat*^{shRNA} are represented as the mean ± SEM. All statistical analysis was done in Microsoft Excel by two sample t-Test assuming unequal variances. All comparisons have been made to the control. * $p < 0.01$, ** $p < 0.001$, *** $p < 0.0001$.

Function of scat is required for the development of larval sensory neurons

Peripheral nervous system dysfunction is one set of symptoms associated with ALS [289]. In some cases of sALS severe sensory neuropathy is observed [290]. Neurodegeneration in the wobbler mouse is not motor neuron specific. Paravalbumin-positive GABAergic interneurons are reduced in the motor cortex of pre-symptomatic wobbler mice 15 to 25 days of age [223]. It has been speculated that loss of GABAergic interneurons may be a precursor to motor neuron degeneration seen in wobbler mice [291]. Peripheral motor neurons and sensory neurons share many mechanisms of axonal degeneration [292]. Previously, neurodegeneration associated with *LRRK2* mutations in PD models has been observed in dopaminergic neurons and peripheral sensory neurons [293]. As a result, we speculated that scat function may be involved in regulation of peripheral sensory neurons. *Drosophila* larvae have well characterized segmentally stereotyped sensory neurons that are grouped into classes I through IV. Classes are defined by their dendritic morphologies, class IV neurons exhibiting the most complex neuronal arbors [294, 295].

We wanted to determine if scat function is involved in neuron development other than that seen in motor neuron axons. To do this we tested loss of scat function on the development of dendritic arbors in larval sensory neurons. We drove expression of Gal4-inducable *UAS-CD4-tdTomato* in conjunction with our previously described *scat* shRNA using a strong sensory neuron specific driver *ppkGal4* [296]. This allowed us to fluorescently label sensory neurons for live cell imaging while producing sensory neuron specific *scat* KD. Since we observed such significant morphological alteration due to scat

dysfunction in larval NMJs we speculated that other types of neuron development may also be affected.

Dysfunction of RNA-binding proteins implicated in neurological disorders have previously been found to regulate the control of sensory neuron dendritic morphology [296]. We observed a significant decrease in the average branch length and longest shortest path in Class IV ddaC sensory neurons with *scat* KD compared to *ppkGla4>UAS-CD4-tdTomato* control larvae (Fig. 11B,11D). It is assumed that physiological signaling follows the shortest path through neurons as fewer synaptic edges correlates with faster and higher-fidelity signaling. To this end, longest shortest path is used to describe the longest distance of optimal signal travel through a neuron [297]. We did not see any significant differences in the number of neurite junctions or neurite branches (Fig. 11C, 11E). It should be noted that *ppkGal4>scat shRNA* larvae show a shift in dendritic branch distribution with a large number of neurite branches located in the periphery of axons that is not seen in controls (Fig. 11A). Similar changes in branch distribution have been observed in the ddaC neurons of *Drosophila* with mutations in *dynein light intermediate chain* (*Dlic2*) and *Turtle* (*Tutl*), in both cases associated with neuron dysfunction [298, 299]. Taken together, these data suggest that scat, in part, is involved in the development of Class IV ddaC sensory neuron dendrites.

Conclusions

Disruption of Vps54 function in the wobbler mouse causes neurodegeneration. However, it is unclear how the disruption of this GARP complex subunit leads to neuron dysfunction. We disrupted expression of the Vps54 *Drosophila* ortholog scat in neuron

specific tissue of larvae to examine its effects. We show that mutants with global knockout and motor neuron-specific knockdown of *scat* display severe synaptic hyperplasia of the NMJ. Motor neuron knockdown of *scat* causes partial disruption of the localization of tSNARE, Syntaxin-16, to the TGN; however, no impact on endosomal pools. Overexpression of Rab GTPases Rab5, Rab7, and Rab11 in *trans* with the knockdown of *scat* in motor neurons suppresses the hyperplasia phenotype previously observed. Conversely, overexpression of dominant negative Rab7 with motor neuron specific *scat* knockdown decreases postsynaptic Dlg and GluRIIB levels but does not alter the levels of additional GluR subunit GluRIIA. Finally, we show that disruption of scat in class IV ddaC sensory neurons causes morphological changes in dendritic neurite localization. Taken together, these data suggest that motor neuron axon development and postsynaptic density composition are regulated by *scat* and Rab7 through an unknown transsynaptic mechanism. We also show that the functional requirement of scat is not isolated to motor neuron axons but is involved in peripheral sensory neuron development as well.

CHAPTER 3: THE ROLE OF SCAT IN AGE PROGRESSIVE NEURODEGENERATION

Introduction

Neurodegenerative diseases are severe and often fatal neurological disorders associated with reduced function, or loss of function of neurological components. This degeneration commonly leads to cognitive impairment and motor dysfunction. The primary risk factor associated with neurodegeneration is aging [4]. As a great portion of the general population continues to age, the prevalence of such disorders has increased [3]. Identification of genetic mutations in such disorders have highlighted several intracellular pathways involved in disease pathogenesis. These genes can be categorized by their control or assistance in; RNA metabolism, axonal and cytoskeletal dynamics, and protein trafficking [7].

Endocytic trafficking has been implicated in several specialized processes in neurons including axon guidance and outgrowth, synaptic plasticity, and axonal transport [244]. Axon growth requires constant replenishment of membrane, membrane proteins, and signaling molecules. For example, axon growth is controlled by small GTPases; Rab8, Rab10, Rab13, and Rab21, which all localize to the TGN or vesicles derived from the TGN

[300]. Rab5 regulates axon and dendrite growth and branching in cultured neurons and acts as a marker for early endosomes [301, 302]. Rab7, classically a marker for late endosomes, causes neuritogenesis disruption when mutated [303-305], while Rab11-positive endosomes promote axonal growth [306]. Rab11 mediates endosome recycling to the TGN and plasma membrane and is commonly used as a marker for recycling endosomes [307].

Here, we show that loss-of-function of scat recapitulates wobbler mouse male sterility and neurodegenerative phenotypes including: reduced lifespan, decreased muscle size, locomotor defects, and reduced body size. Interestingly we see a sexually dimorphic difference between male and female mutants, with females demonstrating more severe neurodegenerative phenotypes overall. We also show that *scat* may be genetically interacting with small GTPase, Rab11, in adult motor neurons to regulate these phenotypes.

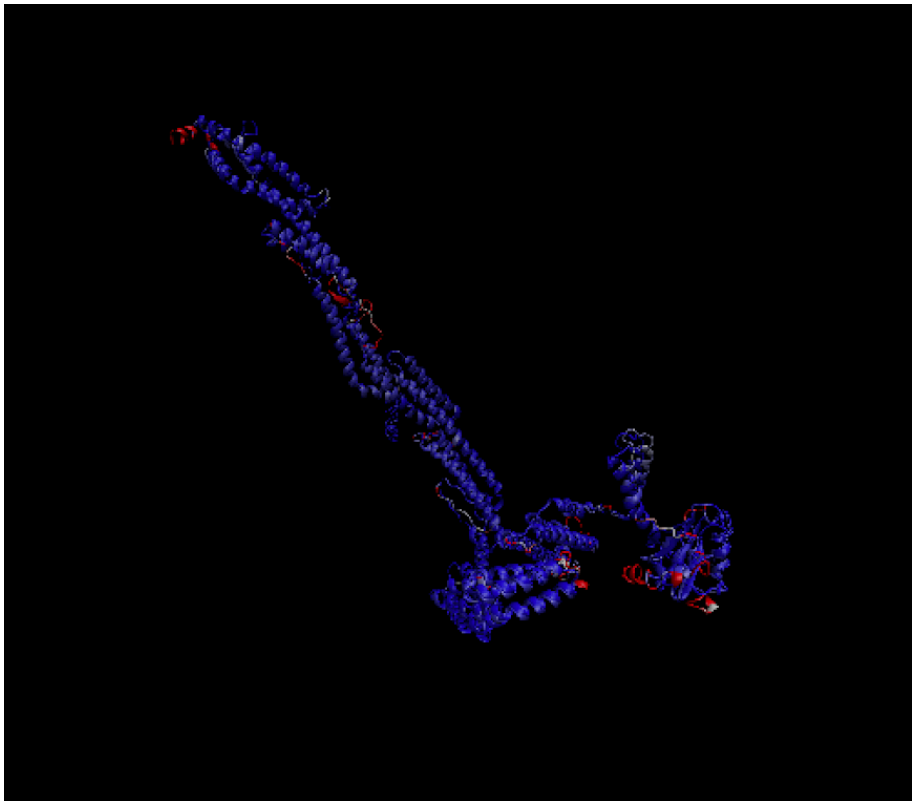

Figure 12. Modeled representation of mammalian Vps54 and scat similarity. Comparison of expected protein structure between mammalian Vps54 [308] and *Drosophila* scat modeled using Chimera software by UCSF. Model displayed upon wild type scat predicted structure. Peptides that are very similar are represented by blue and very dissimilar peptides are represented by red.

Results and Discussion

Development of new "wobbler" flies

Several multi-subunit tethering complexes have been found to play a role in different steps of the endo-lysosomal trafficking pathway [309, 310]. Tethering complexes required for endosomal trafficking must recognize specific membrane associated factors on both the endosome and recipient compartment. Separate domains found in tethering complex subunits determines the specificity of endosome recruitment. Previous studies have shown that the C-terminal domain within Vps54 is required for its recruitment to polarized endocytic compartments [210]. Within the five-stranded antiparallel coiled-coil bundle structure of the C-terminal domain there are an additional set of sub domains: C, D, and E. The Vps54 D domain has a high resemblance to the D domain found within other multi-subunit tethering complexes [311-314]. Interactions between different subunits within the GARP complex are believed to occur at the C domain, formed by the first and second helixes within the C-terminus. The E sub-domain contains hydrophobic contacts between the third and fourth helical structures. This hydrophobic groove is where the L967Q wobbler point mutation occurs, it has been suggested that the mutation of hydrophobic leucine to hydrophilic glutamine imposes different steric constraints resulting in the destabilization of Vps54 [215]. The N-terminal domain within Vps54 is believed to interact with the TGN [210].

To determine the similarity between mammalian Vps54 and scat we compared their peptide sequences for expected protein structures [308] (Fig. 12). It can be clearly seen that majority of peptides in scat and Vps54 share very similar qualities, represented in blue

(Fig. 12). The high degree of similarity between the two protein sequences results in very similar protein structures, and likely similar functional domains. The wild type scat predicted protein structure shows an antiparallel coiled-coil bundle at the C-terminus, similar to that described for Vps54 [208]. However, at the very C-terminus of the scat protein there is an unstructured domain that is not found in the crystal structure or models of the C-terminal domain of Vps54 (Fig. 13B). This small difference can be seen by the high degree of dissimilarity at the C-terminus between scat and Vps54 (Fig. 12).

We wanted to make *scat* mutants with variable protein structures to better characterize the effects of loss of scat function in *Drosophila*. To accomplish this, we utilized the mobile P-element insertion located in the $scat^{1}$ allele. After mobilizing the P-element insertion to different parts of the *scat* allele, it was excised causing a partial deletion of allelic sequence resulting in new in-frame stop codons (Fig. 13A). The Δ*244 scat* mutant allele produced a peptide that is likely unstable in its tertiary structure and is therefore quickly degraded, thus creating a global scat null model [315]. The estimated TM-score of our 3D model is an extremely low 0.27±0.08, indicating that there is very little matching of our peptide with other known proteins, likely because more similar peptides are not stable in this configuration and as such are degraded. The Δ*244* mutant also has a very high root-mean-square deviation (RMSD) of atomic position, 13.7±4.0Å, demonstrating very little similarity to other known proteins, which further supports our claim that the peptide is likely quickly degraded post translationally. The estimated TM-score of our Δ*312 scat* mutant peptide is 0.48±0.15 with an estimated RMSD of 10.6±4.6Å. This RMSD value matches very similarly, RMSD=1.16Å, to a stable ataxia telangiectasia-

mutated and Rad3-related (ATR) protein, suggesting that this truncated mutant is stably expressed in mutant individuals, although the mutant structure does not mirror the wild type protein N-terminus structure (Fig. 13B) [316-319].

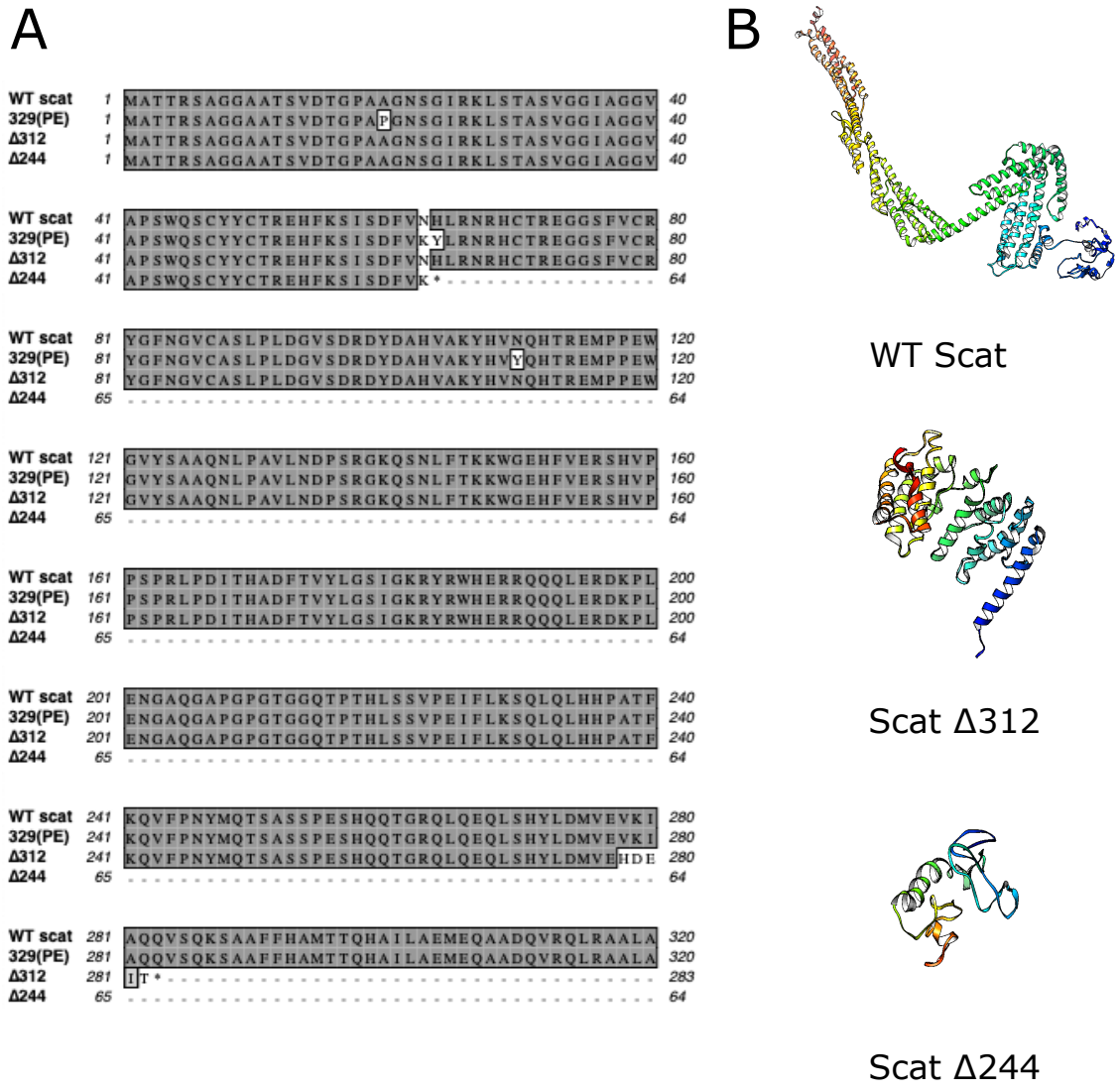

Figure 13. Modeled representation of *scat* mutations. *scat* mutant flies developed by Prajal Patel and Emily Starke. (A) Alignment of scat mutant peptides, wild type scat and 329(PE) peptides continue until 990aa and 989aa respectively and have perfect alignment from position 320+ (B) Three dimensional predicted molecular structures of mutant proteins. Wild type scat was compared to Vps54 protein structure previously described (Schindler 2015). Δ*312* model C-score=-.198, estimated TM-score=0.48±0.15, estimated RMDS=10.6±4.6Å. Δ*244* model C-score=-4.19, estimated TM-score=0.27±0.08, estimated RMDS=13.7±4.0Å. Visual models produced by Chimera software by UCSF.

Mutant flies show characteristic wobbler phenotypes

Both scat loss of function mutations cause male sterility

To determine if our *scat* mutant flies could be used to model age progressive motor neuron degeneration, we first needed to verify that they shared characteristic phenotypes of cellular dysfunction with those seen in the wobbler mouse. One of the most well documented characteristics of the wobbler mouse is male sterility [229]. Defects in spermatogenesis have also been well documented in the $scat^{1}$, scat null mutants. Specifically, sperm cells developed dysfunctional morphology showing reduced motility and production [235]. In both Δ*312* and Δ*244* mutants we observed complete male sterility in homozygotes (datum not shown). Conversely, the *329(PE)* genetic control showed a complete rescue of male fertility and viability, therefore suggesting full functional rescue to wild type spermatogenesis phenotype (datum not shown).

Loss of scat function decreases average lifespan

In mice, complete loss of function of Vps54 causes embryonic lethality and severe developmental defects of motor neurons and cardiac muscle tissue [217]. All studies researching Vps54 effects on longevity and motor neuron defects in adult mice have only been studied in knockdown models. The non-lethal wobbler mouse missense mutation causes reduced functionality of Vps54 but not complete loss of function providing a non-lethal model for aging [220]. This is not the case in flies, mutations leading to complete loss of function of scat only show partial lethality. Eclosion rates allow for the measure of individuals that survive metamorphosis to reach full maturity. We found that Δ*244* mutants

had only 50% (n=25/50) of all wandering third instar larvae survive metamorphosis and develop into mature adults. Similarly, we found that Δ*312* mutants had even fewer, only 46% (n=23/50), of all larvae surviving to reach full maturity (Fig. 14D).

Mice homozygous for the wobbler mutation show a severe decrease in survival rate. It is previously been reported that the median lifespan for wobbler mice is around 100 days of age, which is three times shorter than healthy individuals [320]. We wanted to determine if scat loss-of-function has a similar effect in our *scat* mutants. Much like the wobbler mouse we found *scat* mutants to have significantly reduced lifespan compared to both wild type and *329(PE)* controls ($p<0.0001$). Compared with *329(PE)*, Δ*312* adults showed a 36% and 40% reduction of median lifespan for males (28 days) and females (29 days) respectively. Δ*244* mutants had an even greater, 36% (28 days) in males and 44% (25 days) in females, reduction of median lifespan compared to *329(PE)* controls (male=47 days, females=45 days). As expected, there were no significant differences between *329(PE)* control mutants and wild type flies (male=48 days, females=56 days), providing further evidence to support that a complete rescue of scat function occurred due to the precise excision of the original P-element (Fig. 14A).

Reduced longevity can be found in many neurodegenerative disorders including, ALS, Parkinson's disease, and Alzheimer's disease [321-323]. In ALS the degeneration of motor neurons leads to contractile muscle weakness, first of peripheral limbs and shortly followed by weakness and loss of function of bulbar and respiratory muscle systems critical for survival. This progression usually occurs within 3-5 years of symptom onset and plays a major role in the reduced longevity of affected individuals [324]. Reduced lifespan has

also been observed in other ALS *Drosophila* models. Flies with a loss-of-function mutation in *caz*, the fly ortholog of *FUS*, show a 57% decrease in median lifespan compared with controls. Loss-of-function of *TDP-43* fly ortholog *tbph* has an even more severe affect, reducing median lifespan by 88.4% compared to control animals [325]. Similar to other *Drosophila* ALS models, our results demonstrate that homozygous mutations causing complete loss-of-function of scat leads to a significant decrease in median lifespan of adult *Drosophila* (Fig. 14A). We also see a decreased number of mutant larvae surviving pupation (Fig. 14D).

Neuron hyperexcitability exhibited by bang sensitivity in scat mutants

Hyperexcitability of cortical neurons in humans has been recorded prior to the onset of clinical symptoms of fALS [326]. Similarly, cortical hyperexcitability caused by reduced GABAergic inhibition has been observed in the wobbler mouse [223]. A characteristic phenotype of hyperexcitability in *Drosophila* manifests as epileptic seizure due to external stimulus. In particular a mechanical stimulus or a "bang" can lead to temporary paralysis and seizure, commonly known as the bang sensitivity phenotype [327-329]. We tested for bang sensitivity in adult female flies by monitoring populations for the presence of intermittent seizure immediately following spatial agitation. Specifically, flies were collected in empty vials, vortexed for 10 seconds, and observed for the following 30 seconds. Flies that exhibited bang sensitivity were unable to climb up the sides of the vial and remained at the bottom. We found that both Δ*312* mutants and Δ*244* mutants have

significantly more ($p<0.0005$) individuals prone to exhibit bang sensitivity when compared with wild type and *329(PE)* controls (Fig. 14B).

The bang sensitivity phenotype has been seen in flies with disruption of neural excitability but can also be seen in flies with mutations in genes involved in mitochondrial function, in both cases the phenotype becomes more prevalent with age [330]. Dysfunction of mitochondrial respiration has been observed in the wobbler mouse model [331] and other motor neuron pathologies have been observed in mouse models with mitochondrial abnormalities or dysfunction [332]. Altered mitochondrial morphology has been observed in both spinal motor neurons and skeletal muscle in ALS patients and mouse models [232]. Our datum shows that scat loss-of-function results in neuronal hyperexcitability (Fig. 14B). However, we cannot speak to the cause of this hyperexcitability or in which neurons it may be occurring. It is possible that reduced GABAergic inhibition or mitochondrial dysfunction, similar to that previously described in the wobbler mouse, could be the cause of bang sensitivity in our *scat* mutants, however, further testing would be required to determine the specific cause.

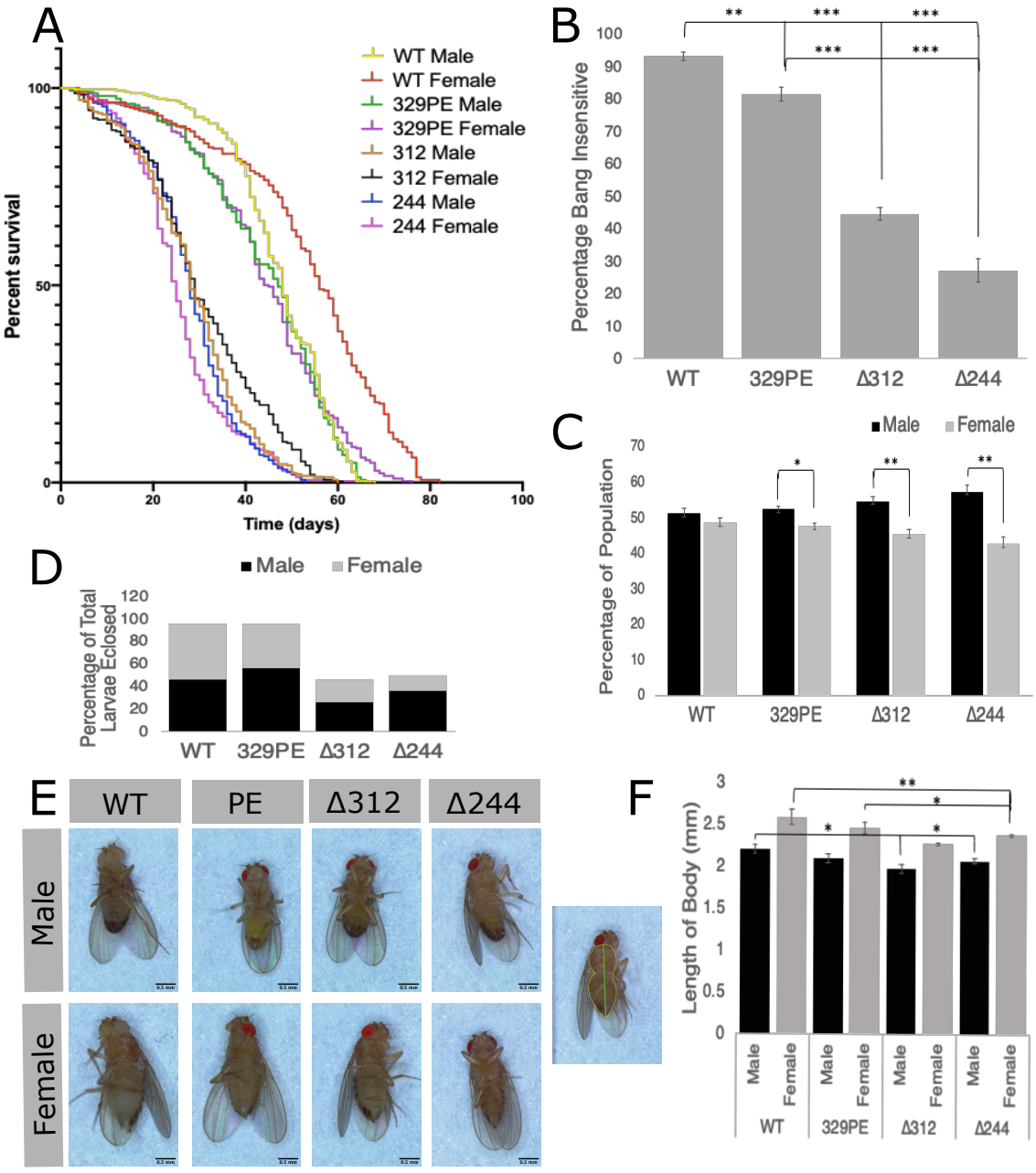

Figure 14. *scat* mutants have reduced longevity, general neural dysfunction and sexually dimorphic morphological changes in body size. (A) Lifespan analysis of indicated genotypes separated by gender. Analysis was done using 300 flies per cohort. Median lifespan for male wild type, *scat 329(PE)*, *scat* Δ*312*, and *scat* Δ*244* are 48, 47, 28, and 28 days respectively. Median lifespan for female wild type, *scat 329(PE)*, *scat* Δ*312*, and *scat* Δ*244* are 56, 45, 29, and 25 days respectively. (B) Bang insensitivity assay of female flies of indicated genotypes 2 days post eclosion. Flies were collected within 24 hours of eclosion, given an overnight rest period and assayed (n=100). (C) Gender ratio of indicated genotypes presented in percentage of population. Flies were randomly collected after pupal eclosion and sexed (n=100). (D) Proportion of flies that survive pupation and associated gender ratios. Wandering instar larvae collected (n=50) allowed time to

pupate and adult flies collected and sexed. (E) Images of representative adult flies for indicated genotype and gender illustrate size differences in mutants. Far right image labeled with example body area measurement in yellow and body length measurement in green. (F) Quantification of body length of adult flies of indicated genotypes and genders. Length in mm was recorded from rostral most region to caudal end of the abdomen (n=5). Statistics: (A) ANOVA Δ*312* and Δ*244* of both genders to control and *329(PE)* $p<0.0001$. (B,C,F) T-Test, *= $p<0.05$, **=$p<0.005$, ***=$p<0.0005$.

Changes in body size occur in scat mutants

A reduction of body size is also exhibited in *scat* mutants, similar to what has been seen in the wobbler mouse [333]. Generally, in *Drosophila*, females are notably larger than otherwise identical males [334]. Qualitatively, it can be seen that female Δ*312* and Δ*244* mutants appear much smaller than wild type and *329(PE)* control flies (Fig. 14E). It also can be noted that the size of males generally appeared to remain the same despite *scat* mutations.

To quantitatively determine the differences in size we observed, we measured body length between anterior and posterior points. Male mutants showed no difference in length compared to genetically matched *329(PE)* controls. In female flies we found that Δ*312* mutants showed no statistical difference from either control group, however, Δ*244* mutants were significantly shorter in body length compared to both wild type and *329(PE)* female controls (Fig. 14F). We describe overall body area as the region of the thorax and abdomen as shown by the yellow outline in Fig. 14E. We saw a significant decrease body area of both female Δ*312* and Δ*244* mutants compared to controls (Fig. 15).

There is not a clear link between body size and neurological function as different neurological disorders vary in their link to overall body mass. However, some neurological disorders, such as late onset AD and ALS, are associated with reduced body mass. Interestingly, mitochondrial dysfunction is commonly found to cause obesity and increase in body size. Abnormal mitochondrial function results in lipid accumulation caused by defects in secretion of adipokines, fatty acid oxidation, and glucose homeostasis within

adipocytes [335]. This suggests that the role of mitochondrial dysfunction may not impact the bang sensitivity phenotype that was observed in our *scat* mutants.

Rapid weight loss has long been used as an identifying feature of late onset neurodegenerative disorders such as AD [336]. In many cases of ALS rapid weight loss is the result of muscle atrophy following denervation by motor neurons affected by neurodegeneration [337]. We speculate that the smaller body size we observe in *scat* mutants may be a result of reduced muscle mass in turn.

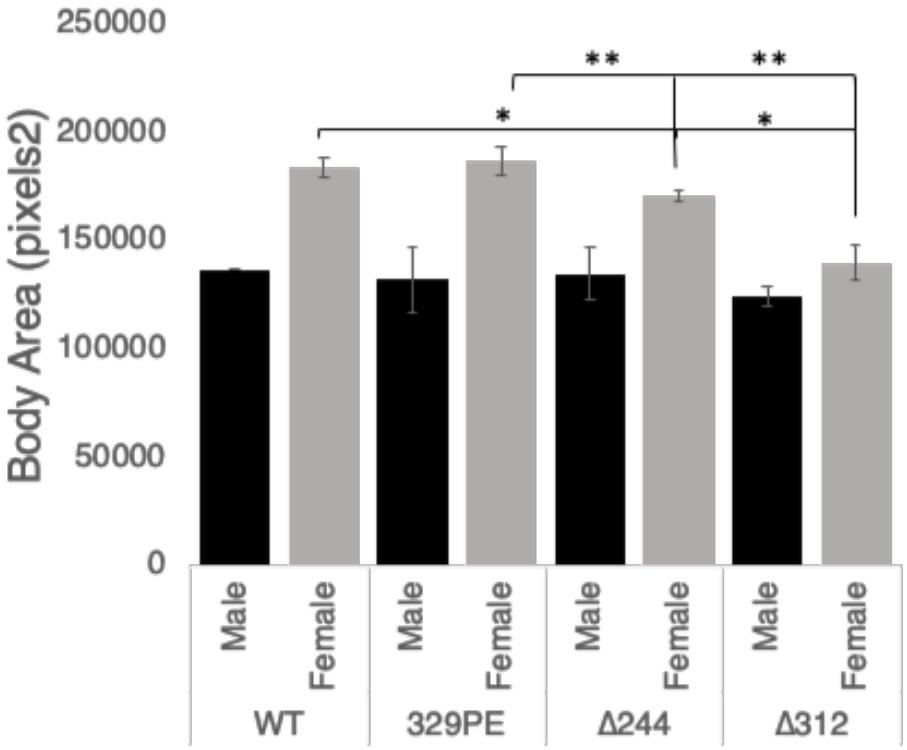

Figure 15. Quantification of body area of adult flies of indicated genotypes and genders. Body area was measured in pixel number collected by measuring total area of the thorax and abdomen together (n=5). Statistics: T-Test, *= $p<0.05$, **=$p<0.005$.

Sexually dimorphic differences in scat mutants

To determine if scat function has a more impactful role in cellular processes predominantly in one gender, we looked into developmental features impacted by neuronal function. Generally, among mammals, females live longer than males, however, in flies, genotype, mating status, and female fecundity all impact which gender is longer-lived [338]. We observed a 16% increase in median lifespan of female wild type flies compared to genotypically paired males. Female *329(PE)* controls had an insignificant 3.5% reduction of median lifespan compared to their male counterparts. Interestingly, scat truncation Δ*312* mutants show an increase in median lifespan of ≤1% in female flies compared to paired males, while female scat deletion Δ*244* mutants showed a notable significant decrease in median lifespan of 11% when compared to males ($p<0.0001$) (Fig. 14A).

Female biased sexual dimorphism is also seen in the gender ratio within each genotypic population of adult flies. Wild type and *329(PE)* populations show only a minor increased presence of males relative to females, 2% and 3% ($p<0.01$) respectively, very close to the expected mendelian ratios. However, in Δ*312* mutant populations, males are present 9% more often than females and even more drastically seen in Δ*244* mutants with males present 14% more ($p<0.001$) (Fig. 14C).

It is also clear that loss of function, or reduced function of scat affects the size of female flies significantly more than males (Fig. 14D). Male mutant flies, although significantly different ($p<0.01$) than wild type, only have reduced average body length of

0.24mm for Δ*312* and 0.13mm for Δ*244*, while female Δ*312* and Δ*244* mutants show an average reduced body length 0.32mm and 0.21mm respectively ($p<0.001$) (Fig. 14F).

Gender differences are not uncommon in neurodegenerative disorders. Parkinson's disease and ALS more commonly effect males [339, 340], while multiple sclerosis is more commonly found in females [341]. We show that loss of function of scat has sexually dimorphic properties effecting females more than males. This can be seen in an even greater reduction of lifespan in female mutant flies compared to male mutants. It can also be found in the rate of developmental success. Female flies show a reduced ability to survive pupation and reach complete maturation to adult form. Generally in flies females are larger than their male counterparts [342]. However, our datum shows a marked decrease in the body size, demonstrated by reduced body length, in female *scat* mutants, while males showed little or no change in body size associated with scat loss of function (Fig. 14D-E).

In mammals, neuroprotective properties of different steroid hormones, specifically estrogen, have been shown [343]. Epidemiological studies suggest that estrogens neuroprotective effect is the reason women with PD have later symptom onset [344]. To the same effect higher prevalence of AD and greater disease severity have been found in women compared to men, the loss of sex hormones during menopause is suggested to be the cause [345]. However, sex differentiation in *Drosophila* is primarily regulated by gene expression of *Sex lethal* and *doublesex* genes rather than steroid hormones [346]. It is possible that the absence of female neuroprotective steroids might account for the sexually dimorphic phenotypes described, however, further exploration is needed to uncover the specific cause of the sexual dimorphism we observed.

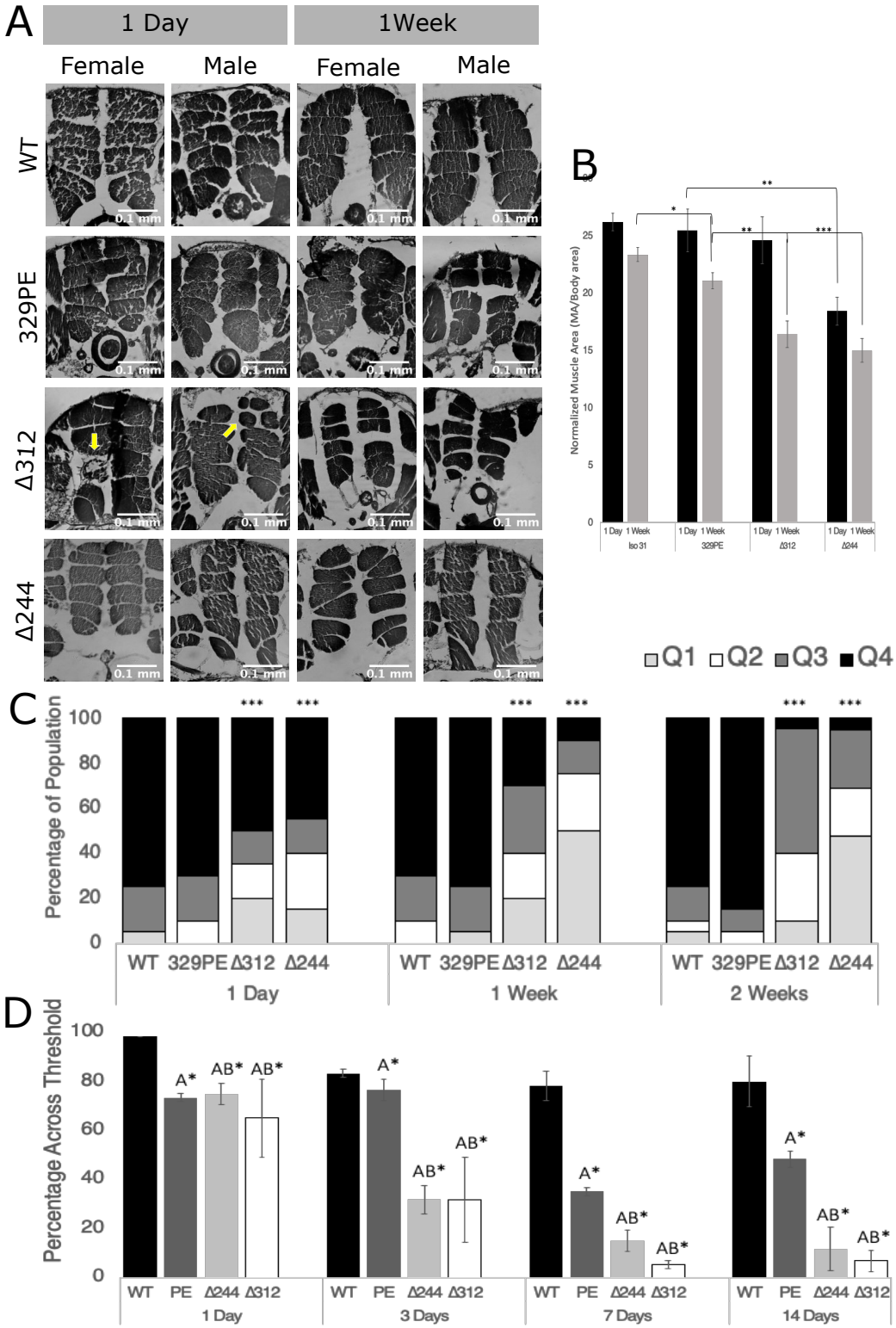
A
1 Day
1Week
Female
Male
Female
Male
WT
329PE
Δ312
Δ244
0.1 mm
B
Normalized Muscle Area (MA/Body area)
1 Day 1 Week
Iso 31
329PE
Δ312
Δ244
Q1 Q2 Q3 Q4
C
Percentage of Population
WT 329PE Δ312 Δ244
1 Day
1 Week
2 Weeks
D
Percentage Across Threshold
WT PE Δ244 Δ312
1 Day
3 Days
7 Days
14 Days

Figure 16. *scat* mutations cause reduced muscle function and size in adult *Drosophila*. (A) Representative H&E staining of thoracic muscle sections of adult flies, gender, age, and genotype indicated. Sections oriented with dorsal side superior in image. Yellow arrows indicate structures of interest. (B) Quantification of dorsal longitudinal muscle area normalized to total area of thoracic section for indicated gender and genotypes (n= 11-20). (C) Spontaneous flight assay showing percentage of female flies that land in each quadrant after being sent into freefall initiating reflexive flight response (n=20). Q1 indicates lowest quadrant, Q4 indicates highest quadrant with Q2 and Q3 indicating accordingly. (D) Negative geotaxis assay showing the percentage of female flies of indicated genotypes and age that cross a 1 cm mark after climbing for 30 seconds (n=20). Statistics: (B) T-test *= $p<0.05$, **= $p<0.005$, ***= $p<0.0005$. (C) Chi-squared analysis ***= $p<0.0005$. (D) Chi-squared analysis A*= $p<0.0005$ compared to wild type, AB*= $p<0.0005$ compared to wild type and *329PE*.

Loss of scat function causes reduced muscle size and locomotor defects

Reduced muscle function in scat mutants

Muscle atrophy and weakness is commonly associated with neurodegenerative disorders involved in the peripheral nervous system such as ALS, MS, Charcot-Marie-Tooth and Parkinson's disease [347-350]. The wobbler mouse, much like ALS patients, exhibits muscle weakness. In the wobbler mouse, muscle weakness is predominantly found to affect the fore limbs. Specifically, this has been observed during behavioral assays such as grid walking that highlight motor defects [217].

To test for locomotor defects associated with primary muscle group function in our models, we performed a spontaneous flight assay to assess the function of flight muscles. Flies have an innate response when entering into freefall to initiate flight [351, 352]. To determine flight locomotor function, we dropped flies into freefall in a 500ml container coated with mineral oil to capture the distance they fell before they were able to right themselves and recover. Flies that have higher functioning flight muscles recover from freefall faster and thus end up in the high quadrants of the container [353]. Only female flies were tested as they had the greatest differences in longevity. At 1 day of age there were no significant differences between wild type and *329(PE)* flies, however, both Δ*312* and Δ*244* mutants showed a significantly larger portion of the population landing in the lower quadrants 35% and 40% respectively when compared to wild type 5% and *329(PE)* 10% ($p<0.0005$). At 7 days the mutants show an even greater portion of flies landing the in lower quadrants, Δ*312* 40% and Δ*244* 75%, while the control flies remained roughly the same ($p<0.0005$). Flies aged 2 weeks show the same trends seen in flies aged 1 week (Fig.

16C). Overall, we found that *scat* mutants had significantly reduced function of flight muscles compared to control animals.

Another primary muscle group that we tested to determine locomotor function were the muscles involved in leg control and climbing. We performed a negative geotaxis assay to determine if muscles involved in leg movements were affected by mutations in *scat*. Flies have an innate escape response to climb up the sides of a container after they have been tapped down to the bottom [352]. Flies were tested 1, 3, 7, and 14 days post eclosion to determine if there was any loss of muscle function with age. Wild type flies showed a 18% reduced locomotor function after the course of 2 weeks, *329(PE)* showed a reduction of 34%, while Δ*312* and Δ*244* flies showed reductions of 89% and 84% respectively. Interestingly, Δ*312* flies at 1 week of age showed the greatest reduction in climbing muscle function, showing a drop of 92%. At just 1 day old *329(PE)*, Δ*312* and Δ*244* flies already showed significantly lower populations of flies able to complete the climbing test ($p<0.0005$) (Fig. 16D). We observed significantly reduced motor function in the limbs of *scat* mutants, not unlike that previously characterized in the wobbler mouse.

We speculate that neuromuscular dysfunction starting in the larval stages may impact adult muscle development resulting in improper development of muscle structure or reduced overall muscle tissue [354]. Locomotor assay results show defects present in *scat* mutants suggesting that muscle function is affected throughout the animal (Fig. 16D).

Reduced thoracic muscle size in scat mutants

A key characteristic of the wobbler mouse is its decreased muscle mass. This has previously been exhibited in wobbler mice with reduced muscle fiber diameter of primary muscles found in both the fore and hind limbs [355]. *Drosophila* dorsal longitudinal muscles have been described as indirect flight muscles, not attached to the wing, rather providing the primary force driving the downstroke of the wing during flight [356]. We speculate that reduced function or size of the muscle would result in lessened flight capability. This correlates with our observations of mutants showing a significantly diminished ability to recover from free fall compared to control groups.

As a result of the diminished locomotor function, we observed we wanted to determine if scat has any effect on muscle morphology. To examine this we collected 10μm sections of fly thoraxes and looked at the 6 bilaterally paired dorsal longitudinal muscles of male and female flies aged 1 day and 7 days. Qualitatively, it is clear that Δ*312* and Δ*244* mutants have smaller individual muscles than the wild type and *329(PE)* controls. It also appears as though in the Δ*312* mutant females there may be some atrophy of individual muscles, while Δ*312* mutant males show possible fractionation of muscles, presumably caused during development of the adult anatomy during metamorphosis (Fig. 16A) [354].

To see quantitative differences between genotypes we measured the total area of all dorsal longitudinal muscles and normalized them to the total area of the thoracic section. We normalized the datum to accommodate minor differences in sections of the thorax as well as to take overall body size differences into account. Measurements were taken from sections of flies aged 1 day and 7 days to see if there was possible age-related muscle

atrophy as well. The datum suggests that normalized muscle area in adult *scat* mutants are significantly less than that of their control counterparts. Specifically, at only 1-day post eclosion, Δ*312* females showed a 6% smaller muscle size than wild type flies and Δ*244* females showed an even greater 30% ($p<0.005$) smaller muscle size than controls. At only 1 day there were no significant differences detected between wild type and *329(PE)* females. The differences in muscle size are even more pronounced in flies aged 7 days. Δ*312* females have average muscle area 30% ($p<0.005$) smaller than wild type, and Δ*244* females a 36% ($p<0.0005$) smaller average muscle area than wild type flies. It was also noted that Δ*312* flies exhibited a 33% decrease in average muscle area between flies age 1 day and flies age 7 days. Δ*244* flies average muscle area decreased by 18.5% between the two age points, which is a rate only slightly higher than that seen in *329(PE)*, 18% and wild type 11% (Fig. 16B). Overall, general muscle size appears to be reduced in *scat* mutants.

We demonstrate that neuronal dysfunction caused by loss of function of scat is likely linked to a decrease in muscle size and locomotor defects. As motor neurons denervate myofibrils, muscle atrophy manifests, preceded by a decrease in sarcolemma permeability. This is commonly seen in neuromuscular disorders as muscle weakness and loss of muscle mass [357]. We show that *sca*t mutants have significantly smaller muscle size and Δ*312* mutant females, in particular, exhibit notable age progressive loss of muscle mass, indicating neuromuscular pathology (Fig. 16A).

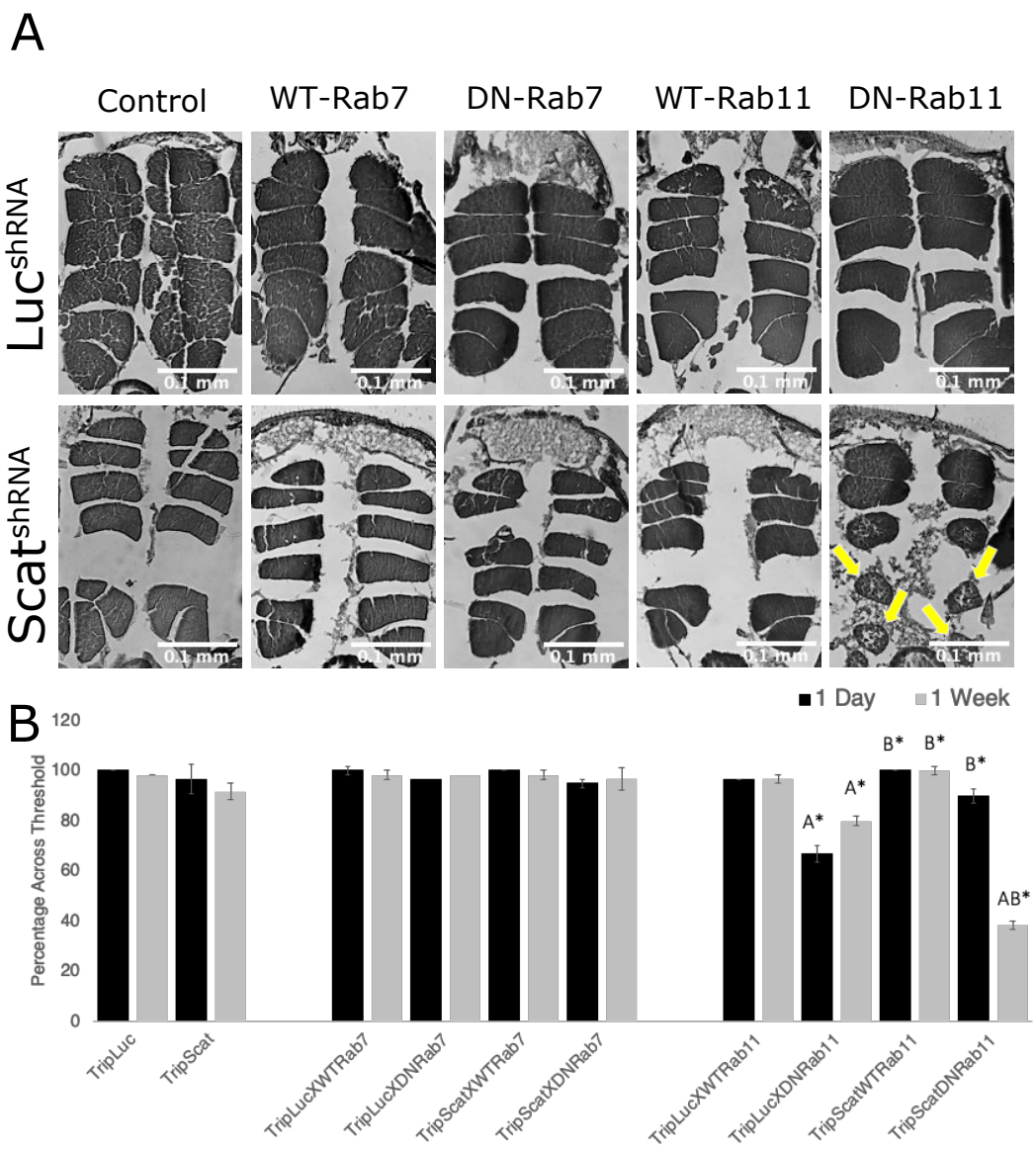

Figure 17. scat interacts with Rab11 causing exacerbated reduced muscle function phenotype. (A) Representative H&E staining of thoracic muscle sections of adult female flies, age and genotype indicated. Sections oriented with dorsal side superior in image. Yellow arrows indicate structures of interest. (B) Negative geotaxis assay showing the percentage of female flies of indicated genotypes and age that cross a 1 cm mark after climbing for 30 seconds (n=20). Statistics: (B) Chi-squared analysis A*= $p<0.005$ compared to Luc^{shRNA} -wild type, B*= $p<0.0005$ compared to Luc^{shRNA} -DN, AB*= $p<0.0005$ compared to both Luc^{shRNA} -wild type and Luc^{shRNA} -DN.

Rab11 interacts with scat regulating muscle atrophy and locomotor function

Knockdown of *scat with DN Rab11 expression exacerbates muscle dysfunction*

We have shown that Rab7 interacts with scat to regulate synaptic integrity at the neuromuscular junction in fly larvae [247]. To see if scat interacts in a similar manner in adult flies, we drove motor neuron specific presynaptic knockdown of *scat* using Gal4-inducable shRNA (s*cat*^{shRNA}) with *C380-Gal4* while concurrently driving overexpression of wild type or dominant negative (DN) forms of Rab7 and Rab11 (Fig. 1A). To test this, we performed a negative geotaxis assay on flies 1 day and 1 week old.

There were no statistical differences in control flies or *scat* knockdown overexpressing wild type or dominant negative Rab7 (Fig. 17B). However, expression of DN Rab11 in the control background show a significant drop in performance both at 1 day ($p<0.0001$) and 1 week ($p<0.005$) old. Conversely, it appears that overexpression of wild type Rab11 does not have any effect on performance (Fig. 17B). The most notable change, however, is seen when DN Rab11 is overexpressed in *scat*^{shRNA} flies, at 1 day old there is a greater proportion of flies (23%) that cross the threshold compared to the control *Luc*^{shRNA} flies overexpressing DN Rab11. After 1 week, however, the performance of *scat*^{shRNA} *DN Rab11* flies is significantly lower ($p<0.0001$) than any other measured variable (Fig. 17B).

A significant age progressive reduction in locomotor function occurred in *scat*^{shRNA} *DN Rab11* flies. Overexpression of DN Rab11 has a minor, but significant, effect on locomotor function on its own and knockdown of *scat* shows a very minor reduction of function on its own (Fig. 17B). At 1 day of age, flies perform better with *scat* knockdown and DN Rab11 compared to control flies only expressing DN Rab11. Taken together, this

suggests that there is an interaction between scat and Rab11 occurring in adults that is associated with aging, which is different from scat and Rab interactions in the larval stages of development.

Rab11 and scat effect thoracic muscle morphology

Since we saw an exacerbation in the reduction of locomotor function in *scat*^{shRNA} *DN Rab11* flies, we wanted to determine if there were any additional changes in muscle morphology. To test this, paraffin embedded sections were taken from the thoraxes of flies to observe muscle morphology of the dorsal longitudinal muscles. Similar to what was seen in *scat* Δ*312* and Δ*244* mutants, overall size of all muscles appears to be much smaller than their control wild type counterparts. Qualitatively, it does not appear that Rab7 has any impact on adult muscle morphology, which is in accordance with the locomotor function datum; however, notable muscle atrophy was observed in *scat*^{shRNA} flies overexpressing the dominant negative form of Rab11 (Fig. 17A).

Rab11 has been observed in recycling endosomes located in larval motor neuron axons and axon terminals [204]. It has also been found to rescue synaptic dysfunction associated with Huntington's disease, a hereditary neurodegenerative disease [358]. Our data suggests that scat and Rab11 are interacting to regulate muscle cell homeostasis.

Overall, our findings suggest that *scat* mutants share many characteristics of the wobbler mouse and would make useful models for the future study of neurodegenerative disorders. We also show evidence for possible mechanistic interactions between scat with Rab11, which may contribute to the disease phenotype that we characterized.

CHAPTER 4: THE WOBBLER FLY; A NEW MODEL FOR NEUROPATHY

The wobbler fly phenotype

Our goal was to characterize *scat* mutants and determine their potential usage as a new "wobbler" fly model in the study of neurodegeneration. The wobbler phenotype is defined by the presence of several characteristics that mirror symptoms observed in human sALS patients. We observed several key traits in *scat* mutants that are also found in the wobbler mouse and are linked with neurodegenerative disorders. In the wobbler mouse model severe muscle weakness is exhibited in the forelimbs, head and neck resulting in unstable or "wobbly" movements [220]. We described reduced locomotor function in both Δ*244* and Δ*312 scat* mutants during behavioral assays (Fig. 16B-C) which parallels the muscle dysfunction characterized in the wobbler mouse [221]. Loss of motor function is preceded by muscular atrophy in the wobbler mouse [221]. We observed similar muscle atrophy in both Δ*244* and Δ*312* mutants (Fig. 16A). We also found that both Δ*244* and Δ*312* mutants are sensitive to outside mechanical stimulus resulting in seizure, which has previously been linked with neuronal hyperexcitability (Fig. 14B). Hyperexcitability is also a trait that has been characterized in the wobbler mouse [223]. We observed reduced lifespan in both Δ*244* and Δ*312* mutants, much like what is seen in the wobbler mouse

[220]. Finally, we observed complete male sterility in both *scat* mutants (datum not shown), mirroring the sterility exhibited in homozygous male wobbler mice [221].

We also observed several characteristics of neuronal dysfunction in *scat* mutants that have not been described in the wobbler mouse. We found that reduction and loss-of-function of scat causes severe synaptic hyperplasia in larvae (Fig. 2), a characteristic unique to flies. We also observed a slight sexual dimorphism in our mutants that has not been previously described, showing a greater neuropathic effect on females than males (Fig. 14-15). Unlike in the wobbler mouse [256], we did not see any effect on localization of endocytic trafficking components with loss of scat function, with the exception of Syntaxin-16 (Fig. 6-7). However, our data, overall, indicates that *scat* mutants share many key characteristics of neurodegenerative pathology with those previously described in the wobbler mouse.

Future directions

Further characterization of the wobbler fly

We observed many similarities of neuropathy between the wobbler mouse and our *scat* mutants. That said, there are other characteristics that have been described in the wobbler mouse model that have yet to be described in *Drosophila*. These include astrogliosis and microgliosis [221], motor neuron degeneration [220], mitochondrial dysfunction [222], neurofilament aggregation [224], axonal transport defects [225] and ubiquitin-positive protein aggregation [226]. Moving forward, it would be advantageous

to explore any parallels between our *scat* mutant flies and the additional wobbler mouse characteristics listed above.

We would like to determine if motor neuron degeneration occurs in *scat* mutant flies. To do this we could utilize a technique known as mosaic analysis with repressible cell markers (MARCM). The use of MARCM in our system would allow for us to fluorescently label individual motor neurons in the legs of adult flies. By identifying individual motor neurons we could then observe if neurodegeneration occurs in *scat* mutants by examining the neurons for reduction of size, fractionation, or overall neuron loss [359]. Similarly, we could use MARCM to label specific microglia and astroglia to observe any similar effects [360].

We could also make use of the many fluorescent dyes and genetically encoded sensors that can be used to measure mitochondrial function in *Drosophila* to observe any differences in *scat* mutants [361]. Similarly, the use of *Drosophila* transgenes that encode fluorescently tagged proteins could allow for us to examine if there are defects in axonal transport, or aggregation of neuronal components within in system.

We showed for the first time that Rab GTPases genetically interact with *scat* during different life cycle stages. Further exploration into the specific mechanisms of these findings would provide a novel insight into the role of endocytic trafficking and neurodegeneration. However, at this time I do not have a suggestion for how to specifically achieve this.

Uses of the wobbler fly

Some research has already been done looking into some of the mechanisms of neuron preservation associated with the wobbler mutation. The work of one group suggests that the inhibition of sphingolipid synthesis by myriocin reduces the neurodegenerative phenotypes seen in the wobbler mouse [320]. Another group found that in vitro, dissociated wobbler mouse motor neurons benefit from treatment of nicotinamide adenine dinucleotide and caffeine, an upstream activator of the enzyme that produces NAD+, nicotinic acid mononucleotide transferase 2 [362]. Energy metabolism defects linked with disruption of cholesterol homeostasis have also been found in the wobbler mouse, however, its link to neurodegeneration is not clear [363]. Much more work needs to be done to determine the mechanisms causing neurodegeneration in the wobbler system. As more mechanisms become clear, treatments, such as those suggested above, can be more readily tested.

Our wobbler fly models allow for a faster throughput system to test many variables that may be associated with the mechanisms responsible for neuron dysregulation and further neurodegeneration. Moving forward our loss of scat function animals can be used to better tease apart components of the endocytic trafficking pathway, and possibly other aspects of cellular function, to determine the functional mechanisms causing the disease phenotype. These flies also allow for a high throughput system of testing to determine the efficacy of different pharmacological treatments.

CHAPTER 5: MATERIALS AND METHODS

Neurodevelopment and scat

Drosophila genetics

The following lines were obtained from the Bloomington Stock Center: *P(PZ)scat1cn1, cn1, Df(2L)Exel8022, UAS-TRiP(HMS01910), UAS-LUC.VALIUM10, tub-Gal4, C380-Gal4, D42- Gal4, 24B-Gal4, UAS-YFP:Rab5, UAS-YFP:Rab5(S43N), UAS-YFP:Rab7, UASYFP: Rab7(T22N), UAS-YFP:Rab11, UAS-YFP:Rab11(S25N). UAS-td:Tomato,ppKGal4* was generously provided by Dr. Eugenia Olesnicky Killian from the UCCS department of biology. The *scat1cn1 and cn1* lines were crossed into *w** to normalize the genetic backgrounds. *w*; cn1* was used as a control to rule out any phenotypes that might be caused by *cn1* homozygosity in the $scat^{1}$ homozygote. The *Df(2L)Exel8022* line deletes the entire *scat* gene plus about 60 kb of flanking genomic DNA including 9 neighboring genes. The Df line does not contain the *cn1* allele. The *UAS-HA:scat* line was made by amplifying the *scat-RA* open reading frame from the *LD22446* cDNA (Berkeley *Drosophila* Genome Project) with a 5' primer containing the HA tag and then cloned into *pUAST*. The genomic rescue line (*scat-HA:scat*) was made by amplifying the *scat* gene and ~350 nt of upstream and ~50 nt of downstream genomic DNA with a 5' primer containing the HA tag and cloned into *pCASPR4*. Both transgenic fly lines were

generated by Bestgene. The *UASHA:scat* (*tub-Gal4>UAS-HA:scat*) and *scat-HA:scat* constructs rescued both $scat^{1}$ semi-lethality and male sterility (datum not shown). Flies with *UAS-td:Tomato,ppKGal4* were crossed with *UAS-TRiP(HMS01910)* ($scat^{shRNA}$) or *UAS-LUC.VALIUM10* (Luc^{shRNA}) to produce flies with sensory neuron specific fluorescence in the desired genetic background. All fly lines and crosses were maintained on standard Bloomington media in a diurnal 25°C incubator. Statistical analysis was done using larvae from each genotype raised under identical conditions.

Immunohistochemistry and confocal microscopy

Larval body wall preps for NMJ and muscle analysis were dissected in Ca2+-free HL3 saline. Unless otherwise indicated, larvae were immunostained as previously described (Nesler et al., 2016). For imaging of the CNS, larval ventral ganglia and proximal axons were explanted and fixed in 4% paraformaldehyde in PBS. For GluRIIA and GluRIIB (and specific experiments with Rab and DLG) antibodies, larvae were fixed with Bouin's solution for 10 minutes. Bouin's solution significantly improved signal-to-noise with the anti-HA, Rab5, and Rab11 antibodies but was not compatible with the anti-Rab7 and dStx16 antibodies. All were blocked in PBS containing 0.3% Triton X-100 (PBST), 2% BSA, and 5% normal goat serum for 30 minutes before incubation overnight with primary antibodies diluted in block. Following washes in PBST, CNS samples were incubated overnight with the appropriate secondary antibodies. All were mounted in DAPI Fluoromount G (Southern Biotech) for confocal microscopy. Primary antibodies used were anti-HA (1:1000) (Sigma; 3F10), Lva (1:50) [251], Stx16 (1:500) (Abcam; ab32340), Dlg

(1:100) (DSHB; 4F3), Hrs (1:100) (DSHB; 27-4), Rab5 (1:800) and Rab11 (1:4000) [258], Rab7 (1:1500) (DSHB), GluRIIA (1:1000) and GluRIIB (1:1000) [364], Brp (1:1000) (DSHB; nc82), and Dylight 649 anti- Hrp (1:1000) (Jackson Labs). The Rab7 and Hrs antibodies were deposited to the DSHB by S. Munro [257], Dlg by C. Goodman [365], and Brp by E. Buchner [285]. Anti-mouse and rabbit secondary antibodies were conjugated to Alexa 488, 568, and 633 (Molecular Probes). Larval sensory neuron imaging was collected in live dendritic arborization sensory neurons of third instar larvae. Larva were anesthetized with 15% chloroform and position between 22x22 mm No 1.5 glass coverslips to immobilize them. Neurons from abdominal segments A4-A6 were imaged with cell bodies positioned in the center of a single lateral boarder of the field of view to ensure consistency of imaging across all neurons. [296]. All imaging was done on an Olympus FV1000 or FV3000 scanning confocal microscope with 40X, 60X, or 100X objectives (N.A. 1.30, 1.42, and 1.40 respectively). When shown, maximum Z projections were assembled from 0.4 μm optical sections using Olympus FV software. All image post-processing was done using Adobe Photoshop or ImageJ2 in open-source Fiji [366, 367]. For colocalization analysis, between 3 and 8 images were examined per experiment. Images were manually thresholded and the Pearson Correlation coefficients calculated using the JACoP plugin for ImageJ2/Fiji [368].

Analysis of bouton number, synapse morphology, active zones and dendrite morphology

The number of type 1 synaptic boutons were manually counted at muscles 6 and 7 (m6/7) in abdominal segment 3 (A3) as previously described [237]. A synaptic bouton was

considered to be a distinctive swelling at the NMJ marked by the presence of both the neuronal membrane marker, Hrp, and the post-synaptic density protein, Dlg [248]. Boutons were quantified by counting the number of Hrp+ and Dlg+ synapses at each NMJ. To account for differences between genotypes in the scaling of NMJs to muscle size, synaptic bouton numbers were normalized to muscle surface area (MSA). MSA was calculated using ImageJ2/Fiji from images of m6/7 obtained using a 20X objective (N.A. 0.85). Branching was determined by counting branch points between strings of boutons at least 3 boutons long. The same NMJs were subjected to analysis using the Morphometrics algorithm, A Fiji-based macro that quantifies morphological features of *Drosophila* synapses [369]. The parameters examined here include total bouton counts, NMJ area, and NMJ length. To validate these results, we compared bouton number determined by the macro with manual counts for *scat* mutant analysis.

While total bouton numbers were not identical, macro counts correlated significantly with manual counts (Pearson correlation coefficient = 0.76; C.I. 95% 0.66-0.84; $p < 0.0001$; n = 91 NMJs). Analysis was done using Fiji version 2.0.0 and the NMJ Morphometrics plugin version 20161129. Settings used were maxima noise tolerance = 500, small particle size = 10, minimum bouton size = 10, and rolling ball radius = 500. NMJ outline and skeleton thresholds were set to “triangle”. To quantify active zone number, NMJs were counterstained with antibodies targeting Brp and Hrp as described above. Maximum Z-projections were processed using the TrackMate plugin for ImageJ2/Fiji [370]. Active zone images were opened in TrackMate using the default calibration settings for the Brp channel. The following additional settings were used: LoG

detector = on, estimated blob diameter = 1 μm, and threshold settings = 100. The results were previewed to ensure accurate detection of found spots and data recorded for all boutons. Sensory neuron dendritic morphology was quantified by Branch number, branch junctions, average branch length, and longest shortest path were quantified in Z-series projections of the neurons using Skeletonize2D/3D and AnalyzeSkeleton ImageJ2/Fiji plugins [371-373].

Behavioral analysis

For the analysis of larval crawling, videos were collected using an iPhone XR (Apple) set in time-lapse video mode (2 frames per second). Ten larvae were collected for each genotype and transferred to the center of a room temperature 15 cm petri dish containing 2% agarose. 45-90 second videos of each larva were collected in triplicate. Videos were trimmed to 90 frames using the Apple photo editing trimming tool selecting for direct path larval movement away from the edge of the petri dish. Files were then converted from .MOV to .TIF series using the export function in ImageJ2/Fiji. Subsequent analysis was done using TrackMate, a Fijibased macro developed for single particle tracking [370]. Images were adjusted to maximize contrast between larva and the background. The parameters were adjusted as follows to analyze larval locomotion. Settings used were: LoG detector, HyperStack displayer, simple LAP tracker, and spot tracking were all turned on. The average velocity was recorded for each replicate.

Analysis of scat expression by quantitative real-time PCR (qRT-PCR)

For qRT-PCR analysis, seven larval ventral ganglia from each genotype were explanted and homogenized in TRIzol reagent (Invitrogen) and total RNA was isolated using a Direct-zol RNA purification kit (Zymogen). RNA concentration and quality were determined using a RNA IQ Assay Kit (Qubit) and a Quibit 4 Fluorometer. RNA quality scores were all above 9.2 indicating that all samples contained high-quality and undegraded RNA. cDNA was synthesized from 1µg of total RNA for each genotype using a double-primed RNA to cDNA EcoDry premix (Clonetech). qPCR primers were designed using Primer3 software to amplify a ~150 nt amplicon near the 3' end of the *scat* mRNA. As an internal reference gene, primers were designed to amplify an amplicon of similar size in the housekeeping gene encoding for ribosomal protein S3 (RpS3). This protein is a core component of the small ribosomal subunit. qRT-PCR was conducted on an iQ5 Real Time PCR System (BioRad) using the SsoAdvanced Universal SYBR Green Supermix (BioRad). Three technical replicants were done for each genotype. Melt curve analysis was done at the end of each run and indicated that neither primer set amplified non-specific products. Threshold cycle (Ct) values for each sample were selected by the iQ5 software. The analysis of differential fold change was done using the Livak (ΔΔCt) method [374].

Primer sequences

The sequences of primers used to generate the *UAS-HA:scat* (inducible) and *scat-HA:scat* (genomic rescue) constructs and for qRT-PCR analysis are listed in the table below.

Primer list:

Cloning of *scat* from LD2244 into pUAST (to generate the inducible HA:Scat line)	
Primer pair	Sequence (5' to 3')
Scat_HAf	GATCTTGCGGCCGCATGGCC ACGACAAGATCCGC
Scat_HAr	GGTACCCTCGAGTTAAGCGTAATCTGGAACATCGTA TGGGTAGTAGAGCCAGATCTCCTCCA
Cloning of *scat* from genomic DNA into pCASPR (to generate the genomic rescue line)	
Primer pair	Sequence (5' to 3')
Scat rescue F1	GATCTTGCGGCCGCGTCAGCTGATTTTGCTCAGA
Scat rescue R1	TCAAGCGTAATCTGGAACATCGTATGGGTAGTAGAGCCAGATCTCCTCCA
Scat rescue F2	TACCCATACGATGTTCCAGATTACGCTTGAGCATTCCGAAGTATTCCATA
Scat rescue R2	GGTACCCTCGAGCTTTCACCCCTAAGTTGCAT
Quantitative RT-PCR experiments (for Fig. S1)	
Primer pair	Sequence (5' to 3')
Scat_qPf	ACGAAACTATCGAGCGGGAC
Scat_qPr	TTGAGCTGCCAATCTCTCGG
RpS3_qPf	TCTTTCTTTTCTGCGCACCA
RpS3_qPr	TCGCATTCATTTTGACGTCG

Statistics

All data was recorded in Excel (Microsoft) and graphed and analyzed in Prism (GraphPad) or Excel (Microsoft). Results were considered to be statistically significant at $p < 0.05$. Results shown throughout the study are mean ± SEM. Data for $scat^{1}$ loss of function and larval crawling velocity were both analyzed by Kruskal-Wallis followed by a Dunn's multiple comparison test to determine significance. Each *scat* RNAi experiment had its own control and was analyzed using a Mann-Whitney U test. The number of synaptic boutons and Brp-positive AZs in genetic interaction experiments were both analyzed by one-way ANOVA followed by a Holm-Sidak multiple comparison test. *ppkGal4*-driven *scat* knockdown sensory neuron analysis was all analyzed by two sample t-Test assuming unequal variances.

Age progressive neurodegeneration and scat

Drosophila genetics

The following fly lines were obtained from the Bloomington Stock Center: *UAS-TRiP(HMS01910), UAS-LUC.VALIUM10, C380-Gal4, UAS-YFP:Rab7, UAS-YFP:Rab7(T22N), UAS-YFP:Rab11, UAS-YFP:Rab11(S25N). w^{1118}* and *P(PZ)scat1cn1.* The *scat1cn1* flies were crossed with w^{1118} to normalize the genetic background. Both *UAS-TRiP(HMS01910)* and *UAS-LUC.VALIUM10* were crossed with *C380-Gal4* to create motor neuron specific expression of genetic variant. Those new *C380-Gal4;UAS* lines were then crossed with *UAS-YFP:Rab* lines to produce the experimental generation of larvae. Three new lines of flies were generated utilizing the mobilizing P-element insertion in the $scat^{1}$ allele. The first new mutant allele (*scat* Δ*312)* was created by deleting a P-element from the 3' end of the *scat* gene and introducing an in-frame stop codon resulting in the loss of 663 amino acids from the polypeptide end. The resulting truncated *scat* Δ*312* protein contains 280 amino acids, 277 of which correspond to the N-terminus of scat. The second new mutant allele *(scat* Δ*244)* was created in the same manner and produces a functionally null truncation consisting of 103 amino acids, 62 of which correspond to the N-terminus of scat. The resulting truncated protein is seemingly not stable and degraded shortly after translation. Both mutant alleles show male sterility and semi-lethality similar to that of the original $scat^{1}$ line. Finally, a line (*scat329(PE)*) was created to act as the *scat* rescue control for genetic background of the new *scat* mutants. This control line was created by precisely excising the P-element insertion from the $scat^{1}$ flies to repair lesions that were created by

the insertion of the P-element originally. This genetic control line rescues the male sterility and semi-lethality phenotypes exhibited by the *scat*^{1} flies.

Drosophila Longevity assay

Adult flies were collected within 24 hours post-eclosion and split into male and female populations. Flies were maintained at 25˚C, 65% humidity and 12:12 hour light-dark on standard Bloomington media and transferred to new vials every 48 hours. The death of individual flies was recorded during the transfer process to new vials. The populations were monitored until all individuals were dead [375]. All data was recorded in Microsoft Excel and further processed using Prism-GraphPad and Microsoft Excel.

Population Gender Ratios

Adult flies were collected at random within 24 hours post-eclosion. Flies were then separated by gender under a dissecting microscope and counted. Data was recorded and processed in Microsoft Excel.

Quantification of adult Drosophila body size

Flies were collected within 24 hours post-eclosion and allowed to age an additional 24 hours for normalization of body size. Flies were anesthetized with CO_2 and the ventral side of the abdomen was imaged using Leica S9i stereo microscope with 10 MP CMOS-camera. The area of the thorax and abdomen, or length from rostral to caudal ends were

determined using open-source Fiji image analysis. Body sizes were recorded and processed in Microsoft Excel.

Whole fly sectioning and staining

Flies were collected within 24 hours post-eclosion and maintain at 25˚C on standard Bloomington media until aged to desired time point. Flies were anesthetized using CO_2 and oriented in embedding collar so that the thorax sat above blades. The collar was placed in a glass container and the tissue was the fixed overnight at 4˚C with Carnoy's fixative. Tissue was the dehydrated by moving the collar from Carnoy's fixative to 40%, 70%, 100% ethanol respectively for 20 minutes at room temperature. Tissue was moved to a 1:1 solution of methyl benzoate: paraffin wax and incubated at 65˚C for an hour. To embed the tissue, the collar was moved to a foil pocket and filled with melted paraffin wax. Once filled, the foil pocket containing the collar was incubated at 65˚C for 2 hours. The pocket was then moved to room temperature and left overnight to allow the wax to harden.

Paraffin embedded tissue was sectioned using a standard microtome into 10 micrometer segments. Paraffin segments were floated in cold water and collected onto charged glass microscope slides stored on coverslip rack at room temperature for 2 hours to dry. Slides were deparaffinized by incubating slides in xylene for 15 minutes.

Tissue was rehydrated before staining by treating slides with 100%, 95%, 80% ethanol and diH_2O for 10 minutes respectively. Tissue was stained by treating slides with Hematoxylin for 5 minutes and Eosin for 30 seconds, with appropriate washes in between treatments (diH_2O, 95% ethanol respectively). Tissue was dehydrated once again by

treating slides with 95% then 100% ethanol for 15 minutes each and stored in xylene overnight at room temperature [376]. Permount, a xylene based mounting media, was used to mount and store stained sections. Sections were imaged using a Laxco SeBa 2 series digital microscope system with a 10X objective (N.A. 1.25).

Quantification of dorsal longitudinal muscle size

Images of paraffin embedded tissue sections were collected using a Laxco SeBa 2 series digital microscope system with a 10X objective (N.A. 1.25). The area of the dorsal longitudinal muscles was determined using open-source Fiji image analysis by tracing around the perimeter of all 12 dorsal longitudinal muscles bundled together excluding any space between individual muscles. The area of the thorax was determined by tracing around the cuticle of the section. Sections with less than 90% intact cuticle were excluded from analysis. Muscle area and thoracic area were recorded and processed in Microsoft Excel.

Spontaneous flight assay

Flies were collected within 24 hours post-eclosion and maintain at 25˚C on standard Bloomington media until aged to desired time point. For behavioral analysis flies were collected and transferred into an empty containment vial. Flies were dropped from containment vial into 500 ml cylinder by a standard funnel. The inside of the cylinder was coated with a thin layer of mineral oil. When dropped into freefall, flies reflexively respond by flying laterally from the drop point, thus getting stuck into the mineral oil coated on the

side of the cylinder. The height of the flies stuck within the cylinder were recorded in Microsoft Excel and data further processed in Prism-GraphPad and Microsoft Excel.

Negative geotaxis assay

Flies were collected within 24 hours post-eclosion and maintain at 25˚C on standard Bloomington media until aged to desired time point. Flies tapped to the bottom of a container exhibit a climbing reflex, where they favor climbing over flight to regain position at the top of a container. For behavioral analysis, flies were transferred into empty *Drosophila* vials. Video of animal behavior was recorded using MacBook Air photobooth video recording software. Flies were tapped down to the bottom of an empty vial and allowed to climb the sides of the vial for 90 seconds, all genotypes were tested in triplicate. Data was analyzed by hand focusing on individual video frames. The number of flies that reflexively climb at least 1 cm in 30 seconds were recorded for each group. Mutant flies exhibit a "bang" phenotype that causes mild seizure like behavior immediately following relocation to the bottom of the vial. To account for recovery differences seen between genotypes the number of flies to cross the threshold was counted only after the first individual crossed the 1 cm threshold. All data was recorded in Microsoft Excel and further processed in Prism-GraphPad.

Bang sensitivity assay

The bang-sensitivity test were performed as previously described [327]. Post eclosion, 100 female flies per genotype were collected under CO_2 and moved to a fresh

food vial, of standard Bloomington media, and allowed overnight recovery. For testing, flies were transferred into an empty vial and stimulated with a vortex mixer at maximum speed for 10 seconds. The bang-sensitive phenotype was scored by the number of flies that did not experience temporary paralysis or seizure lasting more than 20 seconds. Flies were tested and results from several days pooled prior to final data analysis. Data was processed analyzed in Microsoft excel.

REFERENCES

1. Liu, E.Y., C.P. Cali, and E.B. Lee, *RNA metabolism in neurodegenerative disease.* Dis Model Mech, 2017. **10**(5): p. 509-518.
2. Heemels, M.-T., *Neurodegenerative diseases.* Nature, 2016. **539**(7628): p. 179-179.
3. Deal, S.L. and S. Yamamoto, *Unraveling Novel Mechanisms of Neurodegeneration Through a Large-Scale Forward Genetic Screen in Drosophila.* Frontiers in Genetics, 2019. **9**.
4. Niccoli, T. and L. Partridge, *Ageing as a Risk Factor for Disease.* Current Biology, 2012. **22**(17): p. R741-R752.
5. Abeliovich, A. and A.D. Gitler, *Defects in trafficking bridge Parkinson's disease pathology and genetics.* Nature, 2016. **539**(7628): p. 207-216.
6. Canter, R.G., J. Penney, and L.-H. Tsai, *The road to restoring neural circuits for the treatment of Alzheimer's disease.* Nature, 2016. **539**(7628): p. 187-196.
7. Taylor, J.P., R.H. Brown, and D.W. Cleveland, *Decoding ALS: from genes to mechanism.* Nature, 2016. **539**(7628): p. 197-206.
8. Wyss-Coray, T., *Ageing, neurodegeneration and brain rejuvenation.* Nature, 2016. **539**(7628): p. 180-186.
9. Ponomareva, O.Y., K.W. Eliceiri, and M.C. Halloran, *Charcot-Marie-Tooth 2b associated Rab7 mutations cause axon growth and guidance defects during vertebrate sensory neuron development.* 2016. **11**(1).
10. Gitler, A.D., P. Dhillon, and J. Shorter, *Neurodegenerative disease: models, mechanisms, and a new hope.* Dis Model Mech, 2017. **10**(5): p. 499-502.
11. Neumann, M., et al., *Ubiquitinated TDP-43 in frontotemporal lobar degeneration and amyotrophic lateral sclerosis.* Science, 2006. **314**(5796): p. 130-3.
12. Van Deerlin, V.M., et al., *TARDBP mutations in amyotrophic lateral sclerosis with TDP-43 neuropathology: a genetic and histopathological analysis.* Lancet Neurol, 2008. **7**(5): p. 409-16.
13. Gitcho, M.A., et al., *TDP-43 A315T mutation in familial motor neuron disease.* Ann Neurol, 2008. **63**(4): p. 535-8.
14. Kabashi, E., et al., *TARDBP mutations in individuals with sporadic and familial amyotrophic lateral sclerosis.* Nat Genet, 2008. **40**(5): p. 572-4.
15. Sreedharan, J., et al., *TDP-43 mutations in familial and sporadic amyotrophic lateral sclerosis.* Science, 2008. **319**(5870): p. 1668-72.
16. Kwiatkowski, T.J., Jr., et al., *Mutations in the FUS/TLS gene on chromosome 16 cause familial amyotrophic lateral sclerosis.* Science, 2009. **323**(5918): p. 1205-8.
17. Vance, C., et al., *Mutations in FUS, an RNA processing protein, cause familial amyotrophic lateral sclerosis type 6.* Science, 2009. **323**(5918): p. 1208-1211.
18. Costessi, L., et al., *TDP-43 regulates β-adducin (Add2) transcript stability.* RNA Biol, 2014. **11**(10): p. 1280-90.
19. Liu, X., et al., *Long non-coding RNA gadd7 interacts with TDP-43 and regulates Cdk6 mRNA decay.* Embo j, 2012. **31**(23): p. 4415-27.

20. Strong, M.J., et al., *TDP43 is a human low molecular weight neurofilament (hNFL) mRNA-binding protein.* Mol Cell Neurosci, 2007. **35**(2): p. 320-7.
21. Alami, N.H., et al., *Axonal transport of TDP-43 mRNA granules is impaired by ALS-causing mutations.* Neuron, 2014. **81**(3): p. 536-543.
22. Buratti, E., et al., *Nuclear factor TDP-43 and SR proteins promote in vitro and in vivo CFTR exon 9 skipping.* Embo j, 2001. **20**(7): p. 1774-84.
23. Ling, J.P., et al., *TDP-43 repression of nonconserved cryptic exons is compromised in ALS-FTD.* Science, 2015. **349**(6248): p. 650-5.
24. Shiga, A., et al., *Alteration of POLDIP3 splicing associated with loss of function of TDP-43 in tissues affected with ALS.* PLoS One, 2012. **7**(8): p. e43120.
25. Tollervey, J.R., et al., *Characterizing the RNA targets and position-dependent splicing regulation by TDP-43.* Nature Neuroscience, 2011. **14**(4): p. 452-458.
26. Wang, W.-X., et al., *The expression of microRNA miR-107 decreases early in Alzheimer's disease and may accelerate disease progression through regulation of beta-site amyloid precursor protein-cleaving enzyme 1.* The Journal of neuroscience : the official journal of the Society for Neuroscience, 2008. **28**(5): p. 1213-1223.
27. Yang, L., et al., *Oncoprotein TLS interacts with serine-arginine proteins involved in RNA splicing.* J Biol Chem, 1998. **273**(43): p. 27761-4.
28. Kim, H.J., et al., *Mutations in prion-like domains in hnRNPA2B1 and hnRNPA1 cause multisystem proteinopathy and ALS.* Nature, 2013. **495**(7442): p. 467-473.
29. Li, Y.R., et al., *Stress granules as crucibles of ALS pathogenesis.* J Cell Biol, 2013. **201**(3): p. 361-72.
30. Courchaine, E.M., A. Lu, and K.M. Neugebauer, *Droplet organelles?* The EMBO Journal, 2016. **35**(15): p. 1603-1612.
31. Molliex, A., et al., *Phase separation by low complexity domains promotes stress granule assembly and drives pathological fibrillization.* Cell, 2015. **163**(1): p. 123-33.
32. Wolozin, B. and P. Ivanov, *Stress granules and neurodegeneration.* Nature Reviews Neuroscience, 2019. **20**(11): p. 649-666.
33. Fu, L., Y.S. Gao, and E. Sztul, *Transcriptional repression and cell death induced by nuclear aggregates of non-polyglutamine protein.* Neurobiol Dis, 2005. **20**(3): p. 656-65.
34. Polymenidou, M., et al., *Long pre-mRNA depletion and RNA missplicing contribute to neuronal vulnerability from loss of TDP-43.* Nature Neuroscience, 2011. **14**(4): p. 459-468.
35. Lagier-Tourenne, C., et al., *Targeted degradation of sense and antisense C9orf72 RNA foci as therapy for ALS and frontotemporal degeneration.* Proceedings of the National Academy of Sciences, 2013. **110**(47): p. E4530.
36. Rohilla, K.J. and K.T. Gagnon, *RNA biology of disease-associated microsatellite repeat expansions.* Acta Neuropathologica Communications, 2017. **5**(1): p. 63.
37. Iwahashi, C.K., et al., *Protein composition of the intranuclear inclusions of FXTAS.* Brain, 2006. **129**(Pt 1): p. 256-71.

38. Jiang, H., et al., *Myotonic dystrophy type 1 is associated with nuclear foci of mutant RNA, sequestration of muscleblind proteins and deregulated alternative splicing in neurons.* Hum Mol Genet, 2004. **13**(24): p. 3079-88.
39. Lee, Y.B., et al., *Hexanucleotide repeats in ALS/FTD form length-dependent RNA foci, sequester RNA binding proteins, and are neurotoxic.* Cell Rep, 2013. **5**(5): p. 1178-86.
40. Brook, J.D., et al., *Molecular basis of myotonic dystrophy: expansion of a trinucleotide (CTG) repeat at the 3' end of a transcript encoding a protein kinase family member.* Cell, 1992. **68**(4): p. 799-808.
41. Miller, J.W., et al., *Recruitment of human muscleblind proteins to (CUG)(n) expansions associated with myotonic dystrophy.* The EMBO journal, 2000. **19**(17): p. 4439-4448.
42. Batra, R., et al., *Loss of MBNL leads to disruption of developmentally regulated alternative polyadenylation in RNA-mediated disease.* Mol Cell, 2014. **56**(2): p. 311-322.
43. Goodwin, M., et al., *MBNL Sequestration by Toxic RNAs and RNA Misprocessing in the Myotonic Dystrophy Brain.* Cell Rep, 2015. **12**(7): p. 1159-68.
44. Wang, E.T., et al., *Transcriptome-wide regulation of pre-mRNA splicing and mRNA localization by muscleblind proteins.* Cell, 2012. **150**(4): p. 710-24.
45. Jin, P., et al., *Pur alpha binds to rCGG repeats and modulates repeat-mediated neurodegeneration in a Drosophila model of fragile X tremor/ataxia syndrome.* Neuron, 2007. **55**(4): p. 556-564.
46. Sofola, O.A., et al., *RNA-binding proteins hnRNP A2/B1 and CUGBP1 suppress fragile X CGG premutation repeat-induced neurodegeneration in a Drosophila model of FXTAS.* Neuron, 2007. **55**(4): p. 565-71.
47. Sellier, C., et al., *Sam68 sequestration and partial loss of function are associated with splicing alterations in FXTAS patients.* 2010. **29**(7): p. 1248-1261.
48. Sellier, C., et al., *Sequestration of DROSHA and DGCR8 by expanded CGG RNA repeats alters microRNA processing in fragile X-associated tremor/ataxia syndrome.* Cell Rep, 2013. **3**(3): p. 869-80.
49. DeJesus-Hernandez, M., et al., *Expanded GGGGCC hexanucleotide repeat in noncoding region of C9ORF72 causes chromosome 9p-linked FTD and ALS.* Neuron, 2011. **72**(2): p. 245-256.
50. Gendron, T.F., et al., *Antisense transcripts of the expanded C9ORF72 hexanucleotide repeat form nuclear RNA foci and undergo repeat-associated non-ATG translation in c9FTD/ALS.* Acta Neuropathol, 2013. **126**(6): p. 829-44.
51. Renton, A.E., et al., *A hexanucleotide repeat expansion in C9ORF72 is the cause of chromosome 9p21-linked ALS-FTD.* Neuron, 2011. **72**(2): p. 257-68.
52. Zu, T., et al., *RAN proteins and RNA foci from antisense transcripts in C9ORF72 ALS and frontotemporal dementia.* Proceedings of the National Academy of Sciences, 2013. **110**(51): p. E4968.
53. Cooper-Knock, J., et al., *Sequestration of multiple RNA recognition motif-containing proteins by C9orf72 repeat expansions.* Brain, 2014. **137**(Pt 7): p. 2040-51.

54. Hardy, J. and D.J. Selkoe, *The amyloid hypothesis of Alzheimer's disease: progress and problems on the road to therapeutics.* Science, 2002. **297**(5580): p. 353-6.
55. Cech, T.R. and J.A. Steitz, *The noncoding RNA revolution-trashing old rules to forge new ones.* Cell, 2014. **157**(1): p. 77-94.
56. Cairns, N.J., V.M.Y. Lee, and J.Q. Trojanowski, *The cytoskeleton in neurodegenerative diseases.* The Journal of pathology, 2004. **204**(4): p. 438-449.
57. Lariviere, R.C. and J.P. Julien, *Functions of intermediate filaments in neuronal development and disease.* J Neurobiol, 2004. **58**(1): p. 131-48.
58. Hill, W.D., et al., *Epitopes located in spatially separate domains of each neurofilament subunit are present in Parkinson's disease Lewy bodies.* J Comp Neurol, 1991. **309**(1): p. 150-60.
59. Schmidt, M.L., et al., *Epitope map of neurofilament protein domains in cortical and peripheral nervous system Lewy bodies.* The American journal of pathology, 1991. **139**(1): p. 53-65.
60. Jordanova, A., et al., *Mutations in the neurofilament light chain gene (NEFL) cause early onset severe Charcot–Marie–Tooth disease.* Brain, 2003. **126**(3): p. 590-597.
61. De Jonghe, P., et al., *Further evidence that neurofilament light chain gene mutations can cause Charcot-Marie-Tooth disease type 2E.* Ann Neurol, 2001. **49**(2): p. 245-9.
62. Fabrizi, G.M., et al., *Giant axon and neurofilament accumulation in Charcot-Marie-Tooth disease type 2E.* Neurology, 2004. **62**(8): p. 1429-31.
63. Liu, Q., et al., *Neurofilamentopathy in neurodegenerative diseases.* The open neurology journal, 2011. **5**: p. 58-62.
64. Figlewicz, D.A., et al., *Variants of the heavy neurofilament subunit are associated with the development of amyotrophic lateral sclerosis.* Hum Mol Genet, 1994. **3**(10): p. 1757-61.
65. Al-Chalabi, A., et al., *Deletions of the heavy neurofilament subunit tail in amyotrophic lateral sclerosis.* Hum Mol Genet, 1999. **8**(2): p. 157-64.
66. Hutton, M., et al., *Association of missense and 5'-splice-site mutations in tau with the inherited dementia FTDP-17.* Nature, 1998. **393**(6686): p. 702-5.
67. Rizzu, P., et al., *High prevalence of mutations in the microtubule-associated protein tau in a population study of frontotemporal dementia in the Netherlands.* American journal of human genetics, 1999. **64**(2): p. 414-421.
68. Poorkaj, P., et al., *Tau is a candidate gene for chromosome 17 frontotemporal dementia.* Ann Neurol, 1998. **43**(6): p. 815-25.
69. Foster, N.L., et al., *Frontotemporal dementia and parkinsonism linked to chromosome 17: a consensus conference. Conference Participants.* Ann Neurol, 1997. **41**(6): p. 706-15.
70. Spillantini, M.G., et al., *Mutation in the tau gene in familial multiple system tauopathy with presenile dementia.* Proceedings of the National Academy of Sciences of the United States of America, 1998. **95**(13): p. 7737-7741.
71. Cleveland, D.W., S.Y. Hwo, and M.W. Kirschner, *Purification of tau, a microtubule-associated protein that induces assembly of microtubules from purified tubulin.* J Mol Biol, 1977. **116**(2): p. 207-25.

72. Binder, L.I., A. Frankfurter, and L.I. Rebhun, *The distribution of tau in the mammalian central nervous system.* J Cell Biol, 1985. **101**(4): p. 1371-8.
73. Couchie, D., et al., *Primary structure of high molecular weight tau present in the peripheral nervous system.* Proceedings of the National Academy of Sciences of the United States of America, 1992. **89**(10): p. 4378-4381.
74. Goedert, M., et al., *Multiple isoforms of human microtubule-associated protein tau: sequences and localization in neurofibrillary tangles of Alzheimer's disease.* Neuron, 1989. **3**(4): p. 519-26.
75. Goedert, M., et al., *Cloning and sequencing of the cDNA encoding an isoform of microtubule-associated protein tau containing four tandem repeats: differential expression of tau protein mRNAs in human brain.* The EMBO journal, 1989. **8**(2): p. 393-399.
76. Weingarten, M.D., et al., *A protein factor essential for microtubule assembly.* Proc Natl Acad Sci U S A, 1975. **72**(5): p. 1858-62.
77. Lee, G., R.L. Neve, and K.S. Kosik, *The microtubule binding domain of tau protein.* Neuron, 1989. **2**(6): p. 1615-24.
78. Butner, K.A. and M.W. Kirschner, *Tau protein binds to microtubules through a flexible array of distributed weak sites.* J Cell Biol, 1991. **115**(3): p. 717-30.
79. Drechsel, D.N., et al., *Modulation of the dynamic instability of tubulin assembly by the microtubule-associated protein tau.* Molecular biology of the cell, 1992. **3**(10): p. 1141-1154.
80. Yoshida, H. and Y. Ihara, *Tau in paired helical filaments is functionally distinct from fetal tau: assembly incompetence of paired helical filament-tau.* J Neurochem, 1993. **61**(3): p. 1183-6.
81. Bramblett, G.T., et al., *Abnormal tau phosphorylation at Ser396 in Alzheimer's disease recapitulates development and contributes to reduced microtubule binding.* Neuron, 1993. **10**(6): p. 1089-99.
82. Biernat, J., et al., *Phosphorylation of Ser262 strongly reduces binding of tau to microtubules: distinction between PHF-like immunoreactivity and microtubule binding.* Neuron, 1993. **11**(1): p. 153-63.
83. Hasegawa, M., et al., *Characterization of mAb AP422, a novel phosphorylation-dependent monoclonal antibody against tau protein.* FEBS Lett, 1996. **384**(1): p. 25-30.
84. Hoffmann, R., et al., *Unique Alzheimer's disease paired helical filament specific epitopes involve double phosphorylation at specific sites.* Biochemistry, 1997. **36**(26): p. 8114-24.
85. Zheng-Fischhöfer, Q., et al., *Sequential phosphorylation of Tau by glycogen synthase kinase-3beta and protein kinase A at Thr212 and Ser214 generates the Alzheimer-specific epitope of antibody AT100 and requires a paired-helical-filament-like conformation.* Eur J Biochem, 1998. **252**(3): p. 542-52.
86. Lee, V.M., et al., *Monoclonal antibodies distinguish several differentially phosphorylated states of the two largest rat neurofilament subunits (NF-H and NF-M) and demonstrate their existence in the normal nervous system of adult rats.* J Neurosci, 1987. **7**(11): p. 3474-88.

87. Carden, M.J., et al., *Two-stage expression of neurofilament polypeptides during rat neurogenesis with early establishment of adult phosphorylation patterns.* J Neurosci, 1987. **7**(11): p. 3489-504.
88. Schmidt, M.L., et al., *Phosphate dependent and independent neurofilament epitopes in the axonal swellings of patients with motor neuron disease and controls.* Lab Invest, 1987. **56**(3): p. 282-94.
89. Manetto, V., et al., *Phosphorylation of neurofilaments is altered in amyotrophic lateral sclerosis.* J Neuropathol Exp Neurol, 1988. **47**(6): p. 642-53.
90. Leigh, P.N., et al., *Cytoskeletal abnormalities in motor neuron disease. An immunocytochemical study.* Brain, 1989. **112 (Pt 2)**: p. 521-35.
91. Goldstein, M.E., N.H. Sternberger, and L.A. Sternberger, *Phosphorylation protects neurofilaments against proteolysis.* J Neuroimmunol, 1987. **14**(2): p. 149-60.
92. Fliegner, K.H., et al., *Expression of the gene for the neuronal intermediate filament protein alpha-internexin coincides with the onset of neuronal differentiation in the developing rat nervous system.* J Comp Neurol, 1994. **342**(2): p. 161-73.
93. Cairns, N.J., et al., *alpha-internexin is present in the pathological inclusions of neuronal intermediate filament inclusion disease.* The American journal of pathology, 2004. **164**(6): p. 2153-2161.
94. Cairns, N.J., et al., *alpha-Internexin aggregates are abundant in neuronal intermediate filament inclusion disease (NIFID) but rare in other neurodegenerative diseases.* Acta neuropathologica, 2004. **108**(3): p. 213-223.
95. Josephs, K.A., et al., *Neurofilament inclusion body disease: a new proteinopathy?* Brain, 2003. **126**(Pt 10): p. 2291-303.
96. He, C.Z. and A.P. Hays, *Expression of peripherin in ubiquinated inclusions of amyotrophic lateral sclerosis.* J Neurol Sci, 2004. **217**(1): p. 47-54.
97. Strong, M.J., et al., *Phosphorylation state of the native high-molecular-weight neurofilament subunit protein from cervical spinal cord in sporadic amyotrophic lateral sclerosis.* J Neurochem, 2001. **76**(5): p. 1315-25.
98. Roy, S., et al., *Axonal transport defects: a common theme in neurodegenerative diseases.* Acta Neuropathol, 2005. **109**(1): p. 5-13.
99. Ishikawa, T., *Structural biology of cytoplasmic and axonemal dyneins.* Journal of structural biology, 2012. **179**(2): p. 229-234.
100. Wade, R.H., *Microtubules: an overview.* Methods Mol Med, 2007. **137**: p. 1-16.
101. Ballatore, C., et al., *Microtubule stabilizing agents as potential treatment for Alzheimer's disease and related neurodegenerative tauopathies.* Journal of medicinal chemistry, 2012. **55**(21): p. 8979-8996.
102. Brunden, K.R., et al., *Microtubule-stabilizing agents as potential therapeutics for neurodegenerative disease.* Bioorg Med Chem, 2014. **22**(18): p. 5040-9.
103. Johnson, V.E., W. Stewart, and D.H. Smith, *Axonal pathology in traumatic brain injury.* Exp Neurol, 2013. **246**: p. 35-43.
104. Tang-Schomer, M.D., et al., *Partial interruption of axonal transport due to microtubule breakage accounts for the formation of periodic varicosities after traumatic axonal injury.* Exp Neurol, 2012. **233**(1): p. 364-72.

105. Tang-Schomer, M.D., et al., *Mechanical breaking of microtubules in axons during dynamic stretch injury underlies delayed elasticity, microtubule disassembly, and axon degeneration.* Faseb j, 2010. **24**(5): p. 1401-10.
106. Matsuda, W., et al., *Single Nigrostriatal Dopaminergic Neurons Form Widely Spread and Highly Dense Axonal Arborizations in the Neostriatum.* The Journal of Neuroscience, 2009. **29**(2): p. 444.
107. Burré, J., *The Synaptic Function of α-Synuclein.* Journal of Parkinson's disease, 2015. **5**(4): p. 699-713.
108. Lee, H.J., et al., *Impairment of microtubule-dependent trafficking by overexpression of alpha-synuclein.* Eur J Neurosci, 2006. **24**(11): p. 3153-62.
109. Fanara, P., et al., *Cerebrospinal fluid–based kinetic biomarkers of axonal transport in monitoring neurodegeneration.* The Journal of Clinical Investigation, 2012. **122**(9): p. 3159-3169.
110. Haggerty, T., et al., *Hyperphosphorylated Tau in an α-synuclein-overexpressing transgenic model of Parkinson's disease.* The European journal of neuroscience, 2011. **33**(9): p. 1598-1610.
111. Kaul, T., et al., *Region-specific tauopathy and synucleinopathy in brain of the alpha-synuclein overexpressing mouse model of Parkinson's disease.* BMC neuroscience, 2011. **12**: p. 79-79.
112. Wills, J., et al., *Tauopathic changes in the striatum of A53T α-synuclein mutant mouse model of Parkinson's disease.* PloS one, 2011. **6**(3): p. e17953-e17953.
113. Paisán-Ruíz, C., et al., *Cloning of the gene containing mutations that cause PARK8-linked Parkinson's disease.* Neuron, 2004. **44**(4): p. 595-600.
114. Zimprich, A., et al., *Mutations in LRRK2 cause autosomal-dominant parkinsonism with pleomorphic pathology.* Neuron, 2004. **44**(4): p. 601-7.
115. Kawakami, F., et al., *LRRK2 Phosphorylates Tubulin-Associated Tau but Not the Free Molecule: LRRK2-Mediated Regulation of the Tau-Tubulin Association and Neurite Outgrowth.* PLoS ONE, 2012. **7**(1): p. e30834.
116. Kett, L.R., et al., *LRRK2 Parkinson disease mutations enhance its microtubule association.* Hum Mol Genet, 2012. **21**(4): p. 890-9.
117. Kitada, T., et al., *Mutations in the parkin gene cause autosomal recessive juvenile parkinsonism.* Nature, 1998. **392**(6676): p. 605-608.
118. Oliveira, S.A., et al., *Parkin mutations and susceptibility alleles in late-onset Parkinson's disease.* Ann Neurol, 2003. **53**(5): p. 624-9.
119. Ren, Y., et al., *Parkin mutations reduce the complexity of neuronal processes in iPSC-derived human neurons.* Stem Cells, 2015. **33**(1): p. 68-78.
120. Jiang, Q., Y. Ren, and J. Feng, *Direct Binding with Histone Deacetylase 6 Mediates the Reversible Recruitment of Parkin to the Centrosome.* The Journal of Neuroscience, 2008. **28**(48): p. 12993.
121. Williamson, T.L. and D.W. Cleveland, *Slowing of axonal transport is a very early event in the toxicity of ALS-linked SOD1 mutants to motor neurons.* Nat Neurosci, 1999. **2**(1): p. 50-6.

122. Zhang, B., et al., *Neurofilaments and orthograde transport are reduced in ventral root axons of transgenic mice that express human SOD1 with a G93A mutation.* J Cell Biol, 1997. **139**(5): p. 1307-15.
123. Fanara, P., et al., *Stabilization of hyperdynamic microtubules is neuroprotective in amyotrophic lateral sclerosis.* J Biol Chem, 2007. **282**(32): p. 23465-72.
124. Kleele, T., et al., *An assay to image neuronal microtubule dynamics in mice.* Nature Communications, 2014. **5**(1): p. 4827.
125. Münch, C., et al., *Heterozygous R1101K mutation of the DCTN1 gene in a family with ALS and FTD.* Ann Neurol, 2005. **58**(5): p. 777-80.
126. Puls, I., et al., *Mutant dynactin in motor neuron disease.* Nat Genet, 2003. **33**(4): p. 455-6.
127. Cohen, T.J., V.M. Lee, and J.Q. Trojanowski, *TDP-43 functions and pathogenic mechanisms implicated in TDP-43 proteinopathies.* Trends Mol Med, 2011. **17**(11): p. 659-67.
128. Peters, O.M., M. Ghasemi, and R.H. Brown, Jr., *Emerging mechanisms of molecular pathology in ALS.* J Clin Invest, 2015. **125**(5): p. 1767-79.
129. Baldwin, K.R., et al., *Axonal transport defects are a common phenotype inDrosophilamodels of ALS.* 2016: p. ddw105.
130. Farg, M.A., et al., *C9ORF72, implicated in amytrophic lateral sclerosis and frontotemporal dementia, regulates endosomal trafficking.* Human Molecular Genetics, 2014. **23**(13): p. 3579-3595.
131. Goate, A., et al., *Segregation of a missense mutation in the amyloid precursor protein gene with familial Alzheimer's disease.* Nature, 1991. **349**(6311): p. 704-6.
132. Levy-Lahad, E., et al., *Candidate gene for the chromosome 1 familial Alzheimer's disease locus.* Science, 1995. **269**(5226): p. 973-7.
133. Sherrington, R., et al., *Cloning of a gene bearing missense mutations in early-onset familial Alzheimer's disease.* Nature, 1995. **375**(6534): p. 754-760.
134. Zhang, Y.-w., et al., *APP processing in Alzheimer's disease.* Molecular Brain, 2011. **4**(1): p. 3.
135. Selkoe, D.J., *The cell biology of beta-amyloid precursor protein and presenilin in Alzheimer's disease.* Trends Cell Biol, 1998. **8**(11): p. 447-53.
136. Evin, G. and A. Weidemann, *Biogenesis and metabolism of Alzheimer's disease Abeta amyloid peptides.* Peptides, 2002. **23**(7): p. 1285-97.
137. Spoelgen, R., et al., *Interaction of the cytosolic domains of sorLA/LR11 with the amyloid precursor protein (APP) and beta-secretase beta-site APP-cleaving enzyme.* J Neurosci, 2006. **26**(2): p. 418-28.
138. He, X., et al., *Memapsin 2 (beta-secretase) cytosolic domain binds to the VHS domains of GGA1 and GGA2: implications on the endocytosis mechanism of memapsin 2.* FEBS Lett, 2002. **524**(1-3): p. 183-7.
139. Santosa, C., et al., *Decreased expression of GGA3 protein in Alzheimer's disease frontal cortex and increased co-distribution of BACE with the amyloid precursor protein.* Neurobiology of disease, 2011. **43**(1): p. 176-183.
140. Finan, G.M., H. Okada, and T.W. Kim, *BACE1 Retrograde Trafficking Is Uniquely Regulated by the Cytoplasmic Domain of Sortilin.* 2011. **286**(14): p. 12602-12616.

141. Tesco, G., et al., *Depletion of GGA3 stabilizes BACE and enhances beta-secretase activity.* Neuron, 2007. **54**(5): p. 721-37.
142. Pietrzik, C.U., et al., *The cytoplasmic domain of the LDL receptor-related protein regulates multiple steps in APP processing.* Embo j, 2002. **21**(21): p. 5691-700.
143. Trommsdorff, M., et al., *Interaction of cytosolic adaptor proteins with neuronal apolipoprotein E receptors and the amyloid precursor protein.* J Biol Chem, 1998. **273**(50): p. 33556-60.
144. Kounnas, M.Z., et al., *LDL receptor-related protein, a multifunctional ApoE receptor, binds secreted beta-amyloid precursor protein and mediates its degradation.* Cell, 1995. **82**(2): p. 331-40.
145. Cataldo, A.M., et al., *Down syndrome fibroblast model of Alzheimer-related endosome pathology: accelerated endocytosis promotes late endocytic defects.* Am J Pathol, 2008. **173**(2): p. 370-84.
146. Cataldo, A.M., et al., *App gene dosage modulates endosomal abnormalities of Alzheimer's disease in a segmental trisomy 16 mouse model of down syndrome.* J Neurosci, 2003. **23**(17): p. 6788-92.
147. MacLeod, D., et al., *The familial Parkinsonism gene LRRK2 regulates neurite process morphology.* Neuron, 2006. **52**(4): p. 587-93.
148. Heo, H.Y., K.-S. Kim, and W. Seol, *Coordinate Regulation of Neurite Outgrowth by LRRK2 and Its Interactor, Rab5.* Experimental neurobiology, 2010. **19**(2): p. 97-105.
149. Dodson, M.W., et al., *Roles of the Drosophila LRRK2 homolog in Rab7-dependent lysosomal positioning.* Human molecular genetics, 2012. **21**(6): p. 1350-1363.
150. Stafa, K., et al., *GTPase activity and neuronal toxicity of Parkinson's disease-associated LRRK2 is regulated by ArfGAP1.* PLoS Genet, 2012. **8**(2): p. e1002526.
151. Abeliovich, A., et al., *Mice lacking alpha-synuclein display functional deficits in the nigrostriatal dopamine system.* Neuron, 2000. **25**(1): p. 239-52.
152. Cullen, P.J., *Endosomal sorting and signalling: an emerging role for sorting nexins.* Nat Rev Mol Cell Biol, 2008. **9**(7): p. 574-82.
153. Lee, J., et al., *Adaptor protein sorting nexin 17 regulates amyloid precursor protein trafficking and processing in the early endosomes.* J Biol Chem, 2008. **283**(17): p. 11501-8.
154. van Kerkhof, P., et al., *Sorting nexin 17 facilitates LRP recycling in the early endosome.* Embo j, 2005. **24**(16): p. 2851-61.
155. Schöbel, S., et al., *A novel sorting nexin modulates endocytic trafficking and alpha-secretase cleavage of the amyloid precursor protein.* J Biol Chem, 2008. **283**(21): p. 14257-68.
156. Okada, H., et al., *Proteomic identification of sorting nexin 6 as a negative regulator of BACE1-mediated APP processing.* Faseb j, 2010. **24**(8): p. 2783-94.
157. Mizutani, R., et al., *Expression of sorting nexin 12 is regulated in developing cerebral cortical neurons.* Journal of Neuroscience Research, 2012. **90**(4): p. 721-731.

158. Sannerud, R., et al., *ADP ribosylation factor 6 (ARF6) controls amyloid precursor protein (APP) processing by mediating the endosomal sorting of BACE1.* Proc Natl Acad Sci U S A, 2011. **108**(34): p. E559-68.
159. Dugan, J.M., et al., *The Ras-related GTP-binding protein, Rab1B, regulates early steps in exocytic transport and processing of beta-amyloid precursor protein.* J Biol Chem, 1995. **270**(18): p. 10982-9.
160. Maltese, W.A., et al., *Retention of the Alzheimer's amyloid precursor fragment C99 in the endoplasmic reticulum prevents formation of amyloid beta-peptide.* J Biol Chem, 2001. **276**(23): p. 20267-79.
161. Cherry, S., et al., *Charcot-Marie-Tooth 2B mutations in rab7 cause dosage-dependent neurodegeneration due to partial loss of function.* Elife, 2013. **2**: p. e01064.
162. McConlogue, L., et al., *Differential effects of a Rab6 mutant on secretory versus amyloidogenic processing of Alzheimer's beta-amyloid precursor protein.* J Biol Chem, 1996. **271**(3): p. 1343-8.
163. Buggia-Prévot, V., et al., *A function for EHD family proteins in unidirectional retrograde dendritic transport of BACE1 and Alzheimer's disease Aβ production.* Cell reports, 2013. **5**(6): p. 1552-1563.
164. Udayar, V., et al., *A paired RNAi and RabGAP overexpression screen identifies Rab11 as a regulator of β-amyloid production.* Cell Rep, 2013. **5**(6): p. 1536-51.
165. Buggia-Prévot, V., et al., *Axonal BACE1 dynamics and targeting in hippocampal neurons: a role for Rab11 GTPase.* Mol Neurodegener, 2014. **9**: p. 1.
166. Seaman, M.N., *Cargo-selective endosomal sorting for retrieval to the Golgi requires retromer.* J Cell Biol, 2004. **165**(1): p. 111-22.
167. Seaman, M.N.J., *The retromer complex – endosomal protein recycling and beyond.* Journal of Cell Science, 2012. **125**(20): p. 4693.
168. Seaman, M.N., *Recycle your receptors with retromer.* Trends Cell Biol, 2005. **15**(2): p. 68-75.
169. Seaman, M.N.J., *Identification of a novel conserved sorting motif required for retromer-mediated endosome-to-TGN retrieval.* Journal of Cell Science, 2007. **120**(14): p. 2378.
170. Belenkaya, T.Y., et al., *The retromer complex influences Wnt secretion by recycling wntless from endosomes to the trans-Golgi network.* Dev Cell, 2008. **14**(1): p. 120-31.
171. Yang, P.T., et al., *Wnt signaling requires retromer-dependent recycling of MIG-14/Wntless in Wnt-producing cells.* Dev Cell, 2008. **14**(1): p. 140-7.
172. Pan, C.L., et al., *C. elegans AP-2 and retromer control Wnt signaling by regulating mig-14/Wntless.* Dev Cell, 2008. **14**(1): p. 132-9.
173. Kim, E., et al., *Implication of mouse Vps26b-Vps29-Vps35 retromer complex in sortilin trafficking.* Biochem Biophys Res Commun, 2010. **403**(2): p. 167-71.
174. Small, S.A., et al., *Model-guided microarray implicates the retromer complex in Alzheimer's disease.* Ann Neurol, 2005. **58**(6): p. 909-19.
175. Wen, L., et al., *VPS35 haploinsufficiency increases Alzheimer's disease neuropathology.* J Cell Biol, 2011. **195**(5): p. 765-79.

176. Muhammad, A., et al., *Retromer deficiency observed in Alzheimer's disease causes hippocampal dysfunction, neurodegeneration, and Abeta accumulation.* Proceedings of the National Academy of Sciences of the United States of America, 2008. **105**(20): p. 7327-7332.
177. Mecozzi, V.J., et al., *Pharmacological chaperones stabilize retromer to limit APP processing.* Nature chemical biology, 2014. **10**(6): p. 443-449.
178. Zimprich, A., et al., *A mutation in VPS35, encoding a subunit of the retromer complex, causes late-onset Parkinson disease.* Am J Hum Genet, 2011. **89**(1): p. 168-75.
179. Vilariño-Güell, C., et al., *VPS35 mutations in Parkinson disease.* Am J Hum Genet, 2011. **89**(1): p. 162-7.
180. Ando, M., et al., *VPS35 mutation in Japanese patients with typical Parkinson's disease.* Mov Disord, 2012. **27**(11): p. 1413-7.
181. Scherzer, C.R., et al., *Loss of apolipoprotein E receptor LR11 in Alzheimer disease.* Arch Neurol, 2004. **61**(8): p. 1200-5.
182. Rogaeva, E., et al., *The neuronal sortilin-related receptor SORL1 is genetically associated with Alzheimer disease.* Nat Genet, 2007. **39**(2): p. 168-77.
183. Fjorback, A.W., et al., *Retromer binds the FANSHY sorting motif in SorLA to regulate amyloid precursor protein sorting and processing.* J Neurosci, 2012. **32**(4): p. 1467-80.
184. Herskowitz, J.H., et al., *GGA1-mediated endocytic traffic of LR11/SorLA alters APP intracellular distribution and amyloid-β production.* Mol Biol Cell, 2012. **23**(14): p. 2645-57.
185. Okamoto, M. and T.C. Südhof, *Mints, Munc18-interacting proteins in synaptic vesicle exocytosis.* J Biol Chem, 1997. **272**(50): p. 31459-64.
186. Okamoto, M. and T.C. Südhof, *Mint 3: a ubiquitous mint isoform that does not bind to munc18-1 or -2.* Eur J Cell Biol, 1998. **77**(3): p. 161-5.
187. Devon, R.S., et al., *Als2-deficient mice exhibit disturbances in endosome trafficking associated with motor behavioral abnormalities.* Proceedings of the National Academy of Sciences, 2006. **103**(25): p. 9595-9600.
188. Hadano, S., et al., *A gene encoding a putative GTPase regulator is mutated in familial amyotrophic lateral sclerosis 2.* Nature Genetics, 2001. **29**(2): p. 166-173.
189. Maruyama, H., et al., *Mutations of optineurin in amyotrophic lateral sclerosis.* Nature, 2010. **465**(7295): p. 223-6.
190. Stepto, A., et al., *Modelling C9ORF72 hexanucleotide repeat expansion in amyotrophic lateral sclerosis and frontotemporal dementia.* Acta Neuropathologica, 2014. **127**(3): p. 377-389.
191. Waite, A.J., et al., *Reduced C9orf72 protein levels in frontal cortex of amyotrophic lateral sclerosis and frontotemporal degeneration brain with the C9ORF72 hexanucleotide repeat expansion.* Neurobiology of aging, 2014. **35**(7): p. 1779.e5-1779.e13.
192. Yang, Y., et al., *The gene encoding alsin, a protein with three guanine-nucleotide exchange factor domains, is mutated in a form of recessive amyotrophic lateral sclerosis.* Nat Genet, 2001. **29**(2): p. 160-5.

193. Hanein, S., et al., *Identification of the SPG15 Gene, Encoding Spastizin, as a Frequent Cause of Complicated Autosomal-Recessive Spastic Paraplegia, Including Kjellin Syndrome.* The American Journal of Human Genetics, 2008. **82**(4): p. 992-1002.
194. Hazan, J., et al., *Spastin, a new AAA protein, is altered in the most frequent form of autosomal dominant spastic paraplegia.* Nat Genet, 1999. **23**(3): p. 296-303.
195. Patel, H., et al., *SPG20 is mutated in Troyer syndrome, an hereditary spastic paraplegia.* Nat Genet, 2002. **31**(4): p. 347-8.
196. Slabicki, M., et al., *A genome-scale DNA repair RNAi screen identifies SPG48 as a novel gene associated with hereditary spastic paraplegia.* PLoS Biol, 2010. **8**(6): p. e1000408.
197. Zivony-Elboum, Y., et al., *A founder mutation in Vps37A causes autosomal recessive complex hereditary spastic paraparesis.* J Med Genet, 2012. **49**(7): p. 462-72.
198. Shi, Y., et al., *Haploinsufficiency leads to neurodegeneration in C9ORF72 ALS/FTD human induced motor neurons.* Nat Med, 2018. **24**(3): p. 313-325.
199. Zhen, Y. and H. Stenmark, *Cellular functions of Rab GTPases at a glance.* J Cell Sci, 2015. **128**(17): p. 3171-6.
200. Stenmark, H., *Rab GTPases as coordinators of vesicle traffic.* Nat Rev Mol Cell Biol, 2009. **10**(8): p. 513-25.
201. Casper, D., C. Mytilineou, and M. Blum, *EGF enhances the survival of dopamine neurons in rat embryonic mesencephalon primary cell culture.* Journal of Neuroscience Research, 1991. **30**(2): p. 372-381.
202. Kornblum, H.I., et al., *Epidermal growth factor and basic fibroblast growth factor: effects on an overlapping population of neocortical neurons in vitro.* 1990. **535**(2): p. 255-263.
203. Schwenk, B.M., et al., *TDP-43 loss of function inhibits endosomal trafficking and alters trophic signaling in neurons.* The EMBO journal, 2016. **35**(21): p. 2350-2370.
204. Deshpande, M. and A.A. Rodal, *The Crossroads of Synaptic Growth Signaling, Membrane Traffic and Neurological Disease: Insights from Drosophila.* 2016. **17**(2): p. 87-101.
205. Deshpande, M., et al., *Role of BMP receptor traffic in synaptic growth defects in an ALS model.* 2016. **27**(19): p. 2898-2910.
206. Chandran, J., J. Ding, and H. Cai, *Alsin and the molecular pathways of amyotrophic lateral sclerosis.* Molecular neurobiology, 2007. **36**(3): p. 224-231.
207. Lai, C., et al., *Regulation of endosomal motility and degradation by amyotrophic lateral sclerosis 2/alsin.* Molecular Brain, 2009. **2**(1): p. 23.
208. Perez-Victoria, F.J., et al., *Structural basis for the wobbler mouse neurodegenerative disorder caused by mutation in the Vps54 subunit of the GARP complex.* 2010. **107**(29): p. 12860-12865.
209. Perez-Victoria, F.J. and J.S. Bonifacino, *Dual Roles of the Mammalian GARP Complex in Tethering and SNARE Complex Assembly at the trans-Golgi Network.* Molecular and Cellular Biology, 2009. **29**(19): p. 5251-5263.

210. Quenneville, N.R., et al., *Domains within the GARP Subunit Vps54 Confer Separate Functions in Complex Assembly and Early Endosome Recognition.* Molecular Biology of the Cell, 2006. **17**(4): p. 1859-1870.
211. Schindler, C., et al., *EARP is a multisubunit tethering complex involved in endocytic recycling.* Nature Cell Biology, 2015. **17**(5): p. 639-650.
212. Topalidou, I., et al., *The EARP Complex and Its Interactor EIPR-1 Are Required for Cargo Sorting to Dense-Core Vesicles.* PLOS Genetics, 2016. **12**(5): p. e1006074.
213. Conibear, E. and T.H. Stevens, *Vps52p, Vps53p, and Vps54p Form a Novel Multisubunit Complex Required for Protein Sorting at the Yeast Late Golgi.* 2000. **11**(1): p. 305-323.
214. Bonifacino, J.S. and A. Hierro, *Transport according to GARP: receiving retrograde cargo at the trans-Golgi network.* Trends in Cell Biology, 2011. **21**(3): p. 159-167.
215. Pérez-Victoria, F.J., et al., *Structural basis for the wobbler mouse neurodegenerative disorder caused by mutation in the Vps54 subunit of the GARP complex.* Proceedings of the National Academy of Sciences of the United States of America, 2010. **107**(29): p. 12860-12865.
216. Hirata, T., et al., *Post-Golgi anterograde transport requires GARP-dependent endosome-to-TGN retrograde transport.* 2015. **26**(17): p. 3071-3084.
217. Schmitt-John, T., et al., *Mutation of Vps54 causes motor neuron disease and defective spermiogenesis in the wobbler mouse.* Nature genetics, 2005. **37**(11): p. 1213-1215.
218. Karlsson, P., et al., *Loss of Vps54 Function Leads to Vesicle Traffic Impairment, Protein Mis-Sorting and Embryonic Lethality.* International Journal of Molecular Sciences, 2013. **14**(6): p. 10908-10925.
219. Feinstein, M., et al., *VPS53 mutations cause progressive cerebello-cerebral atrophy type 2 (PCCA2).* J Med Genet, 2014. **51**(5): p. 303-8.
220. Schmitt-John, T., *VPS54 and the wobbler mouse.* Frontiers in Neuroscience, 2015. **9**.
221. Duchen, L.W. and S.J. Strich, *An hereditary motor neurone disease with progressive denervation of muscle in the mouse: the mutant 'wobbler'.* 1968. **31**(6): p. 535-542.
222. Santoro, B., et al., *Evidence for chronic mitochondrial impairment in the cervical spinal cord of a murine model of motor neuron disease.* Neurobiol Dis, 2004. **17**(2): p. 349-57.
223. Nieto-Gonzalez, J.L., et al., *Reduced GABAergic inhibition explains cortical hyperexcitability in the wobbler mouse model of ALS.* Cereb Cortex, 2011. **21**(3): p. 625-35.
224. Pernas-Alonso, R., et al., *Regionalized Neurofilament Accumulation and Motoneuron Degeneration Are Linked Phenotypes in Wobbler Neuromuscular Disease.* Neurobiology of Disease, 2001. **8**(4): p. 581-589.
225. Mitsumoto, H., et al., *Impairment of retrograde axonal transport in wobbler mouse motor neuron disease.* Muscle Nerve, 1990. **13**(2): p. 121-6.

226. Dennis, J.S. and B.A. Citron, *Wobbler mice modeling motor neuron disease display elevated transactive response DNA binding protein.* Neuroscience, 2009. **158**(2): p. 745-50.
227. Meisler, M.H., et al., *Evaluation of the Golgi trafficking protein VPS54 (wobbler) as a candidate for ALS.* 2008. **9**(3): p. 141-148.
228. Corrado, L., et al., *VPS54 genetic analysis in ALS Italian cohort.* European Journal of Neurology, 2011. **18**(4): p. e41-e42.
229. Heimann, P., S. Laage, and H. Jockusch, *Defect of sperm assembly in a neurological mutant of the mouse, wobbler (WR).* 1991. **47**(2): p. 77-83.
230. Fári, K., et al., *The role of acroblast formation duringDrosophilaspermatogenesis.* 2016. **5**(8): p. 1102-1110.
231. Paiardi, C., et al., *Failure of acrosome formation and globozoospermia in the wobbler mouse, a Vps54 spontaneous recessive mutant.* Spermatogenesis, 2011. **1**(1): p. 52-62.
232. Moser, J.M., P. Bigini, and T. Schmitt-John, *The wobbler mouse, an ALS animal model.* 2013. **288**(5-6): p. 207-229.
233. Bruzzone, F., et al., *Expression of the deubiquitinating enzyme mUBPy in the mouse brain.* Brain Res, 2008. **1195**: p. 56-66.
234. Berruti, G. and E. Martegani, *The deubiquitinating enzyme mUBPy interacts with the sperm-specific molecular chaperone MSJ-1: the relation with the proteasome, acrosome, and centrosome in mouse male germ cells.* Biol Reprod, 2005. **72**(1): p. 14-21.
235. Castrillon, D.H., et al., *Toward a molecular genetic analysis of spermatogenesis in Drosophila melanogaster: characterization of male-sterile mutants generated by single P element mutagenesis.* Genetics, 1993. **135**(2): p. 489-505.
236. Fabrizio, J.J., et al., *Genetic dissection of sperm individualization in Drosophila melanogaster.* Development, 1998. **125**(10): p. 1833-43.
237. Pradhan, S.J., et al., *The conserved P body component HPat/Pat1 negatively regulates synaptic terminal growth at the larval Drosophila neuromuscular junction.* Journal of cell science, 2012. **125**(Pt 24): p. 6105-6116.
238. Nawalpuri, B., S. Ravindran, and R.S. Muddashetty, *The Role of Dynamic miRISC During Neuronal Development.* Frontiers in Molecular Biosciences, 2020. **7**(8).
239. McGurk, L., A. Berson, and N.M. Bonini, *Drosophilaas anIn VivoModel for Human Neurodegenerative Disease.* Genetics, 2015. **201**(2): p. 377-402.
240. Mhatre, S.D., et al., *Synaptic abnormalities in a Drosophila model of Alzheimer's disease.* Disease Models & Mechanisms, 2014. **7**(3): p. 373.
241. Perry, S., et al., *Developmental arrest of Drosophila larvae elicits presynaptic depression and enables prolonged studies of neurodegeneration.* Development, 2020. **147**(10): p. dev186312.
242. Bier, E., *Drosophila, the golden bug, emerges as a tool for human genetics.* Nat Rev Genet, 2005. **6**(1): p. 9-23.
243. Lloyd, T.E. and J.P. Taylor, *Flightless flies: Drosophila models of neuromuscular disease.* Annals of the New York Academy of Sciences, 2010. **1184**: p. e1-e20.

244. Wojnacki, J. and T. Galli, *Membrane traffic during axon development.* Developmental Neurobiology, 2016. **76**(11): p. 1185-1200.
245. Schreij, A.M.A., E.A. Fon, and P.S. McPherson, *Endocytic membrane trafficking and neurodegenerative disease.* Cellular and Molecular Life Sciences, 2016. **73**(8): p. 1529-1545.
246. Perez-Victoria, F.J., G.A. Mardones, and J.S. Bonifacino, *Requirement of the Human GARP Complex for Mannose 6-phosphate-receptor-dependent Sorting of Cathepsin D to Lysosomes.* 2008. **19**(6): p. 2350-2362.
247. Patel, P.H., et al., *Vps54 regulates Drosophila neuromuscular junction development and interacts genetically with Rab7 to control composition of the postsynaptic density.* Biology Open, 2020. **9**(8): p. bio053421.
248. Menon, K.P., R.A. Carrillo, and K. Zinn, *Development and plasticity of the Drosophila larval neuromuscular junction.* Wiley interdisciplinary reviews. Developmental biology, 2013. **2**(5): p. 647-670.
249. Lahey, T., et al., *The Drosophila tumor suppressor gene dlg is required for normal synaptic bouton structure.* Neuron, 1994. **13**(4): p. 823-35.
250. Berruti, G., M. Ripolone, and M. Ceriani, *USP8, a Regulator of Endosomal Sorting, Is Involved in Mouse Acrosome Biogenesis Through Interaction with the Spermatid ESCRT-0 Complex and Microtubules1.* Biology of Reproduction, 2010. **82**(5): p. 930-939.
251. Sisson, J.C., et al., *Lava lamp, a novel peripheral golgi protein, is required for Drosophila melanogaster cellularization.* J Cell Biol, 2000. **151**(4): p. 905-18.
252. Amessou, M., et al., *Syntaxin 16 and syntaxin 5 are required for efficient retrograde transport of several exogenous and endogenous cargo proteins.* 2007. **120**(8): p. 1457-1468.
253. Lasiecka, Z.M. and B. Winckler, *Mechanisms of polarized membrane trafficking in neurons — Focusing in on endosomes.* 2011. **48**(4): p. 278-287.
254. Conboy, M.J. and M.S. Cyert, *Luv1p/Rki1p/Tcs3p/Vps54p, a yeast protein that localizes to the late Golgi and early endosome, is required for normal vacuolar morphology.* Molecular biology of the cell, 2000. **11**(7): p. 2429-2443.
255. Conibear, E. and T.H. Stevens, *Vps52p, Vps53p, and Vps54p Form a Novel Multisubunit Complex Required for Protein Sorting at the Yeast Late Golgi.* Molecular Biology of the Cell, 2000. **11**(1): p. 305-323.
256. Palmisano, R., et al., *Endosomal accumulation of APP in wobbler motor neurons reflects impaired vesicle trafficking: Implications for human motor neuron disease.* 2011. **12**(1): p. 24.
257. Riedel, F., et al., *An antibody toolkit for the study of membrane traffic in <em>Drosophila melanogaster</em&gt.* Biology Open, 2016. **5**(7): p. 987.
258. Tanaka, T. and A. Nakamura, *The endocytic pathway acts downstream of Oskar in Drosophila germ plasm assembly.* 2008. **135**(6): p. 1107-1117.
259. Conibear, E., *Vps51p Mediates the Association of the GARP (Vps52/53/54) Complex with the Late Golgi t-SNARE Tlg1p.* 2003. **14**(4): p. 1610-1623.

260. Siniossoglou, S. and H.R.B. Pelham, *Vps51p Links the VFT Complex to the SNARE Tlg1p.* 2002. **277**(50): p. 48318-48324.
261. Ho, S.-Y., et al., *Zebrafish fat-free is required for intestinal lipid absorption and Golgi apparatus structure.* 2006. **3**(4): p. 289-300.
262. Pfeffer, S.R., *Rab GTPases: master regulators that establish the secretory and endocytic pathways.* Molecular Biology of the Cell, 2017. **28**(6): p. 712-715.
263. Pfeffer, S. and D. Aivazian, *Targeting Rab GTPases to distinct membrane compartments.* Nat Rev Mol Cell Biol, 2004. **5**(11): p. 886-96.
264. Zhang, J., et al., *Thirty-One Flavors of Drosophila Rab Proteins.* Genetics, 2007. **176**(2): p. 1307-1322.
265. Ozdowski, E.F., et al., *Loss of Drosophila melanogaster p21-activated kinase 3 suppresses defects in synapse structure and function caused by spastin mutations.* Genetics, 2011. **189**(1): p. 123-35.
266. Koh, Y.H., et al., *Regulation of DLG Localization at Synapses by CaMKII-Dependent Phosphorylation.* 1999. **98**(3): p. 353-363.
267. Ghosh, R., et al., *Kismet Positively Regulates Glutamate Receptor Localization and Synaptic Transmission at the Drosophila Neuromuscular Junction.* 2014. **9**(11): p. e113494.
268. Shahidullah, M., et al., *Defects in Synapse Structure and Function Precede Motor Neuron Degeneration in Drosophila Models of FUS-Related ALS.* Journal of Neuroscience, 2013. **33**(50): p. 19590-19598.
269. West, R.J.H., et al., *Rab8, POSH, and TAK1 regulate synaptic growth in a Drosophila model of frontotemporal dementia.* Journal of Cell Biology, 2015. **208**(7): p. 931-947.
270. Zhu, J.-Y., et al., *Knockdown of Hsc70-5/mortalin Induces Loss of Synaptic Mitochondria in a Drosophila Parkinson's Disease Model.* PLoS ONE, 2013. **8**(12): p. e83714.
271. Falk, J., et al., *Rab5 and Rab4 Regulate Axon Elongation in the Xenopus Visual System.* 2014. **34**(2): p. 373-391.
272. van Bergeijk, P., et al., *Optogenetic control of organelle transport and positioning.* Nature, 2015. **518**(7537): p. 111-114.
273. Jin, E.J., et al., *Live Observation of Two Parallel Membrane Degradation Pathways at Axon Terminals.* Current Biology, 2018. **28**(7): p. 1027-1038.e4.
274. Khodosh, R., et al., *Bchs, a BEACH domain protein, antagonizes Rab11 in synapse morphogenesis and other developmental events.* 2006. **133**(23): p. 4655-4665.
275. Sakuma, C., et al., *Drosophila Strip serves as a platform for early endosome organization during axon elongation.* 2014. **5**: p. 5180.
276. Satoh, D., et al., *Spatial control of branching within dendritic arbors by dynein-dependent transport of Rab5-endosomes.* Nat Cell Biol, 2008. **10**(10): p. 1164-71.
277. Chen, K. and D.E. Featherstone, *Discs-large (DLG) is clustered by presynaptic innervation and regulates postsynaptic glutamate receptor subunit composition in Drosophila.* BMC Biology, 2005. **3**(1): p. 1.
278. Sulkowski, M.J., et al., *A Novel, Noncanonical BMP Pathway Modulates Synapse Maturation at the Drosophila Neuromuscular Junction.* 2016. **12**(1): p. e1005810.

279. Deivasigamani, S., et al., *A Presynaptic Regulatory System Acts Transsynaptically via Mon1 to Regulate Glutamate Receptor Levels in Drosophila.* 2015. **201**(2): p. 651-664.
280. Poteryaev, D., et al., *Caenorhabditis elegans SAND-1 is essential for RAB-7 function in endosomal traffic.* The EMBO Journal, 2007. **26**(2): p. 301-312.
281. Yousefian, J., et al., *Dmon1 controls recruitment of Rab7 to maturing endosomes in Drosophila.* 2013. **126**(7): p. 1583-1594.
282. Contractor, A., et al., *Trans-Synaptic Eph Receptor-Ephrin Signaling in Hippocampal Mossy Fiber LTP.* Science, 2002. **296**(5574): p. 1864.
283. Korkut, C. and V. Budnik, *WNTs tune up the neuromuscular junction.* 2009. **10**(9): p. 627-634.
284. Korkut, C., et al., *Regulation of Postsynaptic Retrograde Signaling by Presynaptic Exosome Release.* 2013. **77**(6): p. 1039-1046.
285. Wagh, D.A., et al., *Bruchpilot, a protein with homology to ELKS/CAST, is required for structural integrity and function of synaptic active zones in Drosophila.* Neuron, 2006. **49**(6): p. 833-44.
286. Kittel, R.J., et al., *Bruchpilot promotes active zone assembly, Ca2+ channel clustering, and vesicle release.* Science, 2006. **312**(5776): p. 1051-4.
287. Folwell, J., et al., *Abeta exacerbates the neuronal dysfunction caused by human tau expression in a Drosophila model of Alzheimer's disease.* Experimental neurology, 2010. **223**(2): p. 401-409.
288. Mudher, A., et al., *GSK-3β inhibition reverses axonal transport defects and behavioural phenotypes in Drosophila.* Molecular Psychiatry, 2004. **9**(5): p. 522-530.
289. England, J.D. and A.K. Asbury, *Peripheral neuropathy.* Lancet, 2004. **363**(9427): p. 2151-61.
290. Wakabayashi, K., et al., *Sporadic motor neuron disease with severe sensory neuronopathy.* Acta Neuropathol, 1998. **95**(4): p. 426-30.
291. Bonanno, G., et al., *Release of [3H]d-aspartate induced by K+-stimulation is increased in the cervical spinal cord of the wobbler mouse: a model of motor neuron disease.* Neurochemistry International, 2009. **55**(5): p. 302-306.
292. Gentile, F., et al., *The Peripheral Nervous System in Amyotrophic Lateral Sclerosis: Opportunities for Translational Research.* Frontiers in neuroscience, 2019. **13**: p. 601-601.
293. Lin, C.-H., et al., *LRRK2 G2019S Mutation Induces Dendrite Degeneration through Mislocalization and Phosphorylation of Tau by Recruiting Autoactivated GSK3β.* The Journal of Neuroscience, 2010. **30**(39): p. 13138.
294. Brown, H.E., et al., *The function of Drosophila larval class IV dendritic arborization sensory neurons in the larval-pupal transition is separable from their function in mechanical nociception responses.* PloS one, 2017. **12**(9): p. e0184950-e0184950.
295. Grueber, W.B., L.Y. Jan, and Y.N. Jan, *Tiling of the Drosophila epidermis by multidendritic sensory neurons.* Development, 2002. **129**(12): p. 2867-78.

296. Olesnicky, E.C., et al., *Shep interacts with posttranscriptional regulators to control dendrite morphogenesis in sensory neurons.* Dev Biol, 2018. **444**(2): p. 116-128.
297. *Paths, Diffusion, and Navigation*. 2016, Elsevier. p. 207-255.
298. Long, H., et al., *Dendrite branching and self-avoidance are controlled by Turtle, a conserved IgSF protein in <em>Drosophila</em&gt.* Development, 2009. **136**(20): p. 3475.
299. Corty, M.M., B.J. Matthews, and W.B. Grueber, *Molecules and mechanisms of dendrite development in <em>Drosophila</em&gt.* Development, 2009. **136**(7): p. 1049.
300. Villarroel-Campos, D., et al., *Rab-mediated trafficking role in neurite formation.* 2014. **129**(2): p. 240-248.
301. Liu, J., et al., *Nerve Growth Factor-mediated Neurite Outgrowth via Regulation of Rab5.* 2007. **18**(4): p. 1375-1384.
302. Mori, Y., T. Matsui, and M. Fukuda, *Rabex-5 Protein Regulates Dendritic Localization of Small GTPase Rab17 and Neurite Morphogenesis in Hippocampal Neurons.* 2013. **288**(14): p. 9835-9847.
303. Cogli, L., et al., *CMT2B-associated Rab7 mutants inhibit neurite outgrowth.* 2010. **120**(4): p. 491-501.
304. Saxena, S., *The Small GTPase Rab7 Controls the Endosomal Trafficking and Neuritogenic Signaling of the Nerve Growth Factor Receptor TrkA.* 2005. **25**(47): p. 10930-10940.
305. Spinosa, M.R., et al., *Functional Characterization of Rab7 Mutant Proteins Associated with Charcot-Marie-Tooth Type 2B Disease.* 2008. **28**(7): p. 1640-1648.
306. Li, X. and M. DiFiglia, *The recycling endosome and its role in neurological disorders.* Prog Neurobiol, 2012. **97**(2): p. 127-41.
307. Kelly, E.E., C.P. Horgan, and M.W. McCaffrey, *Rab11 proteins in health and disease.* Biochemical Society transactions, 2012. **40**(6): p. 1360-1367.
308. Gerhard, D.S., et al., *The status, quality, and expansion of the NIH full-length cDNA project: the Mammalian Gene Collection (MGC).* Genome Res, 2004. **14**(10b): p. 2121-7.
309. Cai, H., K. Reinisch, and S. Ferro-Novick, *Coats, tethers, Rabs, and SNAREs work together to mediate the intracellular destination of a transport vesicle.* Dev Cell, 2007. **12**(5): p. 671-82.
310. Lupashin, V. and E. Sztul, *Golgi tethering factors.* Biochim Biophys Acta, 2005. **1744**(3): p. 325-39.
311. Tripathi, A., et al., *Structural characterization of Tip20p and Dsl1p, subunits of the Dsl1p vesicle tethering complex.* Nat Struct Mol Biol, 2009. **16**(2): p. 114-23.
312. Wu, S., et al., *Sec15 interacts with Rab11 via a novel domain and affects Rab11 localization in vivo.* Nat Struct Mol Biol, 2005. **12**(10): p. 879-85.
313. Sivaram, M.V., et al., *The structure of the exocyst subunit Sec6p defines a conserved architecture with diverse roles.* Nat Struct Mol Biol, 2006. **13**(6): p. 555-6.

314. Moore, B.A., H.H. Robinson, and Z. Xu, *The Crystal Structure of Mouse Exo70 Reveals Unique Features of the Mammalian Exocyst.* Journal of Molecular Biology, 2007. **371**(2): p. 410-421.
315. A L Goldberg, a. and A.C.S. John, *Intracellular Protein Degradation in Mammalian and Bacterial Cells: Part 2.* Annual Review of Biochemistry, 1976. **45**(1): p. 747-804.
316. Rao, Q., et al., *Cryo-EM structure of human ATR-ATRIP complex.* Cell Res, 2018. **28**(2): p. 143-156.
317. Roy, A., A. Kucukural, and Y. Zhang, *I-TASSER: a unified platform for automated protein structure and function prediction.* Nat Protoc, 2010. **5**(4): p. 725-38.
318. Yang, J., et al., *The I-TASSER Suite: protein structure and function prediction.* Nat Methods, 2015. **12**(1): p. 7-8.
319. Zhang, Y., *I-TASSER server for protein 3D structure prediction.* BMC Bioinformatics, 2008. **9**: p. 40.
320. Petit, C.S., et al., *Inhibition of sphingolipid synthesis improves outcomes and survival in GARP mutant wobbler mice, a model of motor neuron degeneration.* Proceedings of the National Academy of Sciences, 2020. **117**(19): p. 10565-10574.
321. Chiò, A., et al., *Prognostic factors in ALS: A critical review.* Amyotrophic Lateral Sclerosis, 2009. **10**(5-6): p. 310-323.
322. Macleod, A.D., K.S. Taylor, and C.E. Counsell, *Mortality in Parkinson's disease: a systematic review and meta-analysis.* Mov Disord, 2014. **29**(13): p. 1615-22.
323. Tom, S.E., et al., *Characterization of dementia and Alzheimer's disease in an older population: updated incidence and life expectancy with and without dementia.* American journal of public health, 2015. **105**(2): p. 408-413.
324. Orrell, R.W., *Motor neuron disease: systematic reviews of treatment for ALS and SMA.* Br Med Bull, 2010. **93**: p. 145-59.
325. Wang, J.-W., et al., *The ALS-associated proteins FUS and TDP-43 function together to affect Drosophila locomotion and life span.* Journal of Clinical Investigation, 2011. **121**(10): p. 4118-4126.
326. Vucic, S., G.A. Nicholson, and M.C. Kiernan, *Cortical hyperexcitability may precede the onset of familial amyotrophic lateral sclerosis.* Brain, 2008. **131**(Pt 6): p. 1540-50.
327. Kroll, J.R. and M.A. Tanouye, *Rescue of easily shocked mutant seizure sensitivity in Drosophila adults.* J Comp Neurol, 2013. **521**(15): p. 3500-7.
328. Benzer, S., *From the Gene to Behavior.* JAMA, 1971. **218**(7): p. 1015-1022.
329. Ganetzky, B. and C.-F. Wu, *INDIRECT SUPPRESSION INVOLVING BEHAVIORAL MUTANTS WITH ALTERED NERVE EXCITABILITY IN <em>DROSOPHILA MELANOGASTER</em&gt.* Genetics, 1982. **100**(4): p. 597.
330. Reynolds, E.R., *Shortened Lifespan and Other Age-Related Defects in Bang Sensitive Mutants of Drosophila melanogaster.* G3 (Bethesda, Md.), 2018. **8**(12): p. 3953-3960.
331. Xu, G.P., et al., *Dysfunctional mitochondrial respiration in the wobbler mouse brain.* Neurosci Lett, 2001. **300**(3): p. 141-4.

332. Bertamini, M., et al., *Mitochondrial oxidative metabolism in motor neuron degeneration (mnd) mouse central nervous system.* Eur J Neurosci, 2002. **16**(12): p. 2291-6.
333. Dahlke, C., et al., *Inflammation and neuronal death in the motor cortex of the wobbler mouse, an ALS animal model.* Journal of Neuroinflammation, 2015. **12**(1).
334. Carreira, V.P., J. Mensch, and J.J. Fanara, *Body size in Drosophila: genetic architecture, allometries and sexual dimorphism.* Heredity, 2009. **102**(3): p. 246-256.
335. Bournat, J.C. and C.W. Brown, *Mitochondrial dysfunction in obesity.* Current opinion in endocrinology, diabetes, and obesity, 2010. **17**(5): p. 446-452.
336. McKhann, G., et al., *Clinical diagnosis of Alzheimer's disease: report of the NINCDS-ADRDA Work Group under the auspices of Department of Health and Human Services Task Force on Alzheimer's Disease.* Neurology, 1984. **34**(7): p. 939-44.
337. Nakayama, Y., et al., *Body weight variation predicts disease progression after invasive ventilation in amyotrophic lateral sclerosis.* Scientific Reports, 2019. **9**(1): p. 12262.
338. Austad, S.N. and K.E. Fischer, *Sex Differences in Lifespan.* Cell Metabolism, 2016. **23**(6): p. 1022-1033.
339. McCombe, P.A. and R.D. Henderson, *Effects of gender in amyotrophic lateral sclerosis.* Gender Medicine, 2010. **7**(6): p. 557-570.
340. Miller, I.N. and A. Cronin-Golomb, *Gender differences in Parkinson's disease: Clinical characteristics and cognition.* Movement Disorders, 2010. **25**(16): p. 2695-2703.
341. Harbo, H.F., R. Gold, and M. Tintoré, *Sex and gender issues in multiple sclerosis.* Therapeutic Advances in Neurological Disorders, 2013. **6**(4): p. 237-248.
342. Mathews, K.W., M. Cavegn, and M. Zwicky, *Sexual Dimorphism of Body Size Is Controlled by Dosage of the X -Chromosomal Gene Myc and by the Sex-Determining Gene tra in Drosophila.* Genetics, 2017. **205**(3): p. 1215-1228.
343. Zárate, S., T. Stevnsner, and R. Gredilla, *Role of Estrogen and Other Sex Hormones in Brain Aging. Neuroprotection and DNA Repair.* Frontiers in Aging Neuroscience, 2017. **9**.
344. Saunders-Pullman, R., et al., *The effect of estrogen replacement on early Parkinson's disease.* Neurology, 1999. **52**(7): p. 1417-21.
345. Ding, F., et al., *Ovariectomy induces a shift in fuel availability and metabolism in the hippocampus of the female transgenic model of familial Alzheimer's.* PLoS One, 2013. **8**(3): p. e59825.
346. Heller, K., *Sex on the Fly.* 2010. **8**(5): p. e1000364.
347. Dyck, P.J. and E.H. Lambert, *Lower motor and primary sensory neuron diseases with peroneal muscular atrophy. I. Neurologic, genetic, and electrophysiologic findings in hereditary polyneuropathies.* Arch Neurol, 1968. **18**(6): p. 603-18.
348. Harding, A.E. and P.K. Thomas, *The clinical features of hereditary motor and sensory neuropathy types I and II.* Brain, 1980. **103**(2): p. 259-80.

349. Leger, B., *Human skeletal muscle atrophy in amyotrophic lateral sclerosis reveals a reduction in Akt and an increase in atrogin-1.* 2006.
350. Peker, N., et al., *Loss of Parkin impairs mitochondrial function and leads to muscle atrophy.* Am J Physiol Cell Physiol, 2018. **315**(2): p. C164-C185.
351. Bender, J.A. and M.A. Frye, *Invertebrate solutions for sensing gravity.* Curr Biol, 2009. **19**(5): p. R186-90.
352. Carpenter, F.W., *The Reactions of the Pomace Fly (Drosophila ampelophila Loew) to Light, Gravity, and Mechanical Stimulation.* The American Naturalist, 1905. **39**(459): p. 157-171.
353. Lehmann, F.-O. and J. Bartussek, *Neural control and precision of flight muscle activation in Drosophila.* Journal of Comparative Physiology A, 2017. **203**(1): p. 1-14.
354. Kuleesha, Y., W.C. Puah, and M. Wasser, *A model of muscle atrophy based on live microscopy of muscle remodelling in Drosophila metamorphosis.* 2016. **3**(2): p. 150517.
355. Hantaï, D., et al., *Beneficial effects of insulin-like growth factor-I on wobbler mouse motoneuron disease.* Journal of the Neurological Sciences, 1995. **129**: p. 122-126.
356. *Dorsal Longitudinal Muscles*, in *Encyclopedia of Entomology*, J.L. Capinera, Editor. 2008, Springer Netherlands: Dordrecht. p. 1236-1236.
357. Cisterna, B.A., C. Cardozo, and J.C. Sã¡Ez, *Neuronal involvement in muscular atrophy.* 2014. **8**.
358. Steinert, J.R., et al., *Rab11 rescues synaptic dysfunction and behavioural deficits in a Drosophila model of Huntington's disease.* Human Molecular Genetics, 2012. **21**(13): p. 2912-2922.
359. Sreedharan, J., et al., *Age-Dependent TDP-43-Mediated Motor Neuron Degeneration Requires GSK3, hat-trick, and xmas-2.* 2015. **25**(16): p. 2130-2136.
360. Wu, J.S. and L. Luo, *A protocol for mosaic analysis with a repressible cell marker (MARCM) in Drosophila.* Nature Protocols, 2006. **1**(6): p. 2583-2589.
361. Gokerkucuk, E.B., M. Tramier, and G. Bertolin, *Imaging Mitochondrial Functions: from Fluorescent Dyes to Genetically-Encoded Sensors.* Genes (Basel), 2020. **11**(2).
362. Zwilling, M., C. Theiss, and V. Matschke, *Caffeine and NAD+ Improve Motor Neural Integrity of Dissociated Wobbler Cells In Vitro.* Antioxidants, 2020. **9**(6): p. 460.
363. Gilleron, J., J.M. Gerdes, and A. Zeigerer, *Metabolic regulation through the endosomal system.* Traffic, 2019.
364. Ramos, C.I., et al., *Neto-Mediated Intracellular Interactions Shape Postsynaptic Composition at the Drosophila Neuromuscular Junction.* PLOS Genetics, 2015. **11**(4): p. e1005191.
365. Parnas, D., et al., *Regulation of Postsynaptic Structure and Protein Localization by the Rho-Type Guanine Nucleotide Exchange Factor dPix.* 2001. **32**(3): p. 415-424.
366. Schindelin, J., et al., *Fiji: an open-source platform for biological-image analysis.* Nature Methods, 2012. **9**(7): p. 676-682.

367. Schindelin, J., et al., *The ImageJ ecosystem: An open platform for biomedical image analysis.* Molecular Reproduction and Development, 2015. **82**(7-8): p. 518-529.
368. Bolte, S. and F.P. Cordelières, *A guided tour into subcellular colocalization analysis in light microscopy.* J Microsc, 2006. **224**(Pt 3): p. 213-32.
369. Nijhof, B., et al., *A New Fiji-Based Algorithm That Systematically Quantifies Nine Synaptic Parameters Provides Insights into Drosophila NMJ Morphometry.* 2016. **12**(3): p. e1004823.
370. Tinevez, J.-Y., et al., *TrackMate: An open and extensible platform for single-particle tracking.* Methods, 2017. **115**: p. 80-90.
371. Arganda-Carreras, I., et al., *3D reconstruction of histological sections: Application to mammary gland tissue.* Microscopy Research and Technique, 2010. **73**(11): p. 1019-1029.
372. Polder, G., H.L.E. Hovens, and A.J. Zweers. *Measuring shoot length of submerged aquatic plants using graph analysis*. in *Proceedings of the ImageJ User and Developer Conference 2010, Mondorf-les-Bains, Luxembourg, 27-29 October 2010*. 2010. Luxembourg: Centre de Recherche Public Henri Tudor.
373. Doube, M., et al., *BoneJ: Free and extensible bone image analysis in ImageJ.* Bone, 2010. **47**(6): p. 1076-1079.
374. Livak, K.J. and T.D. Schmittgen, *Analysis of relative gene expression data using real-time quantitative PCR and the 2(-Delta Delta C(T)) Method.* Methods, 2001. **25**(4): p. 402-8.
375. Piper, M.D.W. and L. Partridge, *Protocols to Study Aging in Drosophila.* Methods in molecular biology (Clifton, N.J.), 2016. **1478**: p. 291-302.
376. Kucherenko, M., et al., *Paraffin-Embedded and Frozen Sections of Drosophila Adult Muscles.* Journal of Visualized Experiments : JoVE, 2010.

APPENDIX: LIST OF ABBREVIATIONS

Parkinson's Disease – PD
Alzheimer's Disease – AD
Amyotrophic lateral sclerosis – ALS
Frontotemporal dementia – FTD
Charcot-Marie-Tooth – CMT
RNA binding protein – RBP
TAR DNA-binding protein-43 – TDP43
Nuclear protein fused in sarcoma – FUS
Muscleblind-like protein – MBNL
microRNA – miRNA
Fragile X-associated tremor/ataxia syndrome – FXTAS
Neuronal intermediate filament inclusion disease – NIFID
Leucine-rich repeat kinase 2 – LRRK2
Superoxide-dismutase-1 – SOD1
Lipoprotein receptor-related protein 1 – LRP1
Synaptojanin – SYNJ1
Sorting nexin – SNX
Sortilin-related receptor with A-type repeats – SorLA
ADP ribosylation factor 6 – ARF6
Endoplasmic reticulum – ER
Alsin – ALS2
Optineurin – OPTN
Spastin – SPG4
Strumpellin – SPG8
Spatacsin – SPG11
Spastizin – SPG15
Manose-6-phosphate receptor – M6PR
Trans-Golgi network - TGN
N-ethylmaleidmide-sensitive fusion protein attachment protein receptors – SNAREs
Golgi-associated retrograde protein – GARP
Syntaxin-16 – Stx16
Syntaxin-6 – Syx6
Endosome-associated recycling protein – EARP
Carboxypeptidase – CPY
Cation-independent mannose 6-phosphate receptor – CI-MPR
Glycosylphophatidylinositol – (GIP)
Neuromuscular junction – NMJ
Central nervous system – CNS
Hemagglutinin – HA
Post synaptic density -PSD
Knockdown – KD
Short hairpin RNA – shRNA

Discs Large – DLG
Glutamate receptor – GluR
Bruchpilot – Brp
Root-mean-square deviation – RMSD
PE-precise excision
WT- wild type
CTE – chronic traumatic encephalopathy
Vacuolar protein sorting – Vps
Munc18 interacting protein – Mint
AB – beta amyloid
APP – beta-amyloid precursor protein
HSP – hereditary spastic paraplegia
EGFR-epidermal growth factor receptor
PLS – primary lateral sclerosis